STRUCTURAL REMODELING OF ALPHA-SYNUCLEIN BY SMALL MOLECULES:

A NOVEL PATH TO NEUROPROTECTIVE THERAPEUTICS

Malcolm James Daniels

A DISSERTATION

in

Pharmacology

Presented to the Faculties of the University of Pennsylvania

in

Partial Fulfillment of the Requirements for the

Degree of Doctor of Philosophy

2018

Supervisor of Dissertation

_____

Harry Ischiropoulos, Ph.D.
Gisela and Dennis Alter Research Professor of Pediatrics and Pharmacology

Graduate Group Chairperson

_____

Julie Blendy, Ph.D.
Professor of Pharmacology

Dissertation Committee
Edward B. Lee, M.D., Ph.D., Assistant Professor of Pathology and Laboratory Medicine (Chair)
Kelly L. Jordan-Sciutto, Ph.D., Chair and Professor of Pathology
Kelvin C. Luk, Ph.D., Research Assistant Professor of Pathology and Laboratory Medicine
E. James Petersson, Ph.D., Associate Professor of Chemistry

STRUCTURAL REMODELING OF ALPHA-SYNUCLEIN BY SMALL MOLECULES:

A NOVEL PATH TO NEUROPROTECTIVE THERAPEUTICS

COPYRIGHT

Dedicated to my grandfather, James Lindemann.

His struggle with Alzheimer's disease led to my research at University of Pennsylvania.

His sense of humor got me through.

ACKNOWLEDGMENT

First, I would like to offer my thanks to Harry Ischiropoulos, whose mentorship made this project possible. I chose to join Harry's lab because I felt he would challenge me to conduct and communicate science to the best of my abilities. He challenged me to do that, and more, over the years. In the entire time I've worked with him I never once felt that he considered me a tool or pair of hands. Instead, he gave freely of his thoughts, time, and caring, things for which I will always be grateful. I don't know if I will be his last graduate mentee. If so, I am deeply humbled.

Thank you to my thesis committee members, Eddie Lee, Kelly Jordan-Sciutto, Kelvin Luk, and E. James Petersson. Their honest feedback and thoughtful guidance have helped make this project what it is today. I am particularly thankful for the varied perspectives with which they have assessed my efforts. (I would also like to thank them for being mercifully easy to schedule.)

I owe a great deal the incredible collaborators that contributed to this work. Telling this story would have been impossible without their expertise and generosity. In particular, I would like to thank Marco, Valerio, Maria Grazia, Roberta, and Isabella from CERM at University of Florence, for welcoming me into their lab and their city.

I feel extremely lucky to have studied within the Pharmacology Graduate Group. Julie Blendy has done an excellent job helming the group throughout my tenure at Penn. Likewise, Sarah Squire has helped me at every step. I would also like to acknowledge the incoming class of 2012. It has taken years to get enough distance from Cell 600 and Med. Chem. to see our study sessions as fun, but I do nevertheless. I know I've found lifelong friends among this group. I am especially thankful for the times I've had with Kaitlyn Maier, Cory Alvey, and Ian Johnston. I owe a great deal to Ian and look forward to seeing more of him in the coming years.

Thanks are also due to all the members of the Ischiropoulos lab. You all helped make the lab feel like a home. Danielle, Scott, and Dick, the members of the long-disbanded α-synuclein data club, were particularly generous with their time in helping build the story that would become Chapter 4.

I owe a great deal of thanks to my incredible partner, Amy. She has taught me so much in our time together. Her love and support made it possible for me to complete this project. Her proofreading also strengthened this document immensely. I am excited to see where our next steps take us.

Finally, I must thank my family for their unwavering support throughout my life. I can say with absolute certainty that I never would come to Penn without them. I consider every member of my family to be a role model. Orville and Olleke have shown me that even friends can be family. Jim and Sally helped me learn to laugh. Ruth has taught me the value of being forthright. I have learned more from Peter than could possibly be recorded here. I am excited to learn more from him in the coming years. But it is my parents who deserve my deepest thanks. Throughout my life they have balanced example with expectation, making me the person I am today. Thank you.

ABSTRACT

STRUCTURAL REMODELING OF ALPHA-SYNUCLEIN BY SMALL MOLECULES: A NOVEL PATH TO NEUROPROTECTIVE THERAPEUTICS

Malcolm James Daniels

Harry Ischiropoulos

Neurodegenerative diseases share the unifying features of insoluble protein aggregates and irreversible neuron loss. Parkinson's disease (PD) is defined by proteinaceous Lewy bodies—which contain α-synuclein—and loss of dopamine neurons leading to motor dysfunction. Growing evidence implicates α-synuclein aggregation as a causal driver of neurodegeneration in certain forms of PD. However, the precise mechanism(s) by which the process or products of α-synuclein aggregation drive neuron death remains unknown. Better understanding of this key question might further development of neuroprotective therapies for PD and related disorders. To address this gap, we reviewed how the native conformation of α-synuclein relates to its physiological function and roles in pathology. We also examined how the mouse brain proteome and phosphoproteome change in response to α-synuclein aggregation using quantitative proteomics. This revealed that proteomic changes were not widespread, but instead were enriched within certain functional areas. For the first time, we found that the immunoproteasome is induced during aggregation, providing a new tunable target for studying α-synuclein aggregation and its connection to toxicity. We also employed nordihydroguaiaretic acid (NDGA) and analogs to study the chemistry and products of phenolic inhibitors of α-synuclein aggregation. We discovered that oxidation-dependent cyclization is required for NDGA analogs to inhibit α-synuclein aggregation and that this inhibition is caused by modification of α-synuclein monomers that retain their conformational dynamics and lipid interactions. Further, we found that these NDGA analog-modified monomers exert a dominant negative effect on aggregation of untreated α-synuclein,

exposing a novel mechanism for inhibiting α-synuclein aggregation. Using transgenic *Caenorhabditis elegans,* we showed that cyclized NDGA can prevent neurodegeneration driven by α-synuclein. These findings outline a novel paradigm for small molecule inhibition of α-synuclein aggregation wherein they act by stabilizing dynamic α-synuclein monomers, preventing aggregation. This in turn prevents aggregation of untreated α-synuclein and reduces neurodegeneration. Together this work underscores the importance of α-synuclein's native structural dynamics and provides several novel tools for future use in untangling the relationship between α-synuclein aggregation and neuron loss in PD and related disorders.

TABLE OF CONTENTS

LIST OF FIGURES

CHAPTER 1: INTRODUCTION

1.1 Neurodegenerative diseases and protein aggregation

The most common neurodegenerative diseases are Alzheimer's disease (AD), Parkinson's disease (PD), Huntington's disease (HD), and Amyotrophic Lateral Sclerosis (ALS). Each disease is characterized by degeneration in distinct regions of the brain, producing neurologically correlated clinical symptoms. However, these diseases share remarkable similarities: the progressive accumulation of proteinaceous inclusions, the progressive loss of neurons, and a lack of curative therapies.

AD is characterized by accumulation of extracellular plaques containing the Aβ peptide fragment (Glenner and Wong, 1984) and intracellular neurofibrillary tangles containing hyper-phosphorylated tau (Lee et al., 1991). PD displays intracellular accumulation of α-synuclein-containing Lewy bodies (Spillantini et al., 1997). In HD, the protein huntingtin forms neuronal intranuclear inclusions (DiFiglia et al., 1997). Most ALS patients develop motor neuron inclusions containing ubiquitin and TDP-43 (Neumann et al., 2006). Increasing evidence suggests a causal link between protein aggregation and neurodegeneration, but the mechanism of neurotoxicity has not been identified. In this study, we examine how the physiological role and pathological aggregation of α-synuclein are influenced by its dynamic structure, and how α-synuclein aggregation changes the brain proteome. We also seek to better understand inhibitors of α-synuclein aggregation in hopes of providing a tool to address this deficit.

1.2 Parkinson's disease

Parkinson's disease (PD) is the most common age-related movement disorder, affecting 1.5-3% of people over the age of 75 (Van Den Eeden et al., 2003; Pringsheim et al., 2014). Incidence is expected to rise as the age of the global population increases (Wirdefeldt et al., 2011). The motor phenotype was first characterized in western medical literature by James Parkinson in *An Essay on the Shaking Palsy* and is defined by resting tremor, rigidity, and

bradykinesia (Parkinson, 1817). More than a century later, a loss of neuromelanin pigmentation of the substantia nigra pars compacta (SNpc) was described in PD (Trétiakoff, 1919). Ultimately, parkinsonian motor symptoms can be attributed to a loss of dopamine in the SNpc (Ehringer and Hornykiewicz, 1960). While dopamine neuron loss in the SNpc is normal in aging, the pattern of degeneration in PD is distinct, involving greater loss in the ventrolateral and caudal portions (Fearnley and Lees, 1991).

Many PD patients develop symptoms beyond the central motor phenotype. Nearly all PD patients experience some form of sleep disturbance and many experience sensory dysfunction, particularly olfactory (Koller, 1984; Lees et al., 1988). Older and more advanced PD patients often experience dementia (Emre, 2003; Levy et al., 2002).

1.2.1 Genetics

Up to 10% of PD cases are familial, driven by both dominant and recessive genetic inheritance (Hernandez et al., 2016). Autosomal dominant forms of familial PD are driven by mutations in many genes (e.g. SNCA, LRRK2, VPS35, UCHL1) (Maraganore et al., 2004; Paisán-Ruíz et al., 2004; Vilariño-Güell et al., 2011; Zimprich et al., 2004, 2011). LRRK2 mutations are the most common cause of familial PD cases, found in ~10% of patients (Paisán-Ruíz et al., 2008). Autosomal recessive forms of PD are caused by mutations in other genes, such as PARK2, PINK1, and PARK7 (encoding Parkin, Pten-induced putative kinase 1, and DJ-1, respectively) (Bonifati et al., 2003; Kitada et al., 1998; Valente et al., 2001, 2004). Many of the autosomal recessive forms of PD caused by mutations in these three genes are juvenile onset.

While most PD cases are sporadic, with age as the greatest risk factor, genetic risk factors can still contribute to disease. Genome-wide association studies have found PD risk alleles across many genes previously identified in familial PD (SNCA, LRRK2, PARK16) as well as others encoding proteins involved in pathology (MAPT, encoding microtubule-associated protein tau) (Satake et al., 2009; Simón-Sánchez et al., 2009). More recent meta-analysis has

further expanded these findings both in terms of primary and conditional risk alleles (Nalls et al., 2014).

1.2.2 Histopathology

The pathological hallmark of PD is the presence of Lewy bodies. These cellular inclusions were first described by Friedrich Lewy in 1912 and later named Lewy bodies, after their discoverer (Lewy, 1912; Trétiakoff, 1919). Lewy bodies are proteinaceous and were found in the 1980's to contain both neurofilamin and ubiquitin (Goldman et al., 1983; Lennox et al., 1989). Later examination revealed that aggregated α-synuclein is also a major component (Spillantini et al., 1997). In addition to Lewy bodies, pathological neuronal projections termed Lewy neurites are present in PD, and also contain aggregated α-synuclein (Braak et al., 1994; Spillantini et al., 1998).

Sporadic PD cases can be scored based on a stereotypical pattern of the spread of Lewy pathology which progresses to new regions while worsening in those previously affected (Braak et al., 2003). As these stages progress, a rough correlation can be drawn between the neurological functions of the regions affected and the additional symptoms experienced by patients as PD worsens. This could be taken as evidence that Lewy bodies cause neurodegeneration in PD. However, Lewy bodies have been found in tissue from normal patients who lacked both PD symptoms and striatal neurodegeneration (Ding et al., 2006; Markesbery and Jicha, 2009). Conversely, parkinsonian neurodegeneration can occur in the absence of Lewy bodies. In fact, the most common LRRK2 mutation causes early onset PD that lacks any Lewy pathology (Gaig et al., 2007).

1.3 α-Synuclein

Synuclein proteins were first discovered in cholinergic vesicles and nuclei purified from the electric organ of *Torpedo* (Maroteaux et al., 1988). Syn1, later renamed α-synuclein, was first

characterized in rat brains probed with sera against electric organ samples (Maroteaux and Scheller, 1991). A component of the α-synuclein sequence was detected as the non-amyloid component of amyloid plaques in Alzheimer's disease, but was not attributed to α-synuclein until its discovery in humans (Jakes et al., 1994; Uéda et al., 1993). Interest in α-synuclein increased greatly following its identification in Lewy bodies and the discovery of an α-synuclein point mutation in a several kindreds with early-onset familial PD (Polymeropoulos et al., 1997; Spillantini et al., 1997).

1.3.1 Sequence and structure

α-Synuclein is 140 amino acids in length with a calculated molecular mass of 14,460.16 kDa. Its primary sequence is divided into three functionally defined domains. The N-terminal domain (composed of amino acids 1-60) is characterized primarily by lysine-rich imperfect repeats projected to form amphipathic α-helices upon lipid interaction (George et al., 1995; Maroteaux et al., 1988). These elements repeat seven times and contain amino acids 10-86. This region has a greater affinity for acidic phospholipid membranes (Davidson et al., 1998). When bound to lipid membranes, this region can form an extended conformation of two α-helices, or double back to form a hairpin, depending on the curvature of the surface (Trexler and Rhoades, 2009; Ulmer and Bax, 2005). All α-synuclein point mutations (A30P, E46K, H50Q, G51D, A53E, A53T) that cause autosomal dominant forms of PD occur in the N-terminal domain (Appel-Cresswell et al., 2013; Krüger et al., 1998; Lesage et al., 2013; Pasanen et al., 2014; Polymeropoulos et al., 1997; Proukakis et al., 2013; Zarranz et al., 2004).

Amino acids 61-95 compose the NAC or non-amyloid component domain which was named based on its fragmentary identification in amyloid plaques (Uéda et al., 1993). This domain contains an amino acid sequence (71-82) that is both necessary and sufficient for α-synuclein aggregation into fibril aggregates with β-sheet secondary structure (Giasson et al., 2001). The role of the NAC domain in α-synuclein aggregation has been reinforced by repeated

studies (Du et al., 2003). Recent crystallography has highlighted two regions, PreNAC (47-56) and NACore (68-78), both of which can independently aggregate into fibrils, but may also directly interface within the hydrophobic core of full length α-synuclein fibrils (Rodriguez et al., 2015).

The C-terminal domain (composed of amino acids 96-140) is hydrophobic and remains unstructured both when α-synuclein is bound to lipids and aggregated into fibrils (Chen et al., 2007; Ulmer and Bax, 2005). Although the C-terminal domain does not assume β-sheet confirmation during aggregation, C-terminal truncation increases the rate of α-synuclein aggregation (Hoyer et al., 2004; Li et al., 2005). This effect may be explained in part by transient, temperature sensitive, long range interactions between the C-terminal domain and the N-terminal domain (Dedmon et al., 2005). These interactions have been implicated in stabilizing monomeric confirmation of α-synuclein, reducing its propensity to aggregate (Bertoncini et al., 2005a).

The C-terminal domain is the site of many post-translation modifications of α-synuclein, particularly phosphorylation. This includes phosphorylation at serine 129, which was first detected in Lewy body extracts and is used as a marker of pathologically aggregated α-synuclein (Fujiwara et al., 2002). A more exhaustive discussion of α-synuclein post-translational modification can be found in Section 2.4.

Many intramolecular interactions occur with the α-synuclein C-terminal domain. Interactors include neurotransmitters, most notably dopamine, and other small molecules, which are addressed at length in Section 1.4.3 (Conway et al., 2001). α-Synuclein has been shown to interact with several metal ions, some of which are implicated in toxicity. Various metals have been shown to alter α-synuclein conformation and aggregation kinetics (Uversky et al., 2001a). The C-terminal domain is the site of interaction with a wide variety of divalent metal ions including Fe(II), Mn(II), Co(II), and Ni(II) (Binolfi et al., 2006). Uniquely, interaction with Cu(II) is mediated not only by the C-terminal, but also by H50 (Rasia et al., 2005). This interaction induces α-synuclein oligomerization (Paik et al., 1999). Subsequent experiments have shown that similar

conformation changes are caused by interaction with Cu(II) and dopamine at the C-terminal (Ha et al., 2014; Tavassoly et al., 2014).

The interaction between iron, α-synuclein, and PD has been an area of particular interest. α-Synuclein has been found to bind with Fe(II) and Fe(III), the latter inducing α-synuclein oligomerization (Binolfi et al., 2006; Hillmer et al., 2010; Tabner et al., 2002; Uversky et al., 2001a). Environmental exposure to iron and other heavy metals (Gorell et al., 1999), as well as their accumulation in the brain (Hirsch et al., 1991), have been linked to PD. The connection between iron and α-synuclein in PD likely lies in oxidative stress and damage. Oxidative stress is linked to both parkinsonianism and α-synuclein modification (Giasson et al., 2000; Javitch et al., 1985; Krueger et al., 1990; Przedborski et al., 2001; Souza et al., 2000a). Interaction between α-synuclein and Fe(II) can be caused by redox cycling (Hillmer et al., 2010). The ratio of Fe(II)/Fe(III) ions shifts toward Fe(III), while levels of glutathione, a key redox regulator, are depleted in PD brains (Riederer et al., 1989). Recent evidence suggests that α-synuclein acts as a ferrireductase (Davies et al., 2011). It is possible that aggregation of α-synuclein may prevent its reductase activity causing a toxic loss of function during the progression of PD. While α-synuclein may act as a ferrireductase, there is abundant evidence suggesting its chief function is to mediate vesicle fusion/fission in the synapse, further discussed in Section 1.3.2.

The native conformation of α-synuclein has been the subject of several studies and intense debate, especially given the potential of native structural dynamics to alter its propensity to aggregate. This topic is addressed at length in Section 2.4. Following the compilation of that summary, further examination of the native state of α-synuclein has continued to reinforce the importance of the N-terminal KTKEGV consensus repeats in α-synuclein multimer formation and appropriate lipid interaction. KTKEGV repeat mutations designed to perturb multimerization also induce inappropriate lipid interaction and may contribute to both increased α-synuclein aggregation and defects in vesicular trafficking (Dettmer et al., 2017). The protein glucocerebrosidase 1 (GBA1) is involved in lysosomal lipid quality control and loss of function

mutations are strong risk factors for PD (Sidransky et al., 2009). Deficiency in GBA1 has been shown to inhibit α-synuclein multimerization and enhance pathology during α-synuclein aggregation (Kim et al., 2018). Taken together, the growing body of work around the native state of α-synuclein suggests that complex structural dynamics influence both its physiological function and its propensity to aggregate. Therefore, any disturbances of native state—through mutations, changes in lipid interaction, alteration of cellular redox state, etc.—may contribute to α-synuclein dysfunction.

1.3.2 Physiological function

When identified, synucleins were found in the nucleus and presynapse of neurons (Maroteaux et al., 1988). Subsequent studies have failed to reproduce detection of synucleins in the nucleus, but have reinforced their presence in presynaptic terminals (George et al., 1995; Iwai et al., 1995; Maroteaux and Scheller, 1991; Murphy et al., 2000; Withers et al., 1997). Synelfin, later to be renamed α-synuclein, expression was found to increase during Zebra finch song learning, suggesting a role in neurotransmission or long-term potentiation (George et al., 1995).

The identification of α-synuclein in the presynapse, and its implication in neuronal plasticity, led to examination of neuronal function in α-synuclein knockout mice. These mice were found to lack a gross developmental or functional phenotype (Abeliovich et al., 2000). Striatal brain slices from knockout mice displayed higher levels of dopamine release in response to repeated stimuli than those from wildtype mice, suggesting α-synuclein may play a role in regulating neurotransmitter release. Subsequent studies on synuclein double (α and β) and triple (α, β, and γ) knockout mice revealed a high degree of redundancy among the family (Burré et al., 2010; Chandra et al., 2004). Only the triple knockout showed a profound phenotype, which included age-related neurological deficits, premature mortality, and motor symptoms consistent with models of dopamine neuron loss (Burré et al., 2010).

α-Synuclein modulates vesicular trafficking during neurotransmission. While α-synuclein knockout leads to increased vesicular reserve pool in presynaptic terminals (Murphy et al., 2000), α-synuclein overexpression leads to deficits in vesicle fusion and increased vesicular pools in some models (Larsen et al., 2006). α-Synuclein has been shown to regulate the function of SNARE proteins involved in vesicular fission and fusion (Chandra et al., 2005). This work has been further supported by direct evidence of physical interaction between α-synuclein and the v-SNARE synaptobrevin 2 (Burré et al., 2010). α-Synuclein's particular role may lie in facilitating vesicle endocytosis following neurotransmitter release into the synapse (Vargas et al., 2014).

1.3.3 Aggregation and pathogenesis

The Lewy bodies found in sporadic and familial forms of PD contain aggregated α-synuclein (Baba et al., 1998; Spillantini et al., 1997). Rather than amorphous aggregates, the α-synuclein within Lewy bodies exists as unbranched fibrils roughly 10 nm in diameter and ranging from 50 to 700 nm in length (Spillantini et al., 1998). Subsequently, these fibrils were shown to contain α-synuclein with β-sheet secondary structure (Serpell et al., 2000). As such, α-synuclein aggregates show strong structural similarity with Aβ amyloids in Alzheimer's disease and many other proteins that form amyloid-like fibril aggregates (Nelson et al., 2005; Sawaya et al., 2007). Partially resolved structure based on a combination of nuclear magnetic resonance and electron cryomicroscopy revealed an in-register, antiparallel conformation composed of five β-sheet regions (Heise et al., 2005; Tuttle et al., 2016; Vilar et al., 2008). The rate limiting step in fibril formation is the generation of a nucleus, while elongation of existing fibrils is much more rapid (Uversky et al., 2001b; Wood et al., 1999).

All α-synuclein mutations associated with familial forms of the disease alter aggregation kinetics, though not all enhance fibril formation (Appel-Cresswell et al., 2013; Giasson et al., 1999; Krüger et al., 1998; Lesage et al., 2013; Li et al., 2001; Narhi et al., 1999; Pasanen et al., 2014; Proukakis et al., 2013; Zarranz et al., 2004). Additionally, duplication and triplication of the

SNCA gene encoding α-synuclein leads to α-synuclein aggregation and early onset, with age of onset accelerated by greater gene dose (Chartier-Harlin et al., 2004; Singleton et al., 2003). This suggests a causal link between α-synuclein aggregation and neurodegeneration.

Numerous animal models expressing excess α-synuclein or mutant α-synuclein prone to aggregation exhibit neurodegeneration, though none perfectly recapitulates PD. Transgenic mice expressing human wildtype and mutant α-synuclein exhibit inclusion formation and neurodegeneration, though not within the SNpc (Emmer et al., 2011; Giasson et al., 2002; Gomez-Isla et al., 2003; Lee et al., 2002; van der Putten et al., 2000). Lentiviral expression of either wildtype or mutant α-synuclein leads to aggregation and progressive loss of dopaminergic neurons in the SNpc (Lo Bianco et al., 2002; Kirik et al., 2002). Invertebrate models have also been employed to examine α-synuclein toxicity. *Caenorhabditis elegans* and *Drosophila melanogaster* models have been used extensively, showing particular utility for modeling dopaminergic neurodegeneration and motor phenotypes, respectively (Cao et al., 2010; Feany and Bender, 2000; Lakso et al., 2003).

A recent model of neurodegeneration driven by α-synuclein aggregation avoids the use of transgenic models. Instead, a small amount of pre-formed α-synuclein fibrils (PFFs) is injected into the brain of wildtype mice. This induces aggregation of endogenous α-synuclein that spreads from the site of injection along the connectome as well as concomitant progressive neurodegeneration and motor phenotype (Luk et al., 2012b, 2012a). These effects are not observed in transgenic mice lacking the *Snca* gene encoding α-synuclein, demonstrating the role of endogenous α-synuclein (Luk et al., 2012a). These results have been reproduced with intramuscular injection in mice, enteric injection in rats and primates, and intracerebral injection in mice, rats, and primates (Manfredsson et al., 2018; Paumier et al., 2015; Sacino et al., 2014a, 2014b; Shimozawa et al., 2017). Likewise, intracerebral and enteric injection of Lewy body extracts results in spreading, progressive aggregation of endogenous α-synuclein and neurodegeneration (Holmqvist et al., 2014; Recasens et al., 2014). These models provide

compelling evidence that otherwise non-toxic α-synuclein leads to neurodegeneration when undergoing aggregation.

Independent lines of evidence suggest that the propagation of α-synuclein aggregation throughout the brain is caused by cell-to-cell transmission of aggregated α-synuclein seeds. This connectome-based propagation is suggested by the progressive staging of Lewy body pathology in sporadic PD (Braak et al., 2003), the accumulation of aggregates in fetal tissue grafted into the striatum of PD patients (Kordower et al., 2008; Li et al., 2008), and the spread of aggregation away from the site of injection in PFF animal models (Holmqvist et al., 2014; Luk et al., 2012a; Manfredsson et al., 2018; Sacino et al., 2014b). How α-synuclein aggregates escape neurons is unknown, but aggregates have been detected in exosomes and may escape during neurotransmission due to the presynaptic localization of α-synuclein (Danzer et al., 2012). Uptake of α-synuclein aggregates from the synapse may be neuronal endocytosis (Lee et al., 2008). While mechanistic questions remain regarding the specifics of cell-to-cell transfer of α-synuclein aggregates (Tyson et al., 2016), evidence still suggests that propagation is caused by aggregated α-synuclein. In a model of propagation between primary neurons, treatment with antibodies against pathologically aggregated α-synuclein reduces the spread of pathology (Tran et al., 2014). Exogenous PFFs are taken up by neurons and localize to the lysosome. Transient inhibition of lysosomal activity results in greater recruitment of endogenous α-synuclein into aggregates (Karpowicz et al., 2017).

The mechanism by which α-synuclein aggregation leads to neurotoxicity remains an important question in the field. Toxicity is most commonly attributed to a toxic gain of function, rather than a toxic loss of α-synuclein function. This is supported by the fact that α-synuclein knockout does not result in profound dysfunction (Abeliovich et al., 2000). Instead, the most commonly accepted theory is that α-synuclein oligomers present during aggregation drive toxicity. Enhanced oligomer—rather than fibril—formation can drive neurotoxicity caused by α-synuclein mutants associated with familial PD (Conway et al., 2000). Toxicity may be a product of α-

synuclein oligomers causing membrane permeabilization, perhaps leading to metabolic stress as neurons attempt to maintain physiological ion gradients. Certain types of α-synuclein oligomers induce calcium influx through neuronal membranes and display pore-like structure when viewed by atomic force microscopy (Danzer et al., 2007). In fact, many proteins that form amyloid-like species aggregates can exist as oligomers that increase membrane ion-conductance (Kayed et al., 2004). This permeabilization may also affect organellar membranes. α-Synuclein oligomers can disturb mitochondrial ion gradients through this mechanism (Luth et al., 2014). Other potential mechanisms of α-synuclein oligomer toxicity have been proposed including perturbations of microtubule-kinesin transport (Prots et al., 2013) and alterations of vesicular trafficking (Choi et al., 2013). Distinct populations of α-Synuclein oligomers are induced by expression of A53T α-synuclein in mice. Oligomers extracted from regions with α-synuclein inclusions cause *in vitro* neurotoxicity and act as seeds, while those from other regions do not. Further, levels of inclusion formation and neurodegeneration within brain regions do not correlate with the relative abundance of oligomers (Tsika et al., 2010). This suggests that α-synuclein oligomers are not a single entity, but that multiple distinct populations may exist with markedly different attributes and implications for disease. Whether or not oligomers are the sole cause of α-synuclein neurotoxicity, it is increasingly clear that the process of α-synuclein aggregation gives rise to species or events that lead to neurodegeneration and eventual neuron death.

1.4 Therapies targeting α-synuclein

The body of evidence implicating α-synuclein in PD and related disorders has caused substantial interest in PD therapies targeting α-synuclein. Many different methods have been employed and an even greater number proposed.

1.4.1 Expression and clearance

Altering the steady-state level of α-synuclein has long been an area of interest. The promise of these attempts is underscored by the gene-dose dependent onset of familial PD caused by SNCA gene duplication and triplication (Chartier-Harlin et al., 2004; Singleton et al., 2003) as well as the resistance of α-synuclein knockout mice to MPTP, a toxin that leads to parkinsonian neurodegeneration (Dauer et al., 2002; Thomas et al., 2011).

In vivo suppression of α-synuclein expression has been achieved in rodents through delivery of AAV encoding shRNA and by both unprotected and exosome-protected siRNA. (Alarcón-Arís et al., 2018; Benskey et al., 2018; Cooper et al., 2014; Lewis et al., 2008; Zharikov et al., 2015a). These approaches reduce inclusion formation (Cooper et al., 2014). Knockdown also preserves neurons and dopamine biosynthesis, as well as providing resistance to rotenone toxicity (Zharikov et al., 2015a). Promisingly, one group found that α-synuclein expression in the SNpc of mice can be reduced by intranasal delivery of siRNA, opening the door to non-surgical intervention in adults (Alarcón-Arís et al., 2018).

Increasing α-synuclein clearance has shown promise in reducing pathology. Overexpression of transcription factor EB, which regulates the autophagy-lysosomal degradation pathway, reduces α-synuclein aggregation and cytosolic levels while protecting against neurodegeneration. Conversely, inhibition of transcription factor EB expression exacerbates aggregation and neuron loss (Decressac et al., 2013). Glucocerebrosidase (GCase), a lysosomal glycoside hydrolase involved in Gaucher disease pathogenesis, has also been implicated in α-synuclein degradation. Loss of GCase leads to α-synuclein accumulation, while α-synuclein inhibits lysosomal function, potentially creating a pathological feedback loop (Mazzulli et al., 2011). AAV gene therapy increasing GCase expression reduces α-synuclein levels, aggregation, and neurodegeneration in mouse models expressing A53T α-synuclein (Morabito et al., 2017; Rocha et al., 2015; Sardi et al., 2013). Small molecule modulators of GCase activity have also been identified and reduce α-synuclein levels in neurons induced from stem cells derived from

Gaucher disease and parkinsonian patients (Aflaki et al., 2016). Several other lines of evidence also suggest that enhancing autophagy could be therapeutic in PD (Moors et al., 2017).

1.4.2 Immunization and immunotherapy

Modulating immune responses to α-synuclein and α-synuclein aggregates has shown promise in ameliorating pathology. Active immunization—induction of a host immune response through antigen challenge—has been explored in mice. In the first such study, mice were actively immunized with exposure to recombinant human α-synuclein. Mice in which immunization produced a high antibody titer showed reduced levels of both total α-synuclein and inclusions, as well as improved synaptic markers, while those with lower titers did not see a benefit (Masliah et al., 2005). Subsequently, active immunization against α-synuclein has been shown to reduce inclusion levels, neurodegeneration, and motor phenotype in mice, while inducing microglial activation (Mandler et al., 2015).

Passive immunization with various antibodies against total α-synuclein and pathological α-synuclein has also been examined. Transgenic mice expressing human wildtype or mutant (A30P) α-synuclein showed reductions in inclusions and neurodegeneration following treatment with antibodies against native and pathological α-synuclein (Bae et al., 2012; Games et al., 2014; Lindström et al., 2014; Masliah et al., 2011). Passive immunization with Syn303, an antibody against pathological α-synuclein aggregates, reduced α-synuclein inclusions, neurodegeneration, and motor phenotype in wildtype mice treated with α-synuclein PFFs (Tran et al., 2014). The considerable promise of immunotherapy against PD has led to several clinical trials, the most advanced of which is recruiting for a phase 2 trial (NCT03100149, estimated primary completion in 2020) examining the efficacy of the 9E4 antibody (Games et al., 2014; Masliah et al., 2011) to delay motor phenotype in PD patients (Schenk et al., 2017).

1.4.3 Altering aggregation

The strong evidence that α-synuclein aggregation plays a causal role in PD has led to extensive examination of many approaches to modulating that aggregation pathway. Dopamine, and related molecules containing catechol moieties (vicinal hydroxyls on an aromatic ring), were the first small molecules shown to modulate α-synuclein aggregation. They inhibit α-synuclein fibril formation, instead leading to formation of soluble oligomers (Conway et al., 2001). This interaction has been shown to require oxidation of dopamine and can be inhibited by electron donors (Mazzulli et al., 2006; Norris et al., 2005). Dopamine interacts with the α-synuclein C-terminal at residues $Y_{125}EMPS_{129}$ (Herrera et al., 2008; Mazzulli et al., 2007; Norris et al., 2005). This interaction is stabilized by electrostatic interaction with E83 and can be impaired by E83A mutation (Herrera et al., 2008).

The identification of dopamine as an aggregation inhibitor is notable given the selective loss of dopaminergic neurons in PD. As discussed in Section 1.3.3, α-synuclein oligomers have been shown to destabilize neuron membranes and may be responsible for α-synuclein neurotoxicity. Recently, elevation of α-synuclein in mice expressing A53T α-synuclein was shown to enhance neurodegeneration and oligomer formation. The same study found, in *C. elegans,* that increased dopamine levels enhanced neurodegeneration in animals expressing A53T α-synuclein, but not in animals expressing A53T α-synuclein mutated in the $Y_{125}EMPS_{129}$ to abolish dopamine interaction (Mor et al., 2017). These findings represent the most direct evidence to date that direct interaction between dopamine and α-synuclein enhances α-synuclein neurotoxicity.

While dopamine may enhance α-synuclein toxicity through modulating aggregation, studies have also identified potentially neuroprotective modulators. Many of these inhibitors interact directly with α-synuclein and induce formation of oligomeric species. Some share little of their structure or putative chemistry with dopamine, such as Anle138b (Deeg et al., 2015; Wagner et al., 2013) and rifampicin (Li et al., 2004). However, the preponderance of oligomer-inducing aggregation inhibitors are polyphenols, flavonoids, catechols, or lignans that bear vicinal hydroxyl

substitutions on aromatic rings (Ehrnhoefer et al., 2008; Di Giovanni et al., 2010; Masuda et al., 2009; Meng et al., 2010). An ongoing clinical trial is evaluating one such polyphenol, epigallocatechin gallate (EGCG), in multiple system atrophy, a synucleinopathy characterized by inclusion formation in glia (Levin et al., 2016; Wakabayashi et al., 1998). Previous studies characterizing the effects EGCG on α-synuclein aggregation and neurodegeneration are further discussed in Section 4.2.

Other attempts to alter α-synuclein aggregation have endeavored to alter protein-protein interactions. Chaperone proteins such as heat shock proteins (Hsp) 70 and 104 have been shown to reduce α-synuclein aggregation and toxicity. Hsp70 and Hsp40 are present in Lewy bodies and expression of Hsp70 reduced α-synuclein aggregation and neurodegeneration in *D. melanogaster* expressing A30P and A53T α-synuclein (Auluck et al., 2002). Hsp70 reduced α-synuclein aggregation in mice expressing A30P α-synuclein (Klucken et al., 2004). Hsp104 was shown to reduce both α-synuclein aggregation and neurodegeneration in rats expressing A30P α-synuclein (Lo Bianco et al., 2008). Hsp expression can be altered pharmacologically and may represent a druggable target in PD (Kilpatrick et al., 2013; McLean et al., 2004).

Altering α-synuclein-lipid interactions has also been explored as a method to alter aggregation, though rationales and results have varied. The small molecules NPT100-18A and squalamine displace α-synuclein from membranes, reducing α-synuclein oligomers and neurodegeneration (Perni et al., 2017; Wrasidlo et al., 2016). Conversely, phtalocyanine tetrasulfonate has been shown to stabilize lipid-bound α-synuclein and reduce aggregate formation (Fonseca-Ornelas et al., 2014). Markedly altering the dynamics of α-synuclein-lipid interactions may result in side-effects given their role in physiological function and neurotransmission (covered in Section 1.3.2).

1.5 Current study

Strong evidence implies that α-synuclein aggregation plays a causal role in PD pathogenesis. As such, altering α-synuclein aggregation in PD represents a promising target for therapeutics. While the interaction between α-synuclein and dopamine has been well characterized, less is known about interactions between α-synuclein and putatively neuroprotective molecules that alter aggregation. Additionally, many of these small molecules may perturb the native interactions between α-synuclein membranes, either directly, or by inducing membrane destabilizing oligomers.

Chapter 2 reviews α-synuclein's remarkable structural flexibility, considering its role in physiological function and pathological aggregation. We propose a model of the α-synuclein aggregation energy landscape based on the existing literature.

Chapter 3 presents our examination of changes in the mouse brain proteome and phosphoproteome during α-synuclein aggregation. We found that the proteome does not undergo widespread changes. Instead, we identified specific changes in dopamine biosynthesis directly related PD pathophysiology and the model's motor phenotype. Importantly, we quantified changes in levels of proteins not previously implicated in α-synuclein aggregation. We thoroughly explored Lmp7, a subunit of the immunoproteasome, demonstrating that it also changes in PD patient brains and that the immunoproteasome can degrade α-synuclein fibrils. The implication of Lmp7 in PD, as well as the larger brain proteome we generated, provide novel insight into the process of neurodegeneration driven by α-synuclein aggregation and open the door to new therapies.

Chapter 4 contains our exploration the mechanism of action by which nordihydroguaiaretic acid (NDGA), and novel related analogs (Asiamah et al., 2015), inhibit α-synuclein aggregation. We also analyzed the α-synuclein species formed, particularly considering structural dynamics. We found that NDGA must undergo oxidation and cyclization before interacting with α-synuclein in a manner distinct from EGCG and dopamine. We also found that

NDGA renders monomeric α-synuclein resistant to aggregation without altering native lipid interactions. Further, we observed that the presence of NDGA-modified monomers prevents aggregation of untreated α-synuclein. Finally, we found that cyclized NDGA, but not NDGA, reduces α-synuclein-driven dopamine neuron degeneration in *Caenorhabditis elegans.*

Chapter 5 includes a summary of our findings, seeks to contextualize them within the field, and explores their implications for future research and therapeutic development.

CHAPTER 2: DYNAMIC STRUCTURAL FLEXIBILITY OF ALPHA-SYNUCLEIN

Danielle E. Mor[1*], Scott E. Ugras[2*], Malcolm J. Daniels[3*] and Harry Ischiropoulos[1,2,3,4#]

Biomedical graduate studies in [1]Neuroscience, [2]Biochemistry and Molecular Biophysics and [2]Pharmacology, Raymond and Ruth Perelman School of Medicine at the University of Pennsylvania, PA 19104. [4]Children's Hospital of Philadelphia Research Institute and Departments of Pediatrics and Systems Pharmacology and Translational Therapeutics, the Raymond and Ruth Perelman School of Medicine at the University of Pennsylvania, PA 19104

*Authors contributed equally.

#to whom correspondence should be addressed. E-mail: ischirop@mail.med.upenn.edu

(Published in Neurobiology of Disease, April 2016. Volume 88, Page 66-74)

2.1 Abstract

α-Synuclein is a conserved, abundantly expressed protein that is partially localized in pre-synaptic terminals in the central nervous system. The precise biological function(s) and structure of α-synuclein are under investigation. Recently, the native conformation and the presence of naturally occurring multimeric assemblies have come under debate. These are important deliberations because α-synuclein assembles into highly organized amyloid-like fibrils and non-amyloid amorphous aggregates that constitute the neuronal inclusions in Parkinson's disease and related disorders. Therefore understanding the nature of the native and pathological conformations is pivotal from the standpoint of therapeutic interventions that could maintain α-synuclein in its physiological state. In this review, we will discuss the existing evidence that define the physiological states of α-synuclein and highlight how the inherent structural flexibility of this protein may be important in health and disease.

2.2 Introduction

α-Synuclein is a soluble protein that is highly conserved in vertebrates and abundantly expressed in nervous tissue (Jakes et al., 1994). It was first discovered in 1988 in association with purified synaptic vesicles from the *Torpedo* electric ray (Maroteaux et al., 1988). Soon afterward α-synuclein was found to be widely distributed across the mammalian brain and localized to presynaptic nerve terminals, suggesting functions related to neurotransmission (Iwai et al., 1995). Independent of these reports, α-synuclein was identified as the precursor to a hydrophobic peptide found in Alzheimer's disease senile plaques, termed the non-Aβ component of Alzheimer's disease amyloid (NAC) (Uéda et al., 1993). The α-synuclein gene was also dynamically regulated during song learning in zebra finch, supporting a role in synaptic plasticity (George et al., 1995).

The discovery of a mutation in the α-synuclein gene that was associated with autosomal dominant inheritance of Parkinson's disease (PD) provided the impetus for a major shift in α-synuclein research (Polymeropoulos et al., 1997). PD is a neurodegenerative disorder primarily characterized by the loss of dopamine-producing neurons in the *substantia nigra pars compacta* resulting in motor impairment. Since the original publication of the A53T mutation, several mutations, as well as multiplications of the α-synuclein gene have been linked to PD (Chartier-Harlin et al., 2004; Ferese et al., 2015; Krüger et al., 1998; Lesage et al., 2013; Pasanen et al., 2014; Proukakis et al., 2013; Singleton et al., 2003; Zarranz et al., 2004). Furthermore, several antibodies against α-synuclein robustly detect the well-known pathoanatomical features of PD, Lewy bodies and Lewy neurites, in postmortem brain tissue from patients with sporadic PD as well as other related neurodegenerative disorders (Baba et al., 1998; Spillantini et al., 1997; Takeda et al., 1998). The finding that wildtype α-synuclein was detected in Lewy bodies and Lewy neurites prompted the publication of numerous studies that investigated the biochemistry and biology of α-synuclein. Despite the rather impressive body of work several fundamental

questions remain: What is the physiological function of α-synuclein? What is the structure of native α-synuclein? What factors contribute to the induction of aggregation-competent conformational states of α-synuclein? In this review, we will briefly review the evidence for the different biological functions and discuss ongoing efforts to precisely define physiological structures of α-synuclein.

2.3 The physiological function(s) of α-synuclein

The initial studies indicated that α-synuclein is not required for neuronal development or synapse formation, but instead may modulate synaptic activity. In rodents, α-synuclein is detected close to the time of birth and continues to increase until one month of age, when it reaches a steady-state level that is maintained throughout adulthood (Shibayama-Imazu et al., 1993). Similarly, in cultured rat neurons the development of synapses precedes α-synuclein expression and translocation to axonal terminals (Murphy et al., 2000; Withers et al., 1997). The hypothesis that α-synuclein regulates synaptic activity was directly tested in mice lacking α-synuclein. α-Synuclein null mice develop normal brain architecture and synaptic contacts, and do not exhibit gross behavioral phenotypes (Abeliovich et al., 2000). However, subtle abnormalities in activity-dependent neurotransmitter release have been observed. Upon repeated stimulation, dopaminergic synapses from α-synuclein null mice sustain highly elevated dopamine release (Abeliovich et al., 2000; Yavich, 2004). Functional redundancy among α-synuclein and the other synuclein family members, β- and γ-synuclein, may account for the mild phenotypes observed in the single knockout. In α/β-synuclein double knockout mice, synaptic plasticity appears unaltered relative to α-synuclein single knockouts, although dopamine levels in the striatum are reduced (Chandra et al., 2004). The importance of synucleins is particularly highlighted by α/β/γ-synuclein triple knockouts, which have decreased life span and late-onset synaptic dysfunction compared with wildtype mice (Burré et al., 2010; Greten-Harrison et al., 2010). Triple knockouts in another study had motor deficits and decreased striatal dopamine, along with abnormal dopamine

neurotransmission (Anwar et al., 2011). Collectively, these reports emphasize the important role of the synucleins in long-term synaptic maintenance and plasticity.

Synaptic vesicle trafficking. Examination of the role of α-synuclein in the synaptic vesicle cycle has yielded conflicting results. Depletion of α-synuclein from rodent hippocampal neurons both *in vivo* and *in vitro* induces a significant loss of undocked synaptic vesicles, suggesting that α-synuclein acts to replenish or maintain the resting and/or reserve vesicle pools (Cabin et al., 2002; Murphy et al., 2000). In contrast, another study found that increasing α-synuclein in rodent hippocampal neurons reduces the recycling pool of vesicles (Nemani et al., 2010). The effect of α-synuclein on vesicles docked at the plasma membrane prior to exocytosis is similarly unclear. Knockout or knockdown of α-synuclein in rodent hippocampal neurons results in either a decrease or no change in the number of docked vesicles (Cabin et al., 2002; Murphy et al., 2000). Conversely α-synuclein expression in PC12 cells causes an accumulation of vesicles at the plasma membrane and impairment of exocytosis (Larsen et al., 2006). However, in mice modestly overexpressing α-synuclein (levels are not associated with neurotoxicity), hippocampal synapses display a redistribution of vesicles away from the active zone. The density of vesicles in synaptic boutons is also reduced, consistent with α-synuclein-mediated inhibition of vesicle clustering. This is supported by α-synuclein-induced defects in vesicle re-clustering following endocytosis in rat hippocampal neurons (Nemani et al., 2010). Still, opposing results have been obtained from yeast, in which α-synuclein expression results in massive accumulations of vesicles that co-localize with Rab GTPases (Gitler et al., 2008; Soper et al., 2008). Likewise, α-synuclein has been shown to restrict vesicle diffusion away from synapses in mouse hippocampal neurons (Wang et al., 2014). Several lines of evidence, therefore, support the participation of α-synuclein in synaptic vesicle trafficking, though the specific steps for which it may be most important, i.e. vesicle docking, recycling and/or re-clustering, remain unclear.

Chaperone-like activity and neurotransmitter release. α-Synuclein and the other synuclein family members may act as molecular chaperones, facilitating neurotransmitter release.

Cysteine-string protein α (CSPα) is a chaperone that is essential for synaptic health; its deletion in mice leads to a decrease in SNARE protein complexes, nerve terminal degeneration, motor impairment and death. When expressed in CSPα-deficient mice, α-synuclein is able to rescue this degenerative phenotype and restore levels of SNARE complexes in synaptic terminals. Moreover, mice lacking both α-synuclein and CSPα exhibit an exacerbated phenotypic decline (Chandra et al., 2005). These findings suggest that α-synuclein is able to complement the activity of CSPα in promoting synapse integrity. Direct evidence for the interaction of α-synuclein with SNARE complexes was documented by co-immunoprecipitation of α-synuclein with SNARE proteins and specific binding to the vesicle-associated SNARE protein synaptobrevin-2. In mammalian cells and purified *in vitro* systems, α-synuclein dose-dependently facilitates SNARE complex assembly (Burré et al., 2010). Additional support for chaperone-like activity includes sequence homology between α-synuclein and 14-3-3 protein chaperones as well as the association of α-synuclein with 14-3-3 and its binding partners in rat brain (Ostrerova et al., 1999). α-, β-, and γ-synucleins are also able to prevent the aggregation of denatured proteins *in vitro* (Souza et al., 2000b), further supporting a conserved chaperone-like function of synucleins and the existence of several protein-protein interactions that facilitate synaptic function.

Putative role in neurotransmitter synthesis and reuptake. Published evidence indicates that α-synuclein-mediated protein-protein interactions may modulate dopamine synthesis and recycling. α-Synuclein may inhibit the activity of tyrosine hydroxylase (TH), the rate-limiting enzyme in dopamine synthesis. α-Synuclein and TH co-immunoprecipitate from rat striatal tissue and MN9D dopaminergic cells and α-synuclein was shown to inhibit TH activity in MN9D and PC12 cells, potentially through PP2A phosphatase-mediated reduction of serine 40 phosphorylation of TH (Peng, 2005; Perez et al., 2002). α-Synuclein may also interact with and inhibit the activity of aromatic amino acid decarboxylase, which catalyzes the conversion of L-DOPA to dopamine (Tehranian et al., 2006). Thus, α-synuclein may serve as a negative regulator of dopamine synthesis, though further validation of these findings is necessary. Several

reports have also implicated α-synuclein in the regulation of the dopamine transporter (DAT), though the evidence is conflicting with regards to the functional consequences. Direct binding of α-synuclein to DAT has been demonstrated in multiple studies. However, α-synuclein does not appear to alter DAT function, but rather in various cellular contexts can promote or inhibit DAT trafficking to the plasma membrane (Oaks and Sidhu, 2011). Elucidating the relationship between α-synuclein and DAT requires further investigation.

2.4 α-Synuclein structural flexibility

Primary sequence. The primary sequence of α-synuclein consists of 140 amino acids with a predicted molecular mass of 14,460.16 Da and an isoelectric point of 4.67 (Figure 2.1). The sequence of α-synuclein is composed of three functionally defined domains. The N-terminal region (amino acids 1-60) is characterized by the presence of unique and highly conserved sequence of imperfect tandem repeats with a central consensus motif of **K**(A)-**T**(A,V)-**K**(V)-**E**(Q,T)-**G**(Q)-**V**(A). These motifs spanning residues 10-86 are projected to form two amphipathic α-helices and are characteristic of several proteins such as apolipoproteins that bind reversibly to membranes (George et al., 1995; Maroteaux et al., 1988). Indeed the structure of membrane bound α-synuclein contains two α-helices (amino acids 3-37 and 45-92) in a roughly antiparallel arrangement with a short linking region (Ulmer and Bax, 2005). These helices are stabilized by interaction with a variety of phospholipid bilayers, though α-synuclein interacts preferentially with membranes of high curvature and an abundance of acidic phospholipids, properties consistent with those of synaptic vesicles (Davidson et al., 1998; Zhu et al., 2003b). Upon interaction with membranes of low curvature α-synuclein adopts a distinct secondary structure characterized by a single extended helix that includes both previously described helical domains and the linker region (amino acids 38-44) (Ferreon et al., 2009; Georgieva et al., 2010; Trexler and Rhoades, 2009). All known mutations associated with familial PD (A30P, E46K, H50Q, G51D, A53E, and A53T) are found in the N-terminal domain (Krüger et al., 2008; Lesage et al., 2013; Pasanen et

al., 2014; Polymeropoulos et al., 1997; Proukakis et al., 2013; Zarranz et al., 2004). These mutations, with the exception of G51D, A53E, and A30P, increase the propensity of α-synuclein to form insoluble aggregates and produce morphologically distinct aggregate species (Ghosh et al., 2014; Giasson et al., 1999; Greenbaum et al., 2005; Lesage et al., 2013; Mahul-Mellier et al., 2015; Narhi et al., 1999). Though the precise mechanism by which these mutations promote aggregation has not been conclusively shown, evidence implicate an accelerated formation of oligomers (Conway et al., 2000) likely due to the destabilization of the native N-terminal conformation (Bertoncini et al., 2005b; Burré et al., 2015; Coskuner and Wise-Scira, 2013; Dettmer et al., 2015a).

Amino acids 61-95 compose the hydrophobic NAC domain (Uéda et al., 1993). This region contains a sequence of amino acids (71-82) necessary and sufficient for α-synuclein self-assembly into amyloid fibrils (Giasson et al., 2001). Recently the crystal structures of residues 68-78 (termed NACore), and residues 47-56 (PreNAC) were resolved by the use of micro-electron diffraction, revealing that strands in this region stack in-register into β-sheets that are typical of amyloid assemblies (Rodriguez et al., 2015).

The C-terminal domain (96-140) is rich in negatively charged amino acids (contains 10 glutamate and 5 aspartate residues) and was originally proposed to be essential for maintaining the solubility of the protein. The presence of 5 proline residues, which are known to induce turns

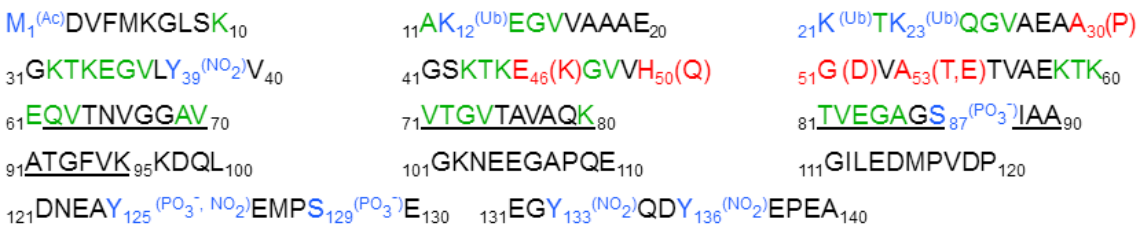

Figure 2.1: Primary sequence of human α-synuclein. Green color indicates the imperfect tandem repeats. Known mutations are indicated in red. The hydrophobic NAC domain is underlined. The major sites of posttranslational modifications identified in vivo are highlighted in blue (Ac, acetylation; Ub, ubiquitination; NO_2, nitration; and PO_3^- phosphorylation).

and disrupt secondary protein structure, suggested that this region is devoid of secondary structure (George et al., 1995; Ulmer and Bax, 2005). However, the C-terminus was shown to form transient, long-range interactions with the N-terminus resulting in the formation of multiple compact monomeric structures (Bertoncini et al., 2005b; Dedmon et al., 2005). These compacted structures of α-synuclein are temperature sensitive and are resistant to aggregation. The data also indicated that at elevated temperatures the C-terminus assumes an extended conformation that liberates N-terminal associations and enables aggregation (Bertoncini et al., 2005b; Dedmon et al., 2005). Moreover, C-terminally truncated forms of α-synuclein aggregate faster than full length protein (Hoyer et al., 2004; Li et al., 2005). Truncated α-synuclein has been detected in the brains of both control (non-disease) and PD patients. Cleavage of full-length protein at residues D115, D119, N122, D125 and Y133 was documented in α-synuclein extracted from LBs (Anderson et al., 2006).

The C-terminus appears to be important for the interaction of α-synuclein with other proteins and for the interaction with small molecules (Burré et al., 2010, 2012; Conway et al., 2001; Mazzulli et al., 2006; Souza et al., 2000a; Woods et al., 2007). Additionally, it contains the major sites of metal binding and post-translational modifications. Binding of iron, copper, and other metals has been shown to influence α-synuclein function and aggregation (Uversky et al., 2001a). Addition of Fe(III), but not Fe(II) to preformed oligomers of α-synuclein accelerates aggregation, raising the question of metal binding at different points during the aggregation process (Kostka et al., 2008). Cu(II) is unique among metals at accelerating aggregation of α-synuclein at physiologically relevant concentrations. The sole histidine residue H50 in α-synuclein was found to be critical for Cu(II) binding (Rasia et al., 2005) whereas other divalent metal ions, including Mn(II), Co(II), Ni(II) and Fe(II), preferentially bind to the C-terminus of α-synuclein at residues D121, N122, and E123 (Binolfi et al., 2006).

Post-translational modifications. α-Synuclein undergoes a number of post-translational modifications, including N-terminal acetylation, serine and tyrosine phosphorylation, lysine

ubiquitination and tyrosine nitration (Barrett and Greenamyre, 2015; Oueslati et al., 2010). α-Synuclein purified under mild conditions is acetylated in the N-terminus. The N-terminal acetylation may account for the formation of an oligomeric form of the protein with partial α-helical structure (Trexler and Rhoades, 2012). However, semisynthetic production of N-terminally acetylated α-synuclein demonstrated that modified and unmodified versions of the protein share similar secondary structure, aggregation propensities, and membrane binding (Fauvet et al., 2012). NMR studies indicated that the first 12 residues undergo a chemical shift due to N-terminal acetylation. This modification also appears to stabilize the helicity of the N-terminus within the context of the full-length protein, and increases the affinity of α-synuclein for lipids (Dikiy and Eliezer, 2014).

Mass spectrometry-based methodologies revealed that α-synuclein extracted from human Lewy bodies was phosphorylated at S129 (Fujiwara et al., 2002). An antibody raised against phosphorylated S129 was then used to show that α-synuclein was phosphorylated at this site only in subjects with disease and that S129 phosphorylated α-synuclein was present only in the Triton-X- and Sarkosyl-insoluble, urea soluble fraction. These data indicated that some form(s) of aggregated α-synuclein and not the soluble protein is targeted for phosphorylation at S129. Indeed *in vitro* data showed that purified fibrils of α-synuclein are substrates for casein kinase 1 or 2 (Waxman and Giasson, 2010). Other data indicated that polo-like kinase (PLK) 2-mediated phosphorylation of S129 increased autophagy-mediated degradation of α-synuclein, suggesting that phosphorylation may be a neuroprotective mechanism to accelerate clearance of aggregated protein (Oueslati et al., 2013). In addition to the monomeric α-synuclein, S129 phosphorylated bands with apparent molecular weight of 22 kDa and 29 kDa were observed in the detergent insoluble extract (Hasegawa et al., 2002). These bands were also immunoreactive with anti-ubiquitin antibodies suggesting that S129 phosphorylated α-synuclein is also targeted for mono- and di-ubiquitination. It has long been established that the core of Lewy bodies stains positive for both α-synuclein and ubiquitin whereas the surrounding halo is immunoreactive for α-

synuclein (Hasegawa et al., 2002). Of the 15 lysine residues in α-synuclein, the major sites of LB-derived α-synuclein undergoing ubiquitination were residues K12, K21, and K23 (Anderson et al., 2006; Hasegawa et al., 2002; Sampathu et al., 2003).

A number of spectroscopic methodologies (CD and NMR) were employed to explore the effect of S129 phosphorylation on the structure of α-synuclein. CD data revealed that phosphorylation of S129 did not affect secondary structure, such that both non-phosphorylated and phosphorylated S129 exhibited random coil structure (Paleologou et al., 2008). NMR data revealed a number of chemical shifts that occur due to phosphorylation. While the residues surrounding S129 exhibited the greatest perturbation, residues 1-90 also exhibited detectable chemical shifts (Paleologou et al., 2008) This likely reflects the previously documented long-range interactions of the C- and N-termini. The potential effects of phosphorylation of S129 on the structure of the protein were not faithfully reproduced by mutation of S129 to either E or D, two common phosphomimics used to study the structural consequences of phosphorylation. For example, phosphorylation at S129 increased the hydrodynamic radius of the protein, whereas S129 E/D mutants did not (Paleologou et al., 2008).

Subsequent studies found additional sites of phosphorylation. Elevated levels of phosphorylated α-synuclein at residue S87 were detected in human brains with Alzheimer's disease, Lewy Body disorders, and multiple system atrophy (Paleologou et al., 2010). S87 phosphorylation alters the biophysical properties of α-synuclein, including inhibition of fibril formation and reduction in membrane binding (Paleologou et al., 2010). Additionally, phosphorylated α-synuclein at residue Y125 was detected in Drosophila expressing human wildtype α-synuclein as well as in human brains, though levels were decreased in disease compared with aged-matched healthy controls (Chen et al., 2009).

The proximity of the α-synuclein phosphorylation sites to the metal binding sites raised the question of how phosphorylation may affect metal ion interactions. This was investigated by the use of C-terminal peptides containing residues 119-132 that were either unmodified,

phosphorylated at Y125 or at S129 (Liu and Franz, 2005). By exploiting the luminescence properties of Tb^{3+}, it was found that phosphorylated Y125 showed enhanced Tb^{3+} binding relative to wildtype or phosphorylated S129. Additionally, phosphorylated Y125 preferentially bound to trivalent rather than divalent metal ions. To investigate this further, longer C-terminal fragments comprised of residues 107-140 that were either unmodified of monophosphorylated at Y125 or S129 were tested for their affinity to various metal ions. By using a fluorescence quenching assay, the dissociation constants of the metal ion complexes and the α-synuclein peptides were determined. These data indicate that either phosphorylation at Y125 or S129 increases the binding affinity for Cu (II) and Fe(II), but not Fe(III). Furthermore, phosphorylated Y125 has a greater affinity for Pb(II) than wildtype, but phosphorylated S129 has an even greater affinity than phosphorylated Y125. Additionally, tandem MS indicated that phosphorylation causes the metal ion binding sites to shift towards the C-terminal end of α-synuclein (Lu et al., 2011).

α-Synuclein within Lewy bodies is nitrated on all four tyrosine residues (Giasson et al., 2000). Chemical nitration of α-synuclein results in the formation of both tyrosine nitrated monomers and nitrated dimers (Souza et al. 2000b). Immunoelectron microscopy confirmed that nitrated monomers and dimers are incorporated into amyloid fibrils. Purified nitrated α-synuclein monomer by itself was unable to form fibrils, whereas the nitrated dimer accelerated aggregation of unmodified α-synuclein (Hodara et al., 2004). Additionally, nitration at residue Y39 in the N-terminus decreased binding to synthetic vesicles and prevented the protein from adopting α-helical conformation (Hodara et al., 2004). These observations were recently confirmed and elegantly expanded by the generation of site-specifically nitrated α-synuclein using protein semisynthetic chemistries (Burai et al. 2015). Using the synthetic nitrated α-synuclein the data showed that nitration did not interfere with phosphorylation of S129 by PLK3 and reaffirmed that intermolecular interactions between the N- and C-terminal regions of α-synuclein are critical in directing nitration-induced oligomerization of α-synuclein (Burai et al. 2015).

Native conformation(s) of α-synuclein. Figure 2.2 depicts the rapid growth in the number of publications identified in PubMed using the term synuclein and highlights key studies that explored the native structure and conformation of the protein. Early biochemical studies of α-synuclein isolated from bacterial expression systems or α-synuclein expressed in rodent tissues indicated that it is monomeric with limited secondary structure. Electrophoretic separation of α-synuclein purified without heating on 6, 10, or 14% acrylamide gels estimated an apparent molecular weight of 20±3 kDa. However, the values of sedimentation coefficient ($S_{20,w}$ = 1.7S), stokes radius (34 Å), analysis on native gels and derivation of the frictional coefficient (f/f_o=2.09) indicated an apparent molecular weight in the range 57-58 kDa (Weinreb et al., 1996). To reconcile this apparently anomalous behavior it was proposed that monomeric α-synuclein achieves minimal structure in simple solutions and this rather extended unstructured conformation resembles a globular protein with a larger apparent molecular weight. This assumption was further corroborated by examination of purified monomeric α-synuclein by CD, FTIR and small angle X-ray scattering, which failed to identify significant secondary structural features. Furthermore, minimal shifts in the spectroscopic features of α-synuclein were observed when the protein was placed in solutions that would increase hydrophobicity and neutralize negative charges indicating that the protein is natively unstructured, joining a growing group of

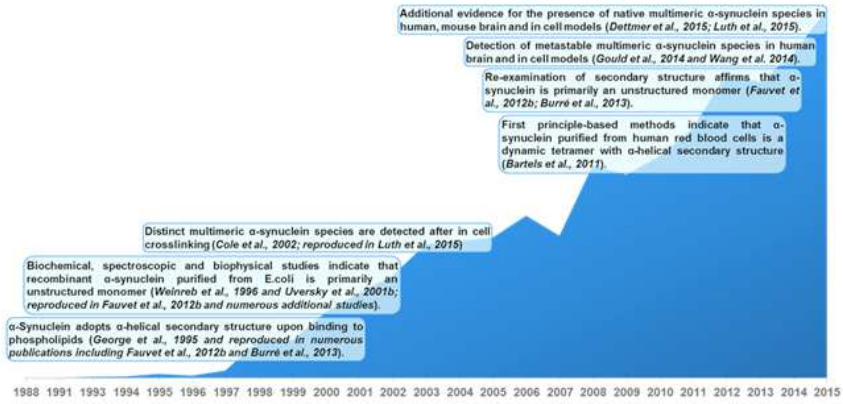

Figure 2.2. **The graph depicts the number of publications** retrieved from PubMed using the search term “alpha synuclein” from a single publication in 1998 to 862 in 2015. Significant milestones that examined the native structure and conformations of α-synuclein are displayed.

proteins sharing similar biochemical and biophysical characteristics (Uversky et al., 2001b). NMR and CD data, however, indicated that α-synuclein assumes increasingly folded secondary structure when exposed to conditions that promote aggregation (low pH and high temperature) or upon interaction with phospholipids. Collectively these data indicated that native α-synuclein is primarily an unstructured monomer, which can assume different compact conformations that resist aggregation, adopts α-helical conformation upon binding to lipids and undergoes conformational changes prior to oligomerization and formation of amyloid fibrils (Uversky et al., 2001b). However, the methodologies employed to quantify the molecular weight of α-synuclein in these elegant studies were not based on first principles and therefore a lingering uncertainty remains regarding the native size of the protein. Moreover, crosslinking experiments in both intact cells expressing α-synuclein and lipid-free lysates revealed the stabilization of high molecular weight α-synuclein multimers (consistent with dimers, trimers, and larger multimers). These multimers were not reduced by dilution of lysates before crosslinking, nor by reducing the concentration of crosslinker from 1 mM to 8 μM, suggesting that they represented endogenous protein complexes (Cole et al., 2002).

Examination of the α-synuclein native state was reignited in 2011 with the publication of results indicating that α-synuclein exists natively as a tetramer, rather than a monomer. Methodologies that are based on first principles were employed to examine the molecular weight and size of α-synuclein extracted under non-denaturing conditions from human red blood cells. Analytical ultracentrifugation produced a sedimentation equilibrium value of 4.78 S, indicating a molecular weight of 57.8 kDa. Analysis of particle geometry by scanning transmission electron microscopy revealed the presence of roughly spherical molecules with a diameter of approximately 3.0-3.5 nm. Automated sampling of 1000 α-synuclein particles showed a distribution of molecular weights between 10 and 175 kDa with a peak distribution at 55 kDa. These findings constitute the most direct measurements of the native molecular weight of α-

synuclein. The tetrameric species were shown to have α-helical conformation and were resistant to aggregation (Bartels et al., 2011).

Complimentary observations were made using recombinant GST-tagged α-synuclein purified from bacterial expression systems under non-denaturing conditions. Single-particle electron microscopy of purified α-synuclein revealed complexes of sizes and internal geometries consistent with trimers and dimers, which were corroborated by measurements of the hydrodynamic radii and elution on native state PAGE. As observed previously, these species were more resistant to aggregation than denatured monomer. CD also showed that several α-synuclein mutations associated with early onset PD (A30P, E46K, A53T) exist in less ordered conformations than wildtype α-synuclein. These mutants were also more prone to aggregation (Wang et al., 2011). However, using the same α-synuclein construct that contains a 10-residue N-terminal extension, which forms multimers when isolated from E. coli, NMR studies indicated that only a small fraction of α-synuclein assembles into α-helical trimers and tetramers and the majority remains as a disordered monomer (Gurry et al., 2013). These data indicated that several potential conformers of α-synuclein may exist in equilibrium. The observation that α-helical trimers and tetramers constitute only a small fraction of the total α-synuclein may explain other studies in which in-cell NMR was used to probe for the structure of α-synuclein and reported primarily the presence of unstructured monomer. NMR data of α-synuclein in intact cells failed to detect stable or highly populated α-synuclein multimers and confirmed the intrinsically disordered nature of the protein in *E. coli* regardless of its purification method (Binolfi et al., 2012). Collectively these studies generated an apparent controversy and stimulated several additional studies that explored the native size and structure of α-synuclein.

A re-examination of the native state of α-synuclein reasserted that the behavior of α-synuclein from various sources was consistent with a disordered monomer. This behavior was observed with protein extracted and isolated under both denaturing and non-denaturing conditions. CD spectra previously attributed to tetrameric assemblies were not reproduced using

isolated monomer, but were replicated with the addition of small unilamellar vesicles. Natively isolated α-synuclein before or after boiling that disrupts secondary structure migrated as high molecular weight α-synuclein bands in native PAGE, which was attributed to the rather expanded size of the unstructured monomer in solution. These findings reaffirmed that the majority of native α-synuclein is a monomer with minimal secondary structure (Fauvet et al., 2012). Further support was provided by similar explorations in the mouse brain, which indicated that the predominant native form of α-synuclein is an unstructured monomer. α-Synuclein exhibited random coil structure in solution, readily aggregated over time, and adopted α-helical structure only upon membrane binding (Burré et al., 2013).

α-Synuclein multimers were detected in postmortem non-diseased human brain using mild protein extraction methods, but no further purification. These α-synuclein multimers had Stokes radii ranging from 33.2-37.5 Å, sedimentation coefficients ranging from 1.4S to 3.8S and apparent molecular weights ranging from 53-70 kDa in native gradient gels. The multimers were detected by anti-α-synuclein antibodies that recognize different epitopes and the multimer identity was confirmed by mass spectrometry. Consistent with previous observations, melting point thermostability analysis showed progressive loss of the α-synuclein multimers and heating of the brain extracts above 55 ^{o}C collapsed the higher molecular weight α-synuclein conformers into the 53 kDa species, which corresponds to the unstructured monomer. These data indicated the presence of α-synuclein conformers, defined as conformationally diverse α-synuclein multimers, in the human brain. Therefore it appears that both monomer and metastable multimers coexist and that interactions with lipids, other proteins, or small molecules may transiently stabilize these species (Gould et al., 2014). This was further supported by controlled bimolecular fluorescence complementation methodologies in different cell types that found α-synuclein metastable conformers assembled in synapses. It was suggested that the function of these multimeric α-synuclein conformers is to restrict recycling of synaptic vesicles and thus reduce neurotransmitter release (Wang et al., 2014).

Additional support for native multimeric species comes from recent studies in which serial purification of α-synuclein from non-pathological human cortical tissue was performed. Removal of lysate components other than protein followed by sequential removal of proteins though size exclusion, anion chromatography, and thiopropyl sepharose 6b separation, resulted in the isolation of >90% pure α-synuclein. Each step of serial purification resulted in a progressive loss of α-synuclein immunoreactive high molecular weight bands observed after disuccinimidyl glutarate crosslinking and SDS-PAGE separation. Analysis of α-synuclein secondary structure by CD found that the sequentially purified protein had greater α-helical content than the recombinant α-synuclein. However, a high degree of variability in secondary structure was observed between purified samples raising questions about the stability of these helical conformations (Luth et al., 2015). Furthermore, crosslinking experiments conducted in brain tissue from mice expressing wildtype or A53T human α-synuclein in the absence of mouse α-synuclein showed that the A53T mutation reduced the presence of soluble multimeric α-synuclein (Dettmer et al., 2015a).

2.5 Concluding remarks and perspectives

Collectively the studies on the native structure indicate a remarkable conformational plasticity and structural flexibility of α-synuclein. The ability of the protein to adopt N-terminal α-helical conformation through its association with lipids has been well documented. The association with lipids has been shown to prevent fibril formation (Martinez et al., 2007; Zhu and Fink, 2003) and may also stabilize physiological multimeric species that together with the monomer regulate SNARE complex assembly and recycling of synaptic vesicles (Burré et al., 2014; Wang et al., 2014). However, other groups have demonstrated a role for phospholipid membranes in promoting pathological α-synuclein aggregation, potentially by acting as a scaffold for amyloid nucleation. This event may preferentially occur at low lipid to protein ratios, when monomeric α-synuclein is free in solution and can participate in nucleation (Galvagnion et al., 2015; Ysselstein et al., 2015).

In figure 2.3 we propose a model which incorporates and summarizes the existing knowledge regarding α-synuclein biology and structure. The steady state levels of α-synuclein are carefully regulated by protein synthesis and removal by several pathways such as the ubiquitin-proteasome pathways and autophagy (Webb et al., 2003). Controlling the steady state levels of this protein by regulating synthesis and degradation may be the first critical defense in preventing aggregation. Conformational change to α-helical rich structures, and stabilization of metastable multimers is achieved by specific interactions with vesicular phospholipids and proteins. The sequestration of α-synuclein in association with membrane vesicles and with other proteins may be of critical importance for preventing aggregation. Therefore these dynamic equilibria maintain functionality and promote assemblies that are resistant to aggregation. Catastrophic events that may include inappropriate post-translational modifications will disassemble the multimers as well as transform aggregation-incompetent monomers to

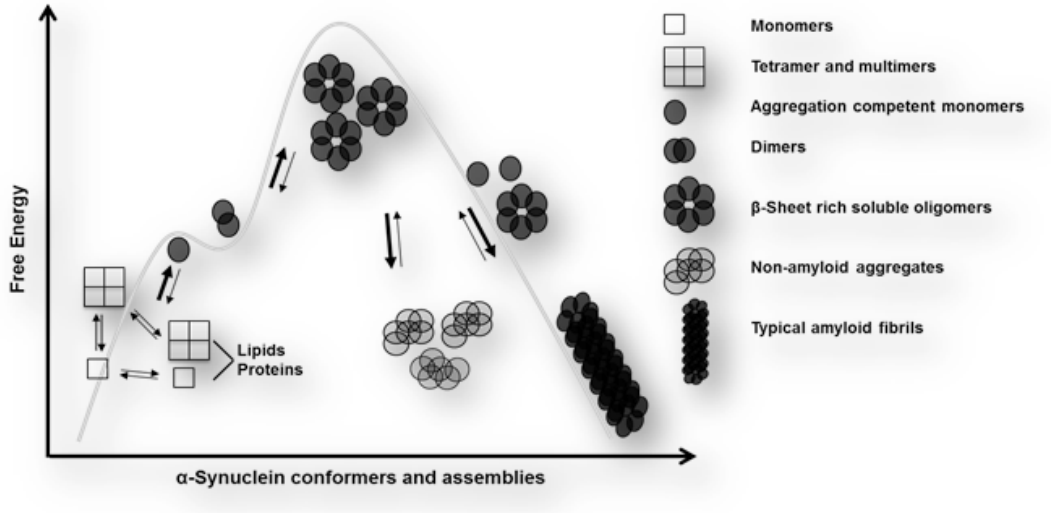

Figure 2.3. **Free energy landscape of possible α-synuclein conformers and multimeric assemblies.** The conversion of native α-synuclein to aggregation-competent monomers may depend on dissociation from stabilizing interactions with lipids and/or proteins as well as dissociation of the metastable tetrameric species. α-Synuclein aggregation-competent monomers can then assemble into dimers and larger oligomeric conformers. The generation of α-synuclein oligomers can rapidly lead to formation of stable amyloid fibrils, or 'off-pathway' amorphous aggregates, both of which have been observed in postmortem brain tissue from patients with PD and related disorders.

aggregation-competent species. The first step in the pathway to amyloid fibril formation is the generation of a dimer that is either held together by hydrophobic interactions induced by increased conformational transition to β-sheet structure or upon covalent cross-linking. Following this nucleation event (Wood et al., 1999) the hydrophobic patch of amino acids between residues 71-82 appears to be primarily responsible for allowing additional α-synuclein monomers to assemble to form oligomeric structures. This transition is the committed rate limiting step for aggregation and must overcome a relatively large thermodynamic requirement that permits the conversion from an unstructured coil to organized β-sheet conformation. Oligomers are soluble in aqueous buffers and can appear spherical or ring-like by atomic force and electron microscopy (Conway et al., 2000; Lashuel et al., 2002). Soluble, high molecular weight oligomers have been extracted from human brain tissue and their levels appear to be increased in PD brain (Sharon et al., 2003) as well as mouse models of α-synuclein aggregation (Tsika et al., 2010). As oligomers grow, they reach an undefined critical length and are able to assume additional quaternary structure. At this stage, these structures may continue to grow in linear β-sheets, forming polarized protofibrils and eventually fibrils. Fibrils may further arrange into protein inclusions although it remains unclear if other proteins within these inclusions anchor these fibrils. Alternatively, oligomers may remain soluble by interacting with small molecules (Conway et al., 2001) or by incorporating post-translationally modified α-synuclein molecules. These structures remain “off the amyloid fibril pathway” and may constitute what has been described in human postmortem tissue as “dots” or “dust-like” amorphous aggregates (Braak et al., 2001; Duda et al., 2002). At this juncture, it remains unclear which of these assemblies are toxic to neurons. Recent data indicate that several conformationally distinct assemblies (possibly different strains) of α-synuclein generated *in vitro* will induce the aggregation of endogenous α-synuclein resulting in neurodegeneration (Guo et al., 2013; Luk et al., 2012a; Peelaerts et al., 2015; Sacino et al., 2014b). The appreciation of different α-synuclein conformers and assemblies as well as their roles in disease may guide potential therapeutic approaches. For example, therapeutic strategies

can be centered on preserving and stabilizing the physiological multimeric conformers as well as preventing monomers from aggregating. Alternatively, sequestration and removal of aggregation-competent monomers and oligomers can be considered.

2.6 Acknowledgments

This work was supported by the National Institutes of Health Grant AG13966; the Intellectual and Developmental Disabilities Center Gant U54 HD086984; and the National Institute of Environmental Health Sciences Center of Excellence in Environmental Toxicology Grant ES013508. DM was supported by National Institutes of Health Ruth L. Kirschstein National Research Service Award Individual Predoctoral Fellowship F31NS087779-01A1. SU was supported by the NIH Chemistry-Biology Interface Training Grant T32GM07133-08. MD was supported by National Institutes of Health Training Grant T32GM008076. HI is the Gisela and Dennis Alter Research Professor of Pediatrics.

CHAPTER 3: INDUCTION OF THE IMMUNOPROTEASOME SUBUNIT LMP7 LINKS PROTEOSTASIS AND IMMUNITY IN ALPHA-SYNUCLEIN AGGREGATION DISORDERS

Scott Ugras[1#], Malcolm J. Daniels[2#], Hossein Fazelinia[3#], Neal S. Gould[3], Anastasia K. Yocum[4], Kelvin C. Luk[5], Esteban Luna[5], Hua Ding[3], Chris McKennan[3,6], Steven Seeholzer[3], Dan Martinez[3], Perry Evans[7], Daniel Brown[8,9], John E. Duda[8,10], and Harry Ischiropoulos[1,3,5,11*]

[1]Biochemistry and Molecular Biophysics Graduate Group, Perelman School of Medicine, University of Pennsylvania, Philadelphia, PA 19104, USA.
[2]Pharmacology Graduate Group, Perelman School of Medicine, University of Pennsylvania, Philadelphia, PA 19104, USA.
[3]Children's Hospital of Philadelphia Research Institute, Philadelphia, PA 19104, USA.
[4]A2IDEA, LLC Ann Arbor, MI 48105, USA.
[5]Center for Neurodegenerative Disease Research, Department of Pathology and Laboratory Medicine, Perelman School of Medicine, University of Pennsylvania, Philadelphia, PA 19104, USA.
[6]Department of Statistics, University of Chicago, Il 60637, USA.
[7]Department of Biomedical and Health Informatics, Children's Hospital of Philadelphia, Philadelphia, PA 19104, USA.
[8]Parkinson's Disease Research, Education and Clinical Center, Michael J. Crescenz VA Medical Center
[9]Department of Neurosurgery, Perelman School of Medicine, University of Pennsylvania
[10]Neurology, Perelman School of Medicine, University of Pennsylvania
[11]Department of Pediatrics, Children's Hospital of Philadelphia, Philadelphia, PA 19104, USA; Department of Systems Pharmacology and Translational Therapeutics, Perelman School of Medicine, University of Pennsylvania, Philadelphia, PA 19104, USA.

#These authors contributed equally
*Corresponding author: ischirop@mail.med.upenn.edu.

(Published in EBioMedicine, May 2018. Volume 31, Pages 307-319)

3.1 Abstract

Accumulation of aggregated α-synuclein into Lewy bodies is thought to contribute to the onset and progression of dopaminergic neuron degeneration in Parkinson's disease (PD) and related disorders. Although protein aggregation is associated with perturbation of proteostasis, how α-synuclein aggregation affects the brain proteome and signaling remains uncertain. In a mouse model of α-synuclein aggregation, 6% of 6,215 proteins and 1.6% of 8,183 phosphopeptides changed in abundance, indicating conservation of proteostasis and phosphorylation signaling. The proteomic analysis confirmed changes in abundance of proteins that regulate dopamine synthesis and transport, synaptic activity and integrity, and unearthed changes in mRNA binding, processing and protein translation. Phosphorylation signaling changes centered on axonal and synaptic cytoskeletal organization and structural integrity. Proteostatic responses included a significant increase in the levels of Lmp7, a component of the immunoproteasome. Increased Lmp7 levels and activity were also quantified in postmortem human brains with PD and dementia with Lewy bodies. Functionally, the immunoproteasome degrades α-synuclein aggregates and generates potentially antigenic peptides. Expression and activity of the immunoproteasome may represent testable targets to induce adaptive responses that maintain proteome integrity and modulate immune responses in protein aggregation disorders.

3.2 Introduction

Cells have developed protein homeostasis networks to maintain proper cellular function and combat potentially toxic protein aggregation. Failure to sustain proteostasis upon protein aggregation may contribute to the pathogenesis of several neurodegenerative diseases of aging such as Parkinson's disease, Alzheimer's disease and Amyotrophic lateral sclerosis (Balch et al., 2008; Douglas and Dillin, 2010; Powers et al., 2009). These diseases are characterized by progressive misfolding and aggregation of proteins and ultimately neuron death.

However, it remains unclear how intracellular aggregation of proteins leads to neuron dysfunction and death. Studies in cellular model systems have shed some light on the pathological mechanisms of endogenous protein aggregation. Dynamic changes in the proteome of cultured cells following intracellular aggregation of artificial synthetic proteins indicated that the formation of amyloid-like aggregates attracted several interacting proteins, which were functionally linked to protein synthesis and quality control (Olzscha et al., 2011). These findings were recently expanded to show that not only artificial synthetic proteins enriched in β-sheet structure but also fragments of mutant huntingtin and TAR DNA-binding protein 43 (TDP-43) peptides, which aggregate in human diseases, cause disturbances in the proteome by interfering with nuclear-cytoplasmic protein and RNA transport (Woerner et al., 2016). Collectively, these studies highlight the impact of protein aggregation on the proteome and proteostasis, and provide the intriguing hypothesis that the re-allocation of cellular resources to combat changes in the proteome upon endogenous protein aggregation leads to dysfunction and ultimately neuron death.

To explore, for the first time, protein aggregation induced changes in the proteome and signaling through phosphorylation *in vivo* we capitalized on the development of a mouse model of α-synuclein aggregation and the use of quantitative mass spectrometry (MS)-based proteomic technologies. α-Synuclein is a 140 amino acid protein that is predominantly localized to vesicles

in pre-synaptic terminals (Davidson et al., 1998; George et al., 1995; Maroteaux et al., 1988) participating in the regulation of neurotransmitter release and synaptic plasticity (Abeliovich et al., 2000; Chandra et al., 2004; Nemani et al., 2010). Several point mutations, as well as multiplications, of the α-synuclein gene are associated with familial Parkinson's disease (PD) (Farrer et al., 2004; Polymeropoulos et al., 1997; Singleton et al., 2003). Moreover, highly organized amyloid-like fibrils and non-amyloid amorphous aggregates of non-mutant α-synuclein are deposited into Lewy bodies, cytoplasmic inclusions that serve as histopathological hallmarks of sporadic PD and other related neurodegenerative disorders (Duda et al., 2002; Giasson et al., 2000; Spillantini et al., 1997).

To investigate the pathological mechanisms of α-synuclein aggregation, Luk et al. developed a mouse model of α-synuclein aggregation (Luk et al., 2012a). In this model, unilateral injection of preformed fibrils (PFFs) of recombinant wild type mouse α-synuclein into the striatum of non-transgenic mice induces progressive aggregation of endogenous α-synuclein, first in regions proximal to the injection site 30 days post injection (dpi) with further involvement of distally interconnected regions by 90 and 180 dpi. Injected mice developed significant dopaminergic neuron degeneration and impaired balance and motor coordination at 180 dpi (Luk et al., 2012a, 2016). Importantly, degeneration and α-synuclein inclusions within the nigrostriatal dopaminergic system are confined to the injected side and absent in the non-injected contralateral side of the brain at 180 dpi. Additionally, injection of PFFs into α-synuclein null (*Snca*$^{-/-}$) mice fails to induce these effects, indicating that endogenous α-synuclein is required for aggregation and dopamine neuron degeneration (Luk et al., 2012a). This PFF injection model has been reproduced in mice, rats and non-human primates (Osterberg et al., 2015; Paumier et al., 2015; Peelaerts et al., 2015; Sacino et al., 2014b; Shimozawa et al., 2017). Therefore, this model (both wild type and *Snca* $^{-/-}$ injected mice) provides an opportunity for *in vivo* study of quantitative changes in the proteome upon aggregation of α-synuclein using MS-based

proteomics and phosphoproteomics when used in combination with Stable Isotope Labeling in Mammals (SILAM) (Wu et al., 2004).

3.3 Methods

Animals. Wild type female, 2-3 month old, C57BL6/C3H mice were obtained from the Jackson Laboratories (Bar Harbor, ME). *Snca*$^{-/-}$ mice were maintained on a C57BL6 background. ^{13}C-Stable Isotope Labeling in Mammals (SILAM) mouse brain tissue (C57BL6 female, L-Lysine-^{13}C6, 97%) was purchased from Cambridge Isotope Laboratories, Inc. All housing, breeding, and procedures were performed according to the NIH Guide for the Care and Use of Experimental Animals and approved by the University of Pennsylvania Institutional Animal Care and Use Committee (IACUC).

Stereotaxic injection of PFFs. For stereotaxic injections, the PFFs were diluted in sterile PBS and fragmented using a Bioruptor bath sonicator (Diagenode, Denville, NJ). Sonication was performed at high power for 10 cycles (30s on, 30s off, at 10°C). Mice were anesthetized with ketamine hydrochloride (100 mg/kg, i.p.) and xylazine (10 mg/kg, i.p.). For each animal, PFFs were stereotaxically targeted into the ventral striatum (AP: +0.2 mm Bregma, lateral: 2.0 mm from midline, depth: 3.6 mm beneath the dura), dorsal striatum (AP: +0.2 mm, lateral: 2.0 mm, depth: 2.6 mm), and overlaying cortex (AP: +0.2 mm, lateral: 2.0 mm, depth: 0.8 mm). Injections were made through a single needle tract using 10 µL syringes (Hamilton, NV) at a rate of 0.1 µL per min (2.5 µL total per site) with the needle in place for ≥ 5 min at each target. Animals were monitored regularly following recovery from surgery. Mice were sacrificed at 90 days post injection by overdose with ketamine/xylazine. For biochemical studies, dorsal striatum and ventral midbrain from ipsilateral and contralateral sides were dissected and stored at -80 °C until used. For histological studies, the brain and spinal cord were removed after transcardial perfusion with PBS and underwent overnight post-fixation in either neutral buffered formalin

(Fisher Scientific) or 70% ethanol (in 150 mM NaCl, pH 7.4), before being processed and embedded in paraffin.

Immunohistochemistry and neuron counting for mouse brain. Immunohistochemistry for α-synuclein phosphorylated at Ser-129 and tyrosine hydroxylase (TH) were performed on 6 µm thick coronal sections as previously described (Luk et al., 2012a). Digitized images of stained sections were acquired using a Perkin Elmer Lamina scanner at 20x magnification. Midbrain dopaminergic neurons belonging to the substantia nigra pars compacta and the ventral tegmental area were quantified from TH-immunostained coronal sections spanning the entire extent of the midbrain (every 9th section). Only intact neurons with visible nuclei and TH positive staining were included in the counting based on established criteria (Fu et al., 2012). Statistical analysis between groups was compared using unpaired t-test.

Sample preparation and LC-MS/MS analysis. For each mouse injected, the midbrain and striatum of the injected and non-injected sides were individual dissected and kept separate. Two midbrain and striatum regions of the injected hemisphere were combined to generate one biological sample for the proteomic analysis. The same approach was employed for the non-injected side. Four biological samples for wild type and three for *Snca*$^{-/-}$ for each injected and non-injected side were analyzed through the proteomic workflow. Homogenates were prepared as described previously (Mertins et al., 2013). Briefly, brains were homogenized with a tissue grinder in cold urea buffer: 8 M urea, 75 mM NaCl, 50 mM Tris HCl pH 8.0, 1 mM EDTA, 2 µg/mL aprotinin (Sigma, A6103), 10 µg/mL leupeptin (Roche, 11017101001), 1 mM PMSF (Sigma, 78830), 10 mM NaF, 5 mM sodium butyrate, 5 mM iodoacetamide (Sigma, A3221), Phosphatase Inhibitor Cocktail 2 (1:100, Sigma, P5726), and Phosphatase Inhibitor Cocktail 3 (1:100, Sigma, P0044). Following 10 min centrifugation at 20,000*g*, protein concentration was determined by a BCA assay (Thermo, 23235). The supernatant was then combined with ^{13}C-labeled brain lysates in a 1:1 ratio (5µg). Samples were reduced for 45 min with 5 mM dithiothreitol followed by alkylation with 20 mM iodoacetamide for 45 min. Samples were then diluted 1:4 with 50 mM Tris

HCl pH 8.0 (to reduce urea concentration to 2 M), then digested overnight with trypsin (Promega, V5111) at 37°C overnight. 1% formic acid was added to the digests to remove urea by pelleting. The tryptic peptides were desalted by ultraMicro-Spin Vydac C18 column (Nestgroup, Inc, SUMSS18V). After peptide separation by high-pH reverse phase chromatography, 95% of peptides were combined in a concatenated pattern into 12 fractions for phosphoproteomic analysis. Lyophilized phosphopeptides fractions were re-suspended in 50% acetonitrile/0.1% trifluoroacetic acid (TFA) and then diluted 1:1 with 100% acetonitrile/0.1% TFA. These samples were then enriched for phosphorylation by incubation with 10 µL immobilized metal affinity chromatography (IMAC) for 30 min. Enriched IMAC beads were the loaded onto C18 silica-packed stage tips washed twice with 50 µL of 80% acetonitrile/0.1% TFA and 100 µL of 1% formic acid. Phosphopeptides were then eluted from IMAC beads with three washes of 70 µL 500 mM dibasic sodium phosphate, pH 7.0, (Sigma, S9763) and 2 washes of 100 µL of 1% formic acid. Elution from stage tips was then performed with 60µL of 50% acetonitrile/0.1% formic acid. Washes were performed on a tabletop centrifuge at a maximum speed of 3,500 *g*. The peptides were analyzed by mass spectrometry (MS) and the data was analyzed with MaxQuant (described below). The SILAM ratio of light/heavy generated from the MaxQuant was converted to $\log_2$ scale and the median of the SILAM ratios therefore was calculated. If the SILAM ratio was close to 1:1, a larger scale sample prep was performed similarly as described above. Protein (2 mg heavy: 2 mg light) was digested with trypsin/Lys-C mix (Promega, V5073) at 1:25 enzyme: protein ratio. This protease mix has been reported to enhance mass spectrometry-based proteomics analysis by reducing the missed cleavages at lysine residue of a given peptide (Mertins et al., 2013). The peptide fragments were desalted on tC18 SepPak cartridge (Waters, WAT036815) and the peptides were lyophilized and stored in -80 °C. For reverse phase-HPLC, the peptides were reconstituted in 20 mM ammonium formate, pH 10.0. Peptide concentration was determined by UV280 before they were separated by high-pH reverse phage chromatography (Acquity UPLC H-Class instrument, Waters) to 72 fractions. Solvent A (2%

acetonitrile, 5mM ammonium formate, pH10) and solvent B (90% acetonitrile, 5mM ammonium formate, pH 10) were used to separate peptides with a ZPRBAX 300Extend-C18 column (4.6mmx250mm, 5 Micron, Agilent). The gradient for separation was 1 mL/min flow rate as at 9 min, 100% A; 13 min, 94% A; 63 min, 71.5%; 68.5 min, 66% A; 81.5 min, 40% A; 83 min; 0% A; at 88-120 min with 1.2 mL/min with 100%A. Five percent of the samples were removed and recombined in a concatenated pattern into 24 fractions for proteomics analysis.

Peptide digests were analyzed on a hybrid LTQ Orbitrap Elite mass spectrometer (Thermofisher Scientific, San Jose, CA) coupled with a NanoLC Ultra (Eksigent Technologies). Mobile phase A consisted of 1% methanol/0.1% formic acid and mobile phase B consisted of 1% methanol/0.1% formic acid/79% acetonitrile. Peptides were eluted into the MS at 200 nl/min with each RP-LC run comprising a 15 min sample load at 3% B and a 90 min linear gradient from 5 to 45% B. The mass spectrometer repetitively scanned m/z from 300 to 1800 (R = 240,000 for LTQ-Orbitrap). FTMS full scan maximum fill time was set to 500 ms, while ion trap MSn fill time was 50 ms; microscans were set at one. FT preview mode, charge state screening, and monoisotopic precursor selection were all enabled with rejection of unassigned and 1+ charge states.

Database searching, construction of the mouse brain reference proteome and proteomic data analysis. Protein identification was performed with MaxQuant (1.5.1.2) using a mouse UniProt database. Carbamidomethyl was defined as a fixed modification. The False Discovery Rate for peptides was set at 1%. Fragment ion tolerance was set to 0.5 Da. The MS/MS tolerance was set at 20 ppm. The minimum peptide length was set at 7 amino acids. The re-quantification option was left unchecked and the match-between-runs was turned on. For a protein to be quantified, the peptide must be identified at least once in light and once in heavy. To construct a unified set of literature and experimental proteins, UniProt accessions were cross-referenced by gene or protein name. For literature proteins, we selected several studies that used MS-based proteomics to identify proteins in the unperturbed mouse brain (Price et al., 2010;

Walther and Mann, 2011; Wang et al., 2006). A reference proteome was generated combining the literature proteome with proteins identified in our experimental runs (Data file S4).

The Light-to-Heavy (L/H) ratio in the non-injected side was divided by the L/H ratio in the injected side to compute the injected/non-injected ratio of ratios. Resulting lists of proteins were analyzed using the Perseus software (http://www.coxdocs.org/doku.php) (Tyanova et al., 2016). The H/L ratios reported by MaxQuant were inverted and log2 transformed. The mean, standard deviation, coefficient of variation, and principle component analysis (PCA) were calculated to examine the precision and repeatability of experiments. We used Z-score to scale the data by subtracting the mean of each column from the values and dividing by the standard deviation of the column. Student's t-test and group averages were calculated and visualized in volcano plots within Perseus. Lists of statistically significant proteins with p-value < 0.05 were selected and DAVID Bioinformatics Resources V6.8 was employed for Gene Ontology (GO) analysis. GO data was visualized using GO plot package in R (Walter et al., 2015). The gene network analysis was performed using GeneMANIA (http://genemania.org/) prediction server (Montojo et al., 2014). Motif-x software tool was used for motif analysis of phosphoproteome using IPI Mouse Proteome as background.

The mass spectrometry proteomics data have been deposited to the ProteomeXchance Consortium via the PRIDE partner repository with the dataset identifier PXD0009647.

Western blot analysis of mouse tissue. Mouse brain samples were extracted using the same method described above for the MS analysis. For each analysis, 5-20 µg of sample was added per lane, separated on 12% Bis-Tris Pre-Cast gels (ThermoFisher) and transferred to PVDF membranes using 7.5% BSA in TBS for blocking. All primary antibodies were used overnight at 1:1000. Antibodies were used against TH (tyrosine hydroxylase; EMD Millipore, 657012 RRID:AB_696697), DAT (dopamine transporter; EMD Millipore, MAB369 RRID:AB_2190413), Ddc (aromatic-L-amino-acid decarboxylase; Abcam, ab3905 RRID:AB_304145), NSE (neuron specific enolase; Abcam, ab53025 RRID:AB_881756), PKC-β2 (protein kinase C beta-2; Abcam,

ab32026 RRID:AB_779042), Akt (protein kinase B; Cell Signaling, 9272 RRID:AB_329827), Lmp7 (proteasome subunit beta type-8; Abcam, ab3329 RRID:AB_303708), and α-synuclein clone D37A6 (Cell Signaling Technology, #4179 RRID:AB_1904156) or clone Syn211 (Sigma-Aldrich Cat# S5566, RRID:AB_261518). Antigen-antibody complexes were detected using an Odyssey LC scanner (LiCor) after incubation with appropriate secondary antibodies. Densitometry was used to quantify intensity of protein bands.

Western blot analysis and proteasome activity of human tissue. Brain samples (amygdala, cortex) from dementia with Lewy bodies and non-disease brains that have been described previously (Rutherford et al., 2013; Waxman et al., 2008) were extracted using high salt buffer containing 1% Triton-X100 (150 mM NaCl, 50 mM Tris, pH 7.6). Protease inhibitors were added to buffer prior to use. To collect triton-soluble fractions, samples were homogenized, sonicated and centrifuged at 15,000 rpm for 30 min. 500 µL of buffer was added to each sample. Protein concentrations were determined by BCA assay (Thermo Fisher). Samples were separated in a 12% Bis-Tris Pre-Cast gel (ThermoFisher) and transferred to a PVDF membrane and blocked using 7.5% BSA in TBS. For each analysis 40 µg of sample was added per lane. All primary antibodies were used overnight at 1:1000. Antibodies were used against Lmp7 (proteasome subunit beta type-8; Abcam, ab3329 RRID:AB_303708), β5 (proteasome subunit beta type-5; Invitrogen, PA1-977 RRID:AB_2172052) and NSE (neuron specific enolase; Abcam, ab53025 RRID:AB_881756). Antigen-antibody complexes were detected using an Odyssey LC scanner (LiCor) after incubation with appropriate secondary antibodies. Densitometry was used to quantify intensity of protein bands. For proteasome activity, the brain samples were homogenized as described above in the absence of protease inhibitors and freshly prepared samples were analyzed using the proteasome activity fluorometric assay (BioVision K245). Assays were performed in a 96-well plate at 37°C using 5 µg of brain lysate per experimental condition. Each condition was analyzed with or without the proteasome inhibitor lactacystin (Enzo Life Science PI104). After 60 min, the fluorescence with inhibitor was subtracted from the

fluorescence without inhibitor in each sample. Three biological replicates were quantified for each experimental condition. Statistical analysis between groups was compared using unpaired t-test.

Immunohistochemistry for human brain. Human brain sections were obtained from the Brain Bank of the Honolulu Asian Aging Study (White and al, 1996). The study is approved by the Kuakini Medical Center Institutional Review Board and participants signed informed consents. Five cases of PD and five healthy controls were examined. DAB and fluorescent Immunohistochemistry for Lmp7, IBA1, and GFAP was performed on 10 µm thick tissue sections. For colorimetric DAB staining, formalin fixed paraffin embedded sections were rehydrated in ethanol and diH_2O and submerged in H_2O_2 for 30 minutes to quench endogenous peroxidase activity. Antigen retrieval was accomplished by microwaving the slides in a pressure cooker with R Buffer U (Electron Microscopy Sciences, 62706-13). The tissue sections were then blocked at room temperature in 2% normal horse serum and incubated with Lmp7 antibody (Abcam, Ab3329, 1:5000) at 4° C for 18 hours. Slides were rinsed in 0.1M Tris and incubated with a biotinylated secondary antibody, ABC, and DAB solution according to Vectastain instructions (Vector Labs, PK-6200 and SK-4100). Images were acquired using a Nikon Eclipse E800 microscope. For fluorescent triple labeling, tissue sections were also rehydrated in ethanol and diH_2O and subjected to the same antigen retrieval and blocking steps as described previously. Slides were then incubated with the same Lmp7 antibody at 1:2500 concentration, along with antibodies against IBA1 (ionized calcium binding adaptor molecule 1; Abcam, ab5076 RRID:AB_2224402, 1:1000) and GFAP (glial fibrillary acidic protein; Millipore, NE1015 RRID:AB_2043416, 1:2000) antibodies at 4° C for 18 hours. Slides were then rinsed in 0.1M Tris and incubated with corresponding Alexa Fluor-conjugated secondary antibodies (Invitrogen, A10042 RRID:AB_2534017; A21202 RRID:AB_141607; A21447 RRID:AB_2535864) for 1 hour at room temperature. Slides were rinsed again in 0.1M Tris and incubated with Hoechst 33342

(Life Technologies, H3570), mounted with Fluormount G (Southern Biotech, 0100-01) and cover-slipped. I mages were acquired using a Nikon A1RSI laser scanning confocal microscope.

In Vitro Degradation Assay. Purified human WT α-synuclein was aggregated at 5 mg/mL for 7 days at 1,400 rpm at 37°C. The fibrils generated from the aggregation of α-synuclein were used as substrate for the *in vitro* degradation assays. Myelin Basic Protein (Sigma M1891) was used at 25 μM and α-synuclein was used at 1 mg/mL. Human Immunoproteasome 20S (Enzo BML-PW8720) and Human Proteasome 20S (Enzo BML-PW9645) were used at a ratio of 0.11:1 proteasome:α-synuclein. Human Proteasome Activator 11S complex (BML-PW9420) was added at a final concentration of 500 nM. Reactions were incubated at 37°C agitating at 600 rpm, and samples were removed at indicated time points. Samples were separated in a 12% Bis-Tris Pre-Cast gel (ThermoFisher) and stained with colloidal blue. Densitometry was used to quantify protein degradation of monomer bands of α-synuclein. Initial time point was considered 100% for each experimental condition. Three biological replicates were quantified for each experimental condition. For mass spectrometry analysis of the immunoproteasome peptides, the samples were removed following the indicated incubation time and frozen prior to processing. For the processing, a modified enhanced filter aided sample preparation (eFASP) was used. Briefly, 10 kDa cutoff microcon filters (Millipore) were first passivated in a solution of 5% Tween 20 overnight to reduce peptide binding, followed by extensive washes with dH_2O. The samples were then transferred to the filters and centrifuged at 14,000 xg for 10 min, retaining the flow through containing the peptides. Sample volume was then reduced to roughly 50 μL by SpeedVac. Contaminants in the sample were removed using C18 Stage Tips (Thermo Electron) and the samples were transferred to autosampler vials. LC-MS/MS conditions and instrument settings proceeded as above with the exception that the samples were not fractionated prior to analysis. The raw data was searched against a database constructed with the human sequence of α-synuclein, proteasome and immunoproteasome subunits using MaxQuant (1.5.1.2) with peptide cleavage set to nonspecific and a FDR of 1%.

Cell treatments. U-251 cells were grown in high glucose DMEM supplemented with 10% FBS, 1% penicillin and streptomycin, 1% glutamine and 1% HEPES. Cells were plated at low density and allowed to adhere for 24h, after which cells were pretreated with 0.1 μg/mL human interferon gamma (Pepro Tech Inc.) alone or in conjunction with the Lmp7 inhibitor ONX 0914 (Cayman Chemicals) at a final concentration of 0.2 μM. Following incubation overnight, 5 μg/mL α-synuclein fibrils were added to the media and incubated for 4d. The cells were washed 3x with PBS and lysed in PBS + 1% Trition-X100. 12 μg of protein was loaded into each lane and the western proceeded as described above. Primary antibodies to α-synuclein (clone Syn211, SigmaAldrich, S5566 RRID:AB_261518), Lmp7 (proteasome subunit beta type-8; Abcam, ab3329), and Actin (Sigma Aldrich, A2066 RRID:AB_476693) were incubated with the membrane at a concentration of 1:1000 overnight at 4°C (Syn211) or for 1 h at room temp (Lmp7, Actin). IR Dye conjugated anti-mouse or anti-rabbit secondary was incubated at 1:5000 for 1 h and the blots were visualized using an Odyssey LC scanner (LiCor).

3.4 Results

Mouse Model of α-Synuclein Aggregation.

To identify proteomic and signaling perturbations induced by the aggregation of α-synuclein, a modified version of the recently developed and independently verified mouse model was employed (Luk et al., 2012a; Osterberg et al., 2015; Sacino et al., 2014b). α-Synuclein aggregation in non-transgenic mice was induced by unilateral injection of PFFs into three locations, the motor cortex, dorsal and ventral-striatum. PFFs were generated by aggregating purified recombinant mouse monomers of α-synuclein to insoluble amyloid-like fibrils exhibiting typical β-sheet secondary structure, then sonicating them to produce smaller, β-sheet PFFs (Fig. 3.S1). The changes in the proteome and phosphoproteome were quantified 90 dpi, a time point that is characterized by aggregation of α-synuclein, but prior to significant dopaminergic neuron loss (Luk et al., 2012a).

Although this model has been extensively validated, dopaminergic neurons belonging to the substantia nigra pars compacta were stereologically quantified from tyrosine hydroxylase (TH) stained coronal sections spanning the entire extent of the midbrain at 90 dpi (Luk et al., 2012a). A non-significant 19 ± 6% loss of substantia nigra dopaminergic neurons was quantified in the injected side of wild type mice, (n=3, t-test, p-value = 0.0507) as compared to the non-injected side (Fig. 3.S2c). In contrast, no changes in TH staining was observed in the injected side of *Snca*$^{-/-}$ mice (Fig. 3.S2c), consistent with the previous results (Luk et al., 2012a). An antibody that recognizes phosphorylated α-synuclein at Ser-129 (pS129), a marker for α-synuclein inclusions in human disorders was used to stain brain tissue obtained at 90 dpi (Anderson et al., 2006; Colom-Cadena et al., 2017; Fujiwara et al., 2002). Consistent with the previous report (Luk et al., 2012a), Lewy body-like inclusions immunoreactive for pS129 were abundant in the substantia nigra (Fig. 3.S2a) and striatum (Fig. 3.S2b) ipsilateral to the injection site by 90 dpi. In contrast, no staining was detected in the same areas on the non-injected side at this time point. Total levels of mouse α-synuclein are unchanged in the injected and non-injected side (Fig. 3.S2e). Moreover, there were no detectable pS129 α-synuclein inclusions in the brains of *Snca*$^{-/-}$ mice injected with PFFs in the same manner (Fig. 3.S2). Collectively, these data confirmed the presence of PFF-triggered α-synuclein aggregation in the ipsilateral injected side of wild type mice, which is associated with mild TH-positive neuron loss, consistent with previous findings in this model (Luk et al., 2012a).

Acquisition and overview of the proteome and phosphoproteome.

A quantitative proteomic workflow depicted in figure 3.1a was implemented to quantify changes in the relative abundance of proteins in both wild type and *Snca*$^{-/-}$ mice. The method incorporated the use of [$^{13}C_6$-lysine]-SILAM mouse brain as an internal “heavy” standard. Detailed examination of the [$^{13}C_6$-lysine]-containing internal reference peptides showed excellent reproducibility (average Pearson correlation coefficient = 0.87, 80% overlap) (Fig. 3.S3). Although the [$^{13}C_6$-lysine] internal standard was derived from the entire brain, whereas the “light”

samples were derived from combining the midbrain and striatum regions only, we report high correlations and tighter spreads of the corresponding heavy-to-light peptide pairs (average Pearson correlation = 0.96) than the heavy-to-heavy peptide pairs (Fig. 3.S3). This improvement likely arises from the coincident sample processing workflow of the SILAM experiment as opposed to the parallel sample processing shown by the heavy-to-heavy comparisons. This analysis validated the use of [$^{13}C_6$-lysine]-SILAM mouse brain as an appropriate standard for accurate proteome quantification.

The quantitative proteomic analysis was restricted to brain regions of pathological interest, which include the midbrain and the striatum. These two regions, dissected from two mice, were combined to generate sufficient protein for the proteomic analysis. Using this approach the proteomic analysis included four replicates derived from the injected and non-injected sides of wild type and three replicates obtained from each side of the similarly injected *Snca*$^{-/-}$ mice. Combined analysis of the replicates in wild type mice applying a false discovery rate of 1% and removal of contaminants and reversed sequences resulted in the identification of 6,508 proteins with a light-to-heavy (L/H) ratio in the injected side, 6,496 in the non-injected side, with 6,215 proteins identified in both sides (Fig. 3.1b). Analysis in the *Snca*$^{-/-}$ mice resulted in the identification of 4,661 proteins with L/H ratio in the injected side, 4,994 in the non-injected side, with 4,460 proteins identified in both sides (Fig. 3.S4a). Immobilized metal affinity chromatography (IMAC) enrichment for phosphopeptides resulted in the identification of 10,058 phosphopeptides in the injected and 10,134 in the non-injected side of the wild type mice; 8,183 phosphopeptides were common between the two sides. Similarly, 10,285 and 9,775 phosphopeptides were identified in the *Snca*$^{-/-}$ mice; 8,031 were shared between the two sides (Data file S1 and Fig. 3.S4b).

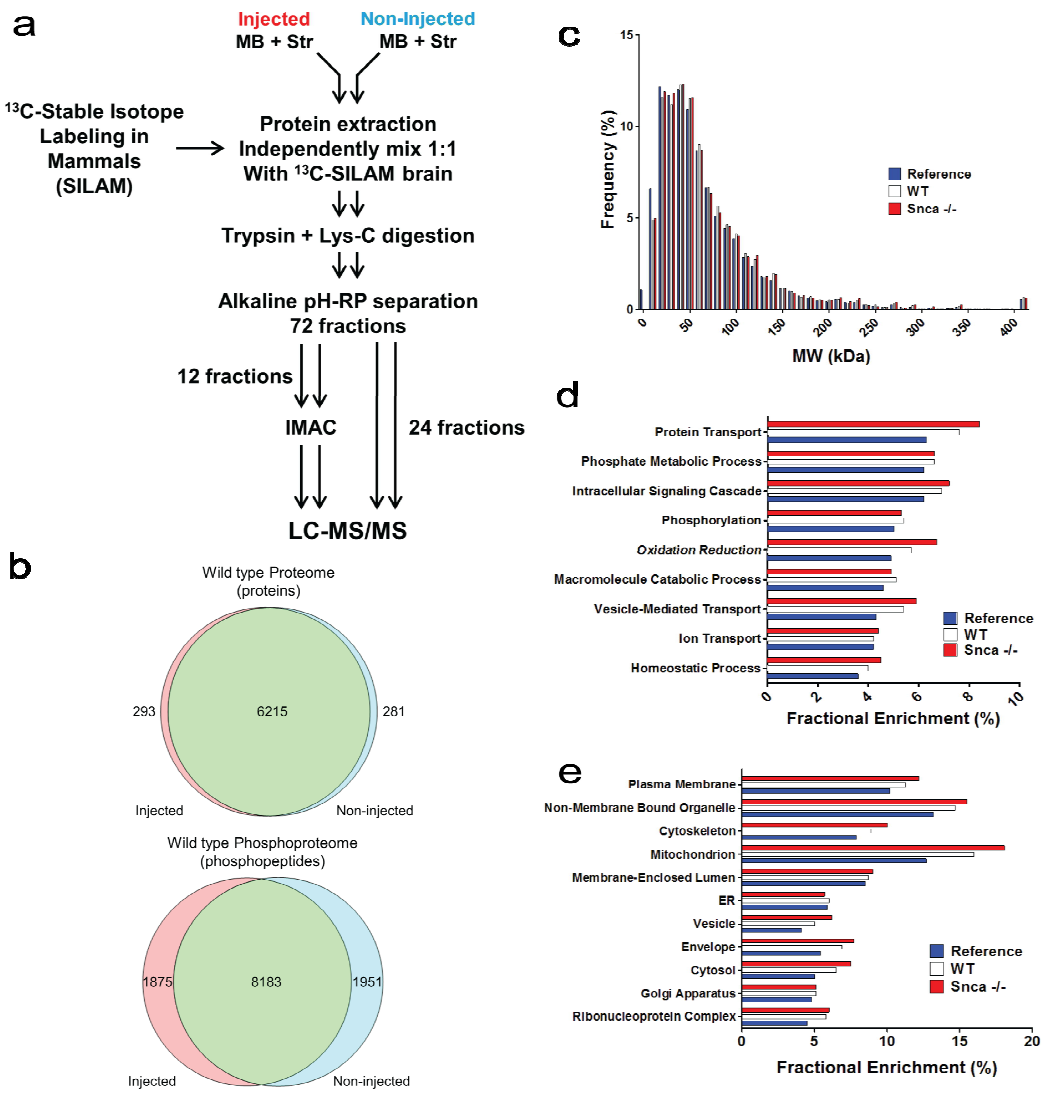

Figure 3.1. Workflow for the acquisition and overall description of proteomes. **(a)** Overview of proteomic workflow. The midbrain and striatum from the brains of two mice were dissected and combined to generate one sample replicate. The ipsilateral injected and the contralateral non-injected sides were kept separate and processed throughout the workflow independently. Immobilized metal affinity chromatography (IMAC) was used to enrich for phosphorylated peptides. **(b)** Venn diagrams depicting the number of proteins and phosphopeptides quantified in 4 independent sample replicates in the injected side and non-injected side in wild type mice. The acquired proteomes in wild type and *Snca*$^{-/-}$ showed typical distribution in terms of molecular weight, cellular location and major biological processes when compared to a whole mouse brain proteome: **(c)** Distribution of the proteins quantified in wild type and *Snca*$^{-/-}$ mice based on protein molecular weight. **(d)** Gene ontology enrichment analysis using cellular components **(e)** Gene enrichment using biological process and KEGG pathways.

In order to determine the extent by which the proteins quantified in this study are reflective of the proteins expressed in the mouse brain, and to protect against potential biases during the acquisition of the proteomic data, we constructed a global mouse brain proteome. For the mouse brain proteome we combined our non-injected wild type proteome with proteins identified by mass spectrometry in unperturbed mouse brain from several existing studies (Price et al., 2010; Sharma et al., 2015; Walther and Mann, 2011; Wang et al., 2006). The resulting proteome comprised of 11,055 unique proteins was curated through UniProt (http://www.uniprot.org). The distribution of the proteins quantified in our study was evaluated based on their molecular weight, cellular localization and biological function against the reference proteome. The proteins quantified were representative of the whole mouse brain proteome covering the entire range of molecular weights >10 kDa to >400 kDa (Fig. 3.1c) all major cellular compartments (Fig. 3.1d) and major biological processes (Fig. 3.1e). Together, these analyses indicated that the number of proteins quantified through this workflow in the midbrain and striatum are compatible with recent studies (Jung et al., 2017; Sharma et al., 2015) and are representative of the proteins expressed in the mouse brain.

Analysis of the proteome and phosphoproteome reveals selective disease-related changes.

Changes in the relative abundance of proteins were quantified by a ratiometric method, dividing the L/H ratio of the non-injected side by the L/H ratio in the injected side. The data was Log2 transformed, the coefficient of variance for each experiment determined, and the data scaled using the standard z-score. Statistically significant changes in proteins (t-test, $p < 0.05$) between the injected and non-injected sides were identified (Data file S2) and typical volcano plots integrating the p-value and the magnitude change were generated. The relative abundance of 377 of 6,215 in wild type and 112 of 4,460 proteins in the *Snca*$^{-/-}$ mice changed significantly in the injected side (Fig. 3.2a; Fig. 3.S5). Similarly, 132 of 8,183 phosphopeptides in wild type and

109 of 8,031 in the *Snca*$^{-/-}$ mice showed significant change (Fig. 3.3a; Fig. 3.S5). There was a minimal overlap between the proteins that showed changes in the injected side of the wild type and *Snca*$^{-/-}$ mice (7 proteins), indicating that the changes in the wild type were driven primarily by the aggregation of α-synuclein. This analysis indicated that aggregation of α-synuclein does not induce large remodeling of the proteome or phosphorylation-dependent signaling. Ontological and functional analysis of the 377 proteins is depicted in the circular plot (Fig. 3.2b) in which the outer circle is a scatter plot for each biological term of the logFC (fold change) of the enriched proteins and the size of the inner trapezoids correspond to the adjusted p-value and the color indicates the z-score. Some of these functional protein clusters (extracellular exosome, synaptic vesicle) have been previously linked to α-synuclein and may represent adaptive response to maintain proteostasis and synaptic function.

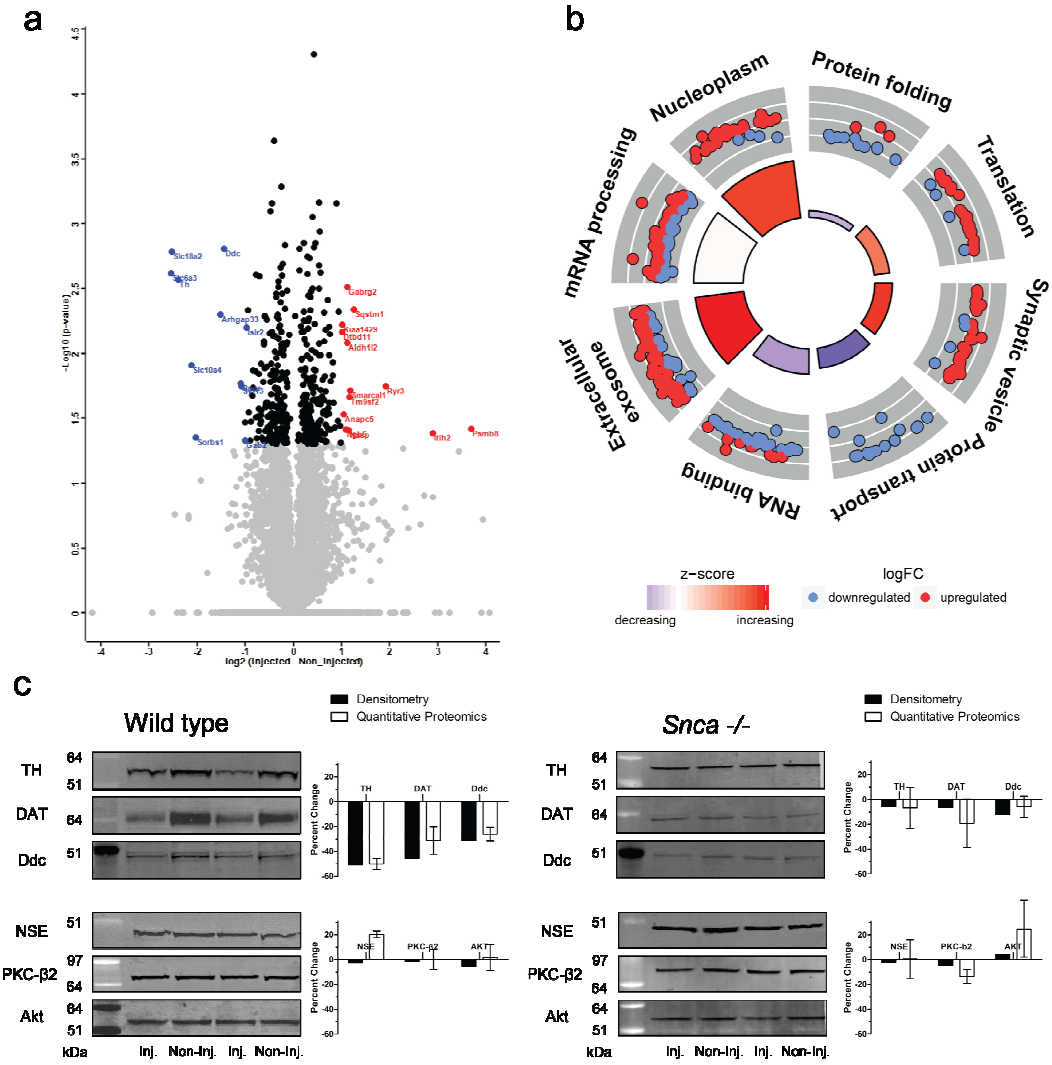

Figure 3.2. Analysis of Quantified Proteins. **(a)** Volcano plot showing the 377 proteins (black circles) that changed significantly ($p < 0.05$) in relative abundance in the injected side as compared to the contralateral non-injected side of wild type mice. The red dots indicate the proteins with >2-fold increase and the blue dots the proteins with >2-fold decrease in relative abundance. **(b)** Ontological analysis of the 377 proteins, which showed significant changes in relative abundance between the ipsilateral injected side and the contralateral non-injected side in the wild type mice. The circular plot depicts the enriched functional networks of proteins. The outer circle is a scatter plot for each biological term of the logFC of the enriched proteins. Within each network, a protein is depicted as a dot, red for upregulated and blue for downregulated. The size of the inner trapezoids correspond to the adjusted p-value and the color indicates the z-score as calculated by GOplot algorithm. **(c)** Representative immunoblots from two independent biological replicates for the significantly changed proteins TH, DAT, and Ddc paired with NSE, PKC-β2 and Akt as unchanged protein controls. The graphs indicate the mean ± sem for protein levels quantified by the SILAM-MS based method and the average of two independent western blot analysis. The relative abundance of NSE, PKC-β2 and Akt did not change in the injected wild type or Snca$^{-/-}$ mice.

The proteomic analysis identified five proteins selectively expressed in dopaminergic neurons among the proteins that decreased in abundance in the injected side of wild type mice. The analysis showed a significant decline in the levels of TH 50 ± 3%, aromatic-L-amino-acid decarboxylase (Ddc) 26 ± 4%, dopamine transporter (DAT; Slc6a3) 31 ± 9%, synaptic vesicular monoamine transporter-2 (VMAT2; Slc18a2) 42 ± 8% and Slc10a4 (specific function is unclear but is specifically expressed in dopaminergic neurons) (Larhammar et al., 2015; Patra et al., 2015) 44 ± 3%. In contrast, the relative abundance of monoamine oxidase A (MAO-A) and catechol-O-methyl transferase (COMT) that metabolize dopamine and are expressed in both glia cells and dopaminergic neurons, did not change significantly (increased by 3 ± 4% and 8 ± 4%, respectively). This finding indicates that, despite possible dilution of the proteome by multiple cell types, our quantitative proteomic approach was capable of identifying specific changes in dopaminergic neurons. Moreover, the decline in the abundance of proteins critical for dopamine synthesis, transport, and recycling exceeded the loss of dopamine neurons (Fig. 3.S2) suggesting ongoing dopamine neuron dysfunction consistent with the progressive injury in the setting of α-synuclein aggregation. As a reference, the abundance of TH, Ddc and DAT did not change in the injected side of *Snca*$^{-/-}$ mice when compared to the contralateral, non-injected side.

Finally, the changes in the levels of TH, DAT and Ddc quantified by SILAM-MS-based methodology were further confirmed by western blot analysis. The western blot analysis matched closely the MS-based quantification showing similar decline in the levels of TH, DAT and Ddc in the injected versus the non-injected side (Fig. 3.2c). The levels of TH, DAT and Ddc were unchanged in the injected side of *Snca*$^{-/-}$ mice when quantified by western blot (Fig. 3.2c). As controls for the western blots, we probed for unchanged proteins as determined by the MS analysis. NSE, PKC-β2 and Akt, showed no change in the levels between injected and non-injected side in wild type and *Snca*$^{-/-}$ mice (Fig. 3.2c) by both MS-based quantification and western.

Although a relatively small number of phosphopeptides showed significant change in the injected side of the wild type mice (132 phosphopeptides identified in 125 proteins, Fig. 3.3a), the data was mined for kinases and functional pathways impacted by α-synuclein aggregation. First, we performed a motif analysis to identify possible sequences targeted by kinase families. This analysis revealed the enrichment for two motifs (Fig. 3.3b). The first motif, X(any amino acid)-X-Serine-Proline is a known minimal sequence motif for phosphorylation by mitogen-activated protein kinases (MAPK), which have been implicated in α-synuclein aggregation related disorders (Ferrer et al., 2001; Iwata et al., 2001; Wilms et al., 2009; Zhu et al., 2003a). The second motif, Arginine-X-X-Serine-X indicates the minimal motif for phosphorylation by Ca^{2+}/calmodulin-dependent protein kinase II (CaMK-II), a serine/threonine kinase enriched at synaptic sites (Miller and Kennedy, 1986; Moriguchi et al., 2012; Picconi et al., 2004). To further explore phosphorylation signal networks, bubble plots of the enriched cellular components and molecular functions were constructed using the z-score and the negative logarithm of the adjusted p-value (Fig. 3.3c). The changes in phosphorylation signaling localize primarily in synapses and axons, and functionally relate to proteins that regulate axonal and synaptic cytoskeletal organization and structural integrity (Fig. 3.3c; Data file S3). Moreover, when the changes in synapse associated phosphopeptides were combined with changes in synaptic vesicle proteins (Fig. 3.2b), the integrated network highlighted numerous physical interactions indicative of functional changes to synaptic architecture and secretory processes in response to α-synuclein aggregation occurring before significant neuron loss (Fig. 3.3d).

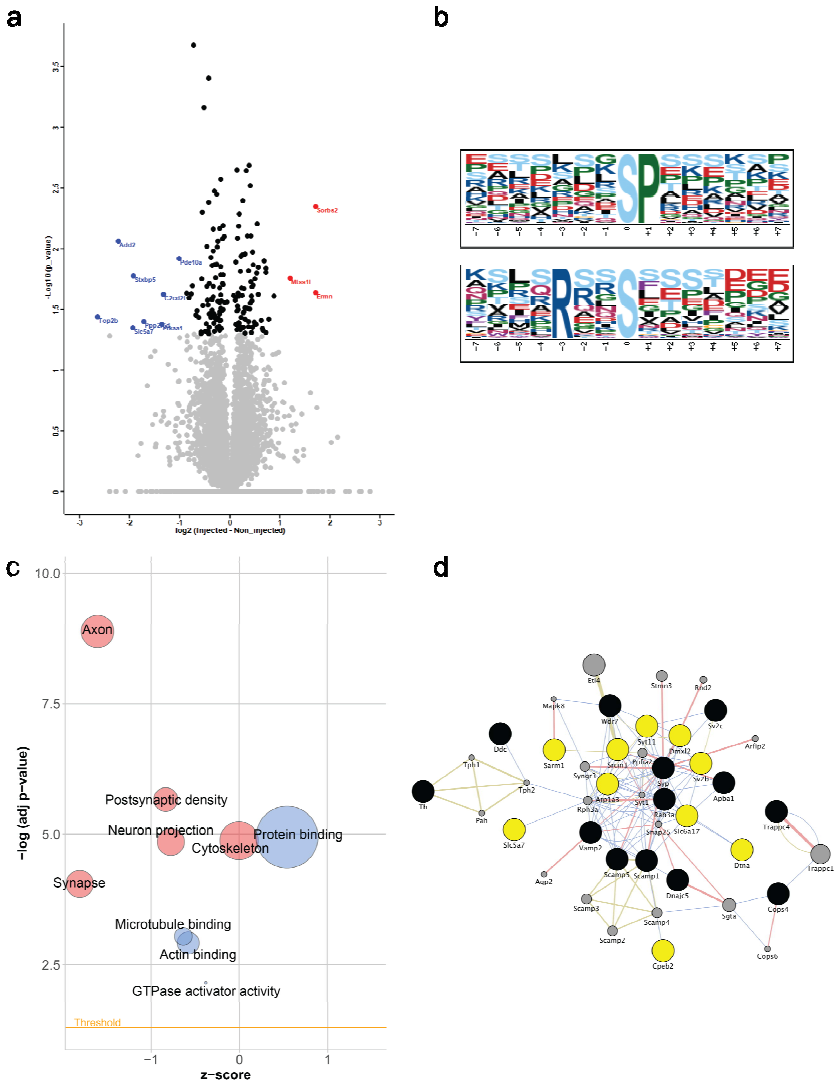

Figure 3.3. Analysis of Quantified Phosphopeptides. (a) Volcano plot showing the 132 phosphorylated proteins (black circles) that changed significantly ($p < 0.05$) in relative abundance in the injected side as compared to the contralateral non-injected side of wild type mice. The red dots indicate the phosphoproteins with >2-fold increase and the blue dots the phosphoproteins with >2-fold decrease in relative abundance. **(b)** Motif analysis of the 132 phosphopeptides, which showed a significant change in relative abundance. Enrichment for two motifs was discovered; the XXSP motif, a known target for phosphorylation by MAP kinase and RXXS indicating substrates for CaMK-II kinase. **(c)** Bubble-plot indicating the cellular components (red) and molecular functions (blue) that were significantly enriched among the 132 phosphopeptides. The area of the displayed circles is proportional to the number of proteins. **(d)** Construction of a synaptic network from the 377 proteins and 132 phosphopeptides. Black circles indicate proteins that are functionally assigned to synaptic vesicles and showed significant changes in relative abundance. The yellow circles indicate phosphoproteins assigned to synapse and showed significant changes in relative abundance. The gray circles are proteins imported based on known interactions. Physical interactions are depicted as pink edges; associations based on co-localization (blue) and shared protein domains (gold).

Upregulation of the Immunoproteasome in α-synuclein aggregation disorders.

Among the significantly changed proteins a prominent increase in the relative levels of the proteasome subunit beta type-8 (Psmb8; common name, low molecular mass protein 7; Lmp7), was quantified in the injected side of wild type mice (Fig. 3.2a). The increase in relative abundance of Lmp7 by MS in the injected side of wild type mice was validated by western blot analysis (Fig. 3.S6 and 3.S7). Lmp7 is one of the three subunits of the catalytic core of the immunoproteasome (Cascio et al., 2001; Driscoll et al., 1993; Gaczynska et al., 1994; Huber et al., 2012), an inducible form of the proteasome assembled in response to inflammatory stimuli, primarily IFNγ (Ebstein et al., 2013; Nathan et al., 2013; Seifert et al., 2010; Yun et al., 2016). The immunoproteasome is defined by the replacement of catalytic subunits β_1, β_2 and β_5 of the proteasome with proteasome subunit beta type-9 (low molecular mass protein 2; Lmp2), proteasome subunit beta type-10 (multicatalytic endopeptidase complex subunit-1; MECL-1) and Lmp7, respectively (Cascio et al., 2001; Driscoll et al., 1993; Gaczynska et al., 1994; Huber et al., 2012).

Since there are no previous studies linking α-synuclein aggregation to immunoproteasome induction and its potential role in proteostasis, we examined whether a similar increase of the immunoproteasome levels and activity occurs in human disease. We compared the levels of Lmp7 in the brains of dementia with Lewy bodies (DLB), which contain aggregated α-synuclein (Duda et al., 2002; Giasson et al., 2000; Waxman et al., 2008), and non-disease control subjects. The analysis revealed a 3-fold increase in the levels of Lmp7 in DLB as compared to controls but no change in the levels of constitutive proteasome catalytic subunit β_5 (Fig. 3.4a and 3.4b). Chymotrypsin-like activity, which is selectively elevated in the immunoproteasome (Gaczynska et al., 1994; Huber et al., 2012), was quantified to evaluate if the increase in protein levels correlates with activity. An 80% increase in the lactacystin-sensitive, chymotrypsin-like activity was quantified in the DLB brain homogenates as compared to controls (Fig. 3.4c).

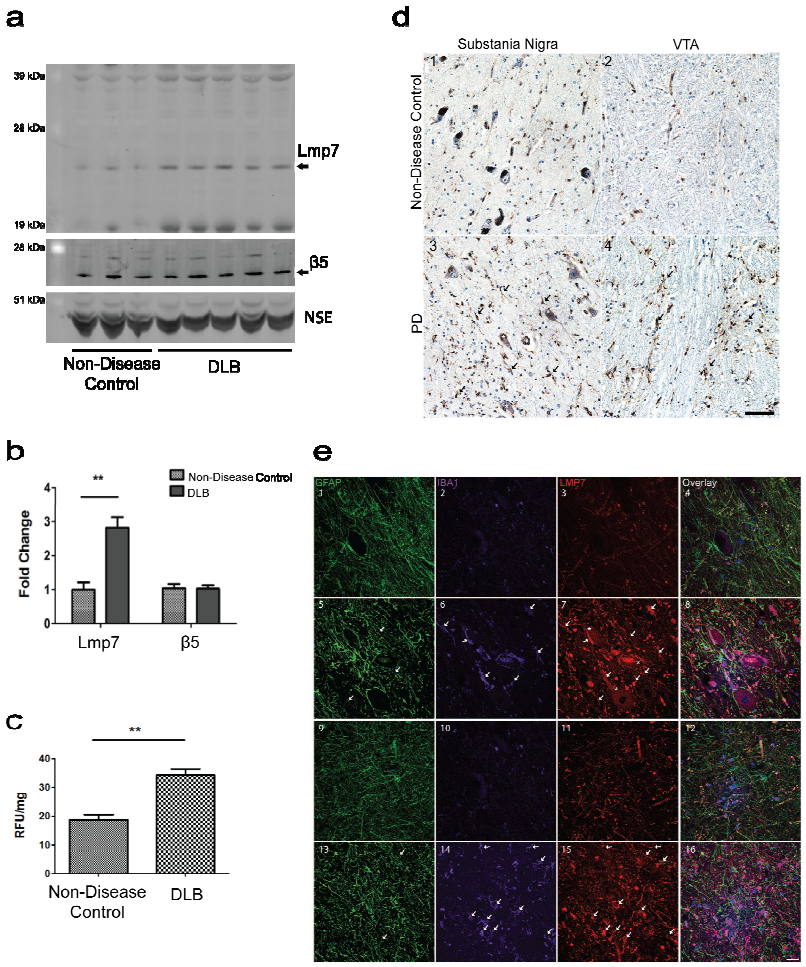

Figure 3.4. The Immunoproteasome in Human Disease Driven by α-Synuclein Aggregation. (a) Representative western blot analysis in human DLB and non-disease control brains for Lmp7 and the proteasome protein β5. **(b)** Densitometric analysis of western blots normalized to the levels of NSE protein indicate a significant increase (**p<0.01, t test) in Lmp7 levels in DLB brains (n=5) compared with controls, (n = 3). **(c)** Concomitant with the increase in Lmp7 protein levels the chymotrypsin-like activity, a proxy for immunoproteasome activity, is increased by 189% in DLB brain compared with control brain (**p<0.01, n = 3, t test). **(d)** Immunohistochemical staining revealed increased immunoreactivity for Lmp7 in PD substantia nigra and VTA. (**d_1**) Representative staining for Lmp7b in control substantia nigra and (**d_2**) VTA. Increased Lmp7 staining in both neurons (asterisks) and glia (arrows) in PD substantia nigra (**d_3**) and VTA (**d_4**). Nuclei were counterstained with hematoxylin (blue). Scale bar = 50 μm. **(e)** Co-localization of Lmp7 with glial markers. Representative fluorescent staining for the astrocyte marker, GFAP; microglial marker, IBA1; and Lmp7. Overlay of GFAP, IBA1, LMP7 and Hoechst nuclear stain is displayed in the right column. Staining in non-disease control substantia nigra (**e_{1-4}**) and in VTA (**e_{5-8}**). Increased staining for Lmp7 in the PD substantia nigra (**e_{9-12}**) and in the VTA (**e_{12-16}**). Lmp7 co-localized with both astrocytes and microglia. Staining increased in glial processes and soma (arrows) and neurons (asterisks) in PD substantia nigra relative to normal controls. Lmp7 staining increased in astrocytes and microglia (arrows) of PD VTA relative to non-disease controls. Scale bar = 20 μm.

Immunohistochemical analysis of PD (n = 5) and non-disease control tissue (n = 5) showed increased staining for Lmp7 in both the substantia nigra and ventral tegmental area (VTA) in PD tissue (Fig. 3.4d). Increased staining for Lmp7 was observed in both neurons and glia in the substantia nigra of PD cases but not in control cases (Fig. 3.4d and 3.4e). Neuronal staining occurred in pigmented and non-pigmented neurons in PD substantia nigra. In PD ventral tegmental area, Lmp7 staining occurred primarily in glia, while neuronal Lmp7 was not detected in PD or control VTA. In glia and neurons, Lmp7 staining was detected throughout both cell bodies and processes. Lmp7 localization was further characterized by fluorescent triple labeling of astrocytes, microglia and Lmp7 (Fig. 3.4e). In the VTA of PD cases, 47 ± 10% of IBA-1 positive cells, a marker for microglia, and 40 ± 4 % of GFAP, an astrocytic marker, co-localized with Lmp7 (n = 4). Overall, the biochemical and histological data demonstrate activation of the immunoproteasome in human diseases characterized by α-synuclein aggregation.

To investigate the potential significance of the immunoproteasome we explored its ability to degrade α-synuclein fibrils *in vitro*. For these experiments, we used the 20S immunoproteasome and the 20S proteasome, which degrade proteins without the need for ubiquitin tagging or the presence of the 19S regulatory particle (Moscovitz et al., 2015). First, we secured that the purified immunoproteasome degraded myelin basic protein (MBP), a selective substrate (Raule et al., 2014). After 22 hours, 96% of MBP was degraded by the immunoproteasome and 69% by the proteasome (Fig. 3.S8). Next, α-synuclein fibrils generated from purified human monomeric α-synuclein with typical β-sheet secondary structure were used as substrate. The immunoproteasome was capable of degrading α-synuclein fibrils in a time dependent manner achieving more than 50% degradation by 72 hours and nearly complete degradation after 5 days of incubation (Fig. 3.5a and 3.5b). We further explored the possible consequences of immunoproteasome-mediated α-synuclein fibril degradation. Since one of the main functions of the immunoproteasome is to produce peptides for antigen presentation, we tested if the degradation products exhibit peptide sequences that have been found to elicit MHC I

and MHC II responses (Sulzer et al., 2017). Mass spectrometry detected 1,111 unique peptide sequences covering the entire 140 α-synuclein amino acid residues (Data file S5). Further refinement of the detected peptides indicated that the immunoproteasome produced multiple peptides within the antigenic regions of α-synuclein (Sulzer et al., 2017), specifically between residues 31-46 and 116-140 (Fig. 3.5c). Finally, to demonstrate that the immunoproteasome degrades α-synuclein fibrils in intact cells, we used U-251 cells, a human glioblastoma cell line that does not express endogenous α-synuclein and minimally detectable basal levels of Lmp7. The only source of α-synuclein in this cell model is the exogenous α-synuclein PFFs added to the culture media. In these cells, α-synuclein PFF uptake appears to be dependent on inflammatory activation as evidence by the lack of uptake of exogenous α-synuclein in PFF only treated cells (Fig. 3.5d). The link between inflammatory activation and α-synuclein uptake has been previously documented (Lee et al., 2010). Concurrent treatment with INFγ induces expression of Lmp7 and intracellular accumulation of exogenous α-synuclein. INFγ only treated cells show the expected increase in Lmp7, but there is no α-synuclein available to detect in these cells. Intracellular accumulation of the exogenous α-synuclein PFFs was quantified in the absence or presence of the Lmp7 specific inhibitor ONX-0914 (Muchamuel et al., 2009). Inhibition of the immunoproteasome results in greater intracellular accumulation of α-synuclein (Fig. 3.5d and 3.5e) without altering Lmp7 levels. Taken together, the data suggest a possible neuroprotective role for the induction of the immunoproteasome to maintain proteostatic networks in response to α-synuclein aggregation.

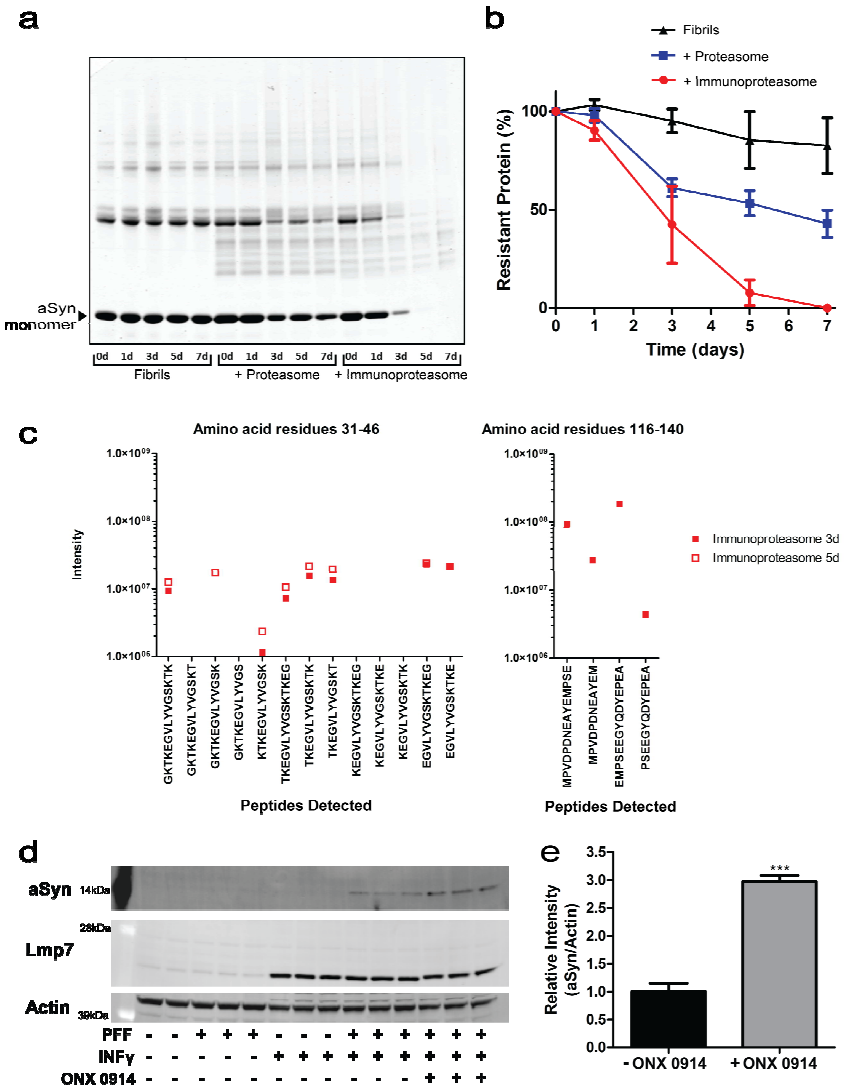

Figure 3.5. Degradation of α-Synuclein preformed fibrils by the immunoprotesome. **(a)** Representative immunoblot for the SDS-soluble fraction of α-synuclein fibrils in the absence or presence of purified 20S proteasome or immunoproteasome for the indicated amount of time. Incubation of pre-formed α-synuclein fibrils with purified 20S proteasome or immunoproteasome resulted in a time-dependent decrease of oligomeric and monomeric α-synuclein. **(b)** Quantification of the ~14kDa α-synuclein band corresponding to monomeric protein in the SDS-soluble fraction. (n = 3). **(c)** Analysis by mass spectrometry of the α-synuclein peptides generated after the degradation of α-synuclein fibrils by the purified immunoproteasome. The relative intensity of the peptides generated within the presumed antigenic regions, residues 31-46 and residues 116-140 is shown after 3 and 5 days of incubation. **(d)** Immunoblot analysis of α-synuclein and Lmp7 in U-251 cells. Cell were treated with 0.1 µg/mL INFγ for 24 hours prior to exposure to α-synuclein preformed fibrils. To ascertain the contribution of immunoproteasome in the degradation of internalized α-synuclein fibrils cells were treated with the Lmp7 specific inhibitor ONX-0914. **(e)** Quantification of the normalized intensity α-synuclein in U-251 cells after induction of Lmp7 and α-synuclein preformed fibril uptake in the absence or presence of the Lmp7 specific inhibitor ONX-0914, (***p<0.001, n=3, t test).

3.5 Discussion

Here, we quantified changes in the proteome and phosphorylation signaling in a validated, non-transgenic mouse model of α-synuclein aggregation. The proteomic approach achieved quantification of more than 6,000 proteins and 8,000 phosphoproteins, with typical representation of proteins based on size, localization, and biological function consistent with similar MS-based proteomic studies using the entire mouse brain (Walther and Mann, 2011) or specific regions of mouse brain (Jung et al., 2017) indicating a reasonable coverage and representation of the proteome. The proteomic workflow enabled the quantification of 46 proteins that have been linked to Parkinson's disease or associated with Lewy body formation and 220 of 226 proteins that were recently linked to α-synuclein (Chung et al., 2017). Contrary to expectations, the changes in the proteome and phosphorylation signaling pathways induced by aggregation of α-synuclein before significant dopaminergic neuron death are minimal and for the most part proteostasis is preserved. Despite the absence of widespread remodeling of the proteome, the data provided unique insights for the responses to protein aggregation, revealing selective changes in protein clusters that participate in dopamine neurotransmission, maintenance of neuronal and synaptic architecture and immune responses. These selective changes were absent in PFF-treated *Snca*$^{-/-}$ mice.

Ontological analysis of the changes in the proteome and phosphoproteome revealed both expected and novel findings. Notably, and consistent with the anticipated pathology, the data revealed selective and significant decrease in the relative abundance of proteins that regulate dopamine biosynthesis (TH, Ddc), transport and storage (VMAT-2) and recycling (DAT). The decline in the levels of TH, Ddc, VMAT-2 and DAT was greater than the magnitude of neuron loss supporting previous observations that alteration in synaptic proteins and function precedes dopaminergic neuron death (Ara et al., 1998; Chung et al., 2009; Garcia-Reitböck et al., 2010; Jackson-Lewis et al., 1995). This observation is further reinforced by the quantification of significant changes in proteins that regulate synaptic vesicles and signaling through

phosphorylation for proteins participating in the organization synaptic architecture and function. These results support previous reports (Chung et al., 2009; Milber et al., 2012; Rockenstein et al., 2014) including observations in humans (Milber et al., 2012; Scott et al., 2010) that perturbations of synaptic protein function and cytoskeletal integrity precede neurodegeneration in α-synuclein aggregation disorders.

Additional pathways impacted by the aggregation of α-synuclein included changes in mRNA processing, binding, protein transport and nucleoplasmic function. These changes are consistent with the alterations in nuclear-cytoplasmic protein and RNA transport observed in models of mutant huntingtin and TDP-43 neurotoxicity (Woerner et al., 2016). Significant changes in relative abundance were also quantified for 112 proteins that are annotated as extracellular and proteins associated with exosomes. Augmentation of extracellular protein release, including exosomes, in response to α-synuclein has been reported (Danzer et al., 2012; Emmanouilidou et al., 2010; Minakaki et al., 2018) and may represent neuronal attempt to remove potential toxic species of α-synuclein, which can be engulfed and degraded by surrounding glia. Although this hypothesis implies a neuroprotective strategy to accommodate proteostasis, it may also propagate α-synuclein toxicity and activate inflammatory and immune glia responses.

The analysis unearthed an increase in the levels of Lmp7, one of the three cardinal subunits of the immunoproteasome, which may represent a response to protein aggregation and activation of innate immunity, since the immunoproteasome is primarily induced by inflammatory stimuli, namely IFNγ (Aki et al., 1994; Heink et al., 2005). Increased Lmp7 levels in the mouse model of α-synuclein aggregation and, critically, in DLB and PD brains has not been previously documented. However, induction of the immunoproteasome is not specific for α-synuclein aggregation. Levels and activity of the immunoproteasome are elevated in postmortem brains of patients with Huntington's and Alzheimer's disease (Aso et al., 2012; Díaz-Hernández et al., 2003; Mishto et al., 2006; Orre et al., 2013). In Huntington's disease, Lmp2-positive staining was

predominantly within neurons and overlapped with approximately 5% of cortical huntingtin protein aggregates (Díaz-Hernández et al., 2003). In the Alzheimer's disease brains increased labeling for the immunoproteasome was associated with reactive glia that surrounded amyloid-β plaques (Mishto et al., 2006; Orre et al., 2013). Taken in conjunction with our findings that Lmp7 staining was increased in both neurons and glia in the substantia nigra and co-localized with microglia in the ventral tegmental area in cases with PD, these data indicate that neurons and glia attempt to counter protein aggregation by inducing the formation of the immunoproteasome.

The immunoproteasome serves at least two known biological functions. The major function relates to the generation of peptides presented by MHC class I molecules on the cell surface for recognition by $CD8^+$ T cells (Driscoll et al., 1993; Gaczynska et al., 1994; Huber et al., 2012; Kincaid et al., 2011). The immunoproteasome also removes ubiquitin-tagged oxidatively-modified misfolded proteins (Ebstein et al., 2013; Nathan et al., 2013; Seifert et al., 2010; Yun et al., 2016). Both of these functions may be critical for protein aggregation diseases and particularly for PD, DLB and related disorders characterized by aggregation of α-synuclein. Our data indicates that the immunoproteasome degrades α-synuclein PFFs *in vitro* and in cells, implicating the induction of the immunoproteasome as a potential pathway for elimination of α-synuclein aggregates. Moreover, the degradation of α-synuclein PFFs resulted in the generation of potentially antigenic peptides that can induce both MHC I and MHC II responses.

Expression of MHC I in dopaminergic neurons in control (non-disease) and PD postmortem tissues has been reported (Cebrián et al., 2014; Lindå et al., 1999). Moreover, the selective expression of MHC I in dopaminergic neurons renders them susceptible to $CD8^+$ T cell mediated injury and death (Cebrián et al., 2014). A recent study has extended these observations to show that peptides derived from α-synuclein elicit both MHC I and MHC II responses to drive cytokine secretion from $CD4^+$ T cells and $CD8^+$ cytotoxic T cells in peripheral mononuclear cells from patients with PD (Sulzer et al., 2017). Therefore, the induction of the immunoproteasome in PD may relate to the degradation of α-synuclein and the generation of

antigenic peptides for T cell presentation. This function may be viewed as detrimental for dopaminergic neurons as activation of T cells elicits cytotoxic effects in neurons.

However, the immunoproteasome may play an important protective role. Primates and mice with longer lifespans have elevated levels of the immunoproteasome (Pickering et al., 2015). This may derive from the role of the immunoproteasome in degrading oxidatively modified, ubiquitin-tagged, aggregated proteins (Ebstein et al., 2013; Nathan et al., 2013; Seifert et al., 2010; Yun et al., 2016). The capacity of the immunoproteasome to degrade proteins modified by oxidants may also be a vital response to neurodegeneration since an association between oxidized proteins and increased immunoproteasome has been reported (Teoh and Davies, 2004). Oxidative stress and oxidized proteins have been long considered in the pathological cascade of neurodegenerative diseases including PD and related α-synuclein aggregation disorders (Giasson et al., 2000; Ischiropoulos and Beckman, 2003; Souza et al., 2000a). Although several forms of autophagy and the lysosomal pathway may participate in clearing α-synuclein and related intermediates such as α-synuclein oligomers (Ebrahimi-Fakhari et al., 2011), the immunoproteasome may be a viable strategy to influence neuroinflammation as well as clearance of potentially toxic α-synuclein species. Given these findings, the timely and appropriate induction of the immunoproteasome by small molecules or other activators may limit the progression of pathology in neurodegenerative disorders. A recent study provided a proof-of-concept for this suggestion by identifying small molecules known to inhibit the p38 MAP kinase arm of MAPK signaling as potent activators of the proteasome (Leestemaker et al., 2017). Interestingly, the activation of the proteasome by the p38 MAPK inhibitors was shown to increase removal of overexpressed α-synuclein in cells providing a foundation for future studies that target the immunoproteasome (Leestemaker et al., 2017).

Data uncovered a significant induction of Lmp7, one of the three principal subunits of the immunoproteasome. The induction of immunoproteasome has been associated with removal of misfolded proteins and preservation of proteostasis. Increased Lmp7 levels were also

documented in postmortem human brain with Parkinson's disease and increased levels and proteolytic activity were documented in postmortem brains with DLB disease, which is characterized by α-synuclein aggregation.

3.6 Acknowledgements

We thank Dr. Benoit Giasson, (Center for Translational Research in Neurodegenerative Disease, University of Florida) for providing the human DLB and control postmortem brains.

3.7 Author contributions

SU participated in all aspects of data collection, generated the samples for MS-based analysis, performed western blot analyses, evaluated the immunoproteasome activity in human brains and helped with the writing of the manuscript. MD and NG generated and analyzed data, generated figures and helped with editing. HF and AKY performed statistical and bioinformatic analyses of the data; HF generated figures. KCL and EL performed the stereotactic injections, evaluated α-synuclein aggregation and neuron viability in the mouse model. HD, CMcK and SS performed the proteomic analysis and supported MS-based data analysis. DM screened and evaluated antibodies used for immunohistochemistry. PE supported the construction of the mouse brain reference proteome and provided bioinformatics support. DB and JED performed and analyzed the immunohistological studies in human tissues. HI planned, organized and participated in the analysis and discussion of all the data and writing of the manuscript. HI is the Gisela and Dennis Alter research professor at the Children's Hospital of Philadelphia Research Institute.

3.8 Supplemental Figures

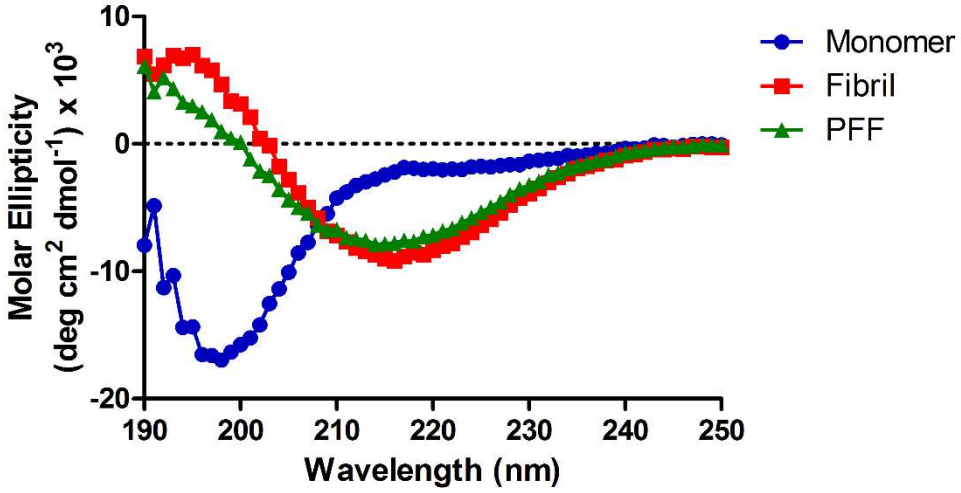

Figure 3.S1. Characterization of mouse α-synuclein fibrils. Purified mouse recombinant wild-type α-synuclein was aggregated by incubating the protein (5 mg/ml) at 37°C under constant shaking at 1,400 rpm for 8 days. Circular Dichroism (CD) spectra of the aggregated proteins revealed the presence of is typical of β-sheet rich structures (red). PFFs generated by sonication of the amyloid-like α-synuclein fibrils retain the β-sheet rich structure (green). The purified recombinant soluble mouse α-synuclein monomer showed a typical unstructured spectrum (blue). CD measurements were obtained in 10 mM potassium phosphate.

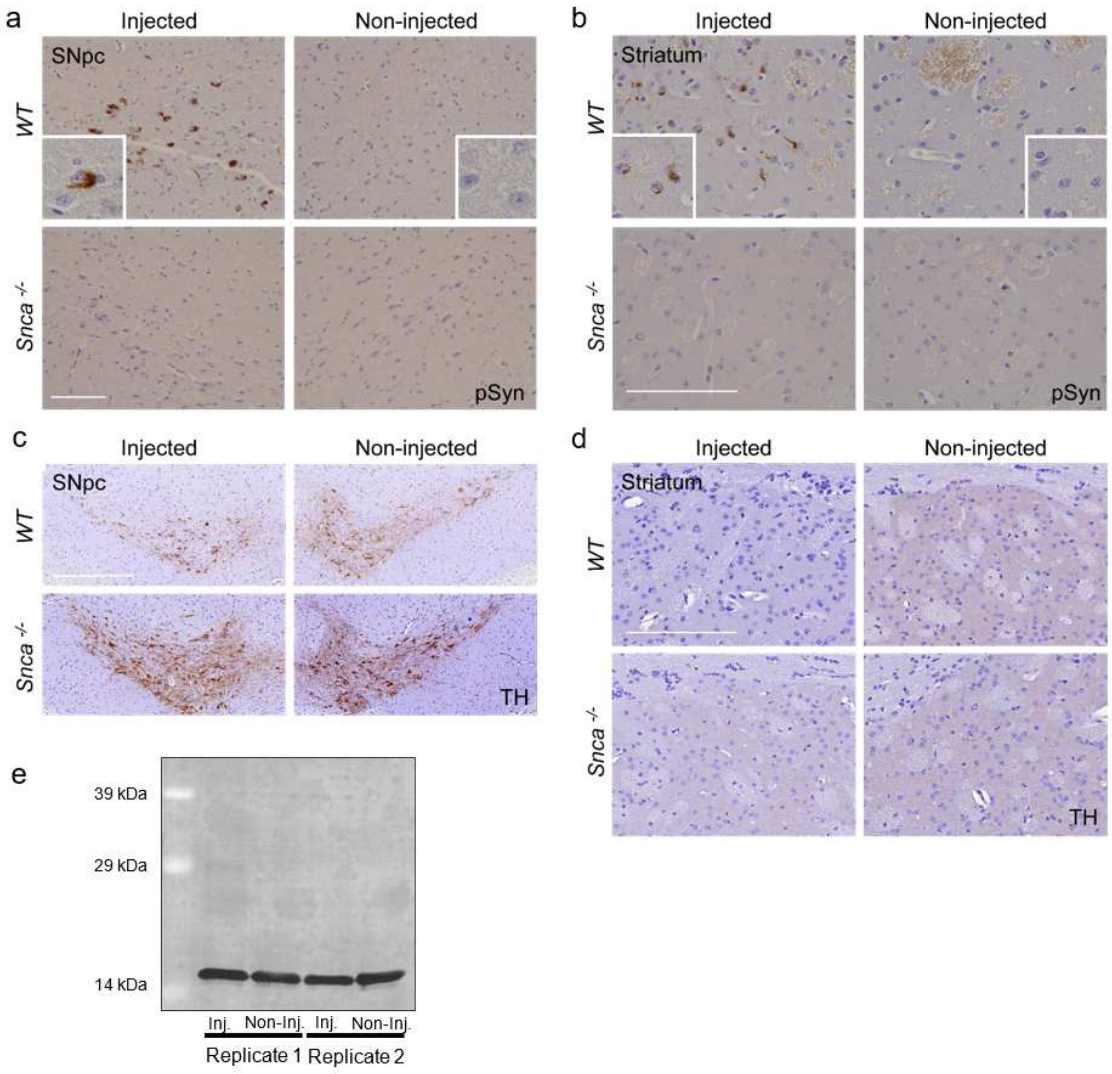

Figure 3.S2. Characterization of wild type and *Snca-/-* mouse models. (a) Representative staining for Ser-129 phosphorylated α-synuclein in the substantia nigra of injected and non-injected wild type and *Snca-/-* mice. Insert is higher magnification of neuronal cytoplasmic inclusions in the injected side; no staining for Ser-129 phosphorylated α-synuclein was found in the non-injected side. Scale bar = 100 μm. (b) Ser-129 phosphorylated α-synuclein in the striatum of injected and non-injected wild type and *Snca-/-* mice. Scale bar = 100 μm. (c) Staining of midbrain tyrosine hydroxylase (TH) positive neurons in the injected and non-injected hemispheres of wild type and *Snca-/-* mice. Scale bar = 500 μm. (d) Immunostaining for TH in striatum of injected and non-injected hemispheres of wild type and *Snca-/-* mice. Scale bar = 100 μm. (e) Western blot of total α-synuclein in the injected and non-injected hemispheres of wild type mice.

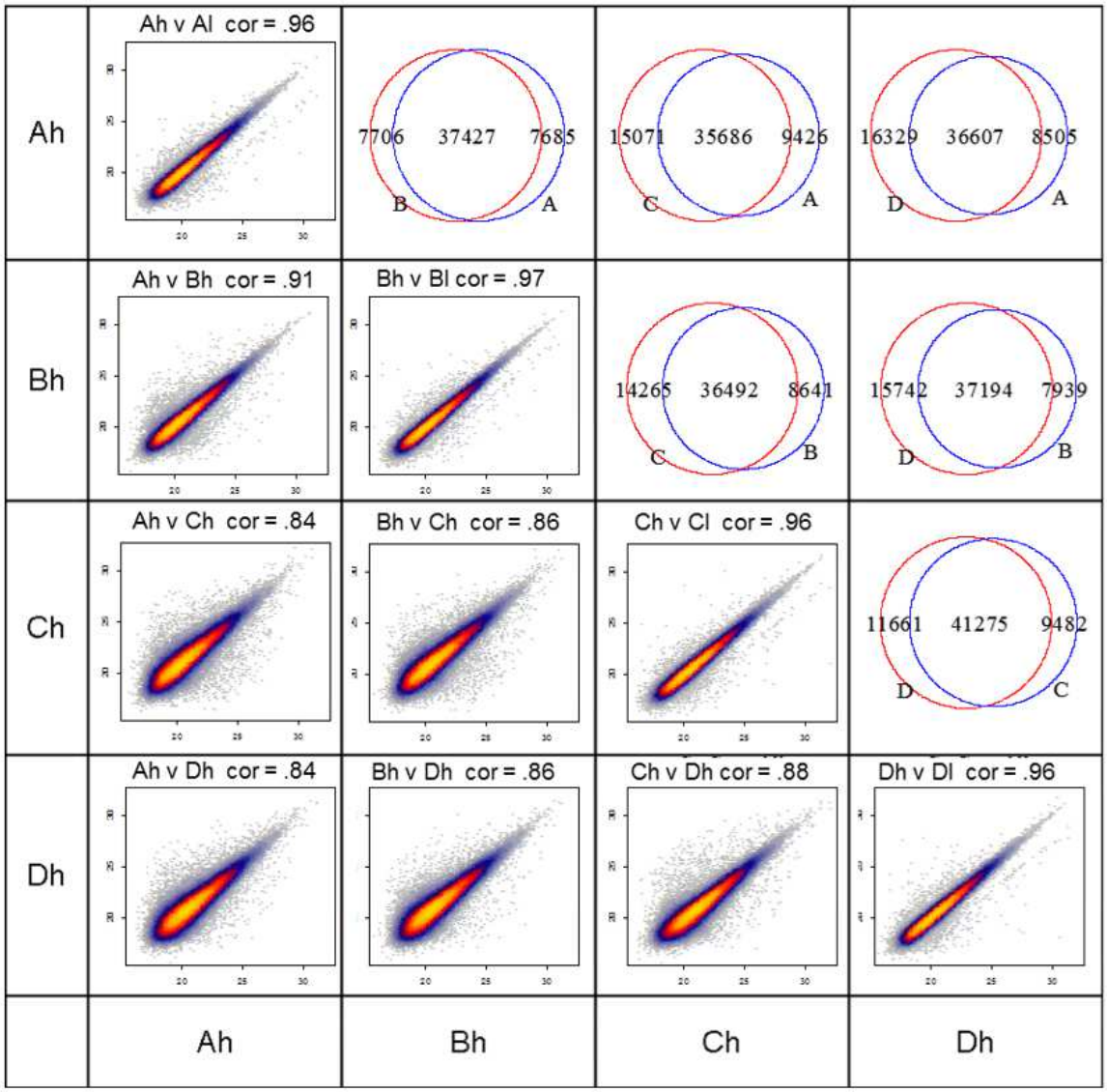

Figure 3.S3. Characterization of [$^{13}C_6$]-lysine-containing tryptic peptide component of SILAM reference proteome. Log2 [intensity] of individual heavy peptides for each of 4 biological replicate experiments (Ah, Bh, Ch, and Dh) are shown plotted each against the others below the diagonal. Area proportional Venn diagrams with accompanying peptide counts for each comparison are shown above the diagonal. Along the diagonal are the corresponding heavy vs light pairs for each experiment. As expected, histograms of peptide intensities unique to each experiment in the pairwise comparisons (non-overlap regions of Venn diagrams) were very heavily weighted toward the lowest quintile of intensities (not shown). Pearson correlation coefficients for each of the heavy:heavy biological replicate pairwise plots and for the heavy:light plots are shown along the diagonal. High correlations and tighter spreads of the corresponding heavy:light peptide pairs (average Pearson correlation = 0.96) than the heavy:heavy peptide pairs is observed. This is likely due to the coincident sample processing workflow of the SILAM experiment. In all, approximately 30,000 heavy peptides were quantified across all four biological replicates which corresponds closely to the number of heavy:light ratios for peptides determined across the same.

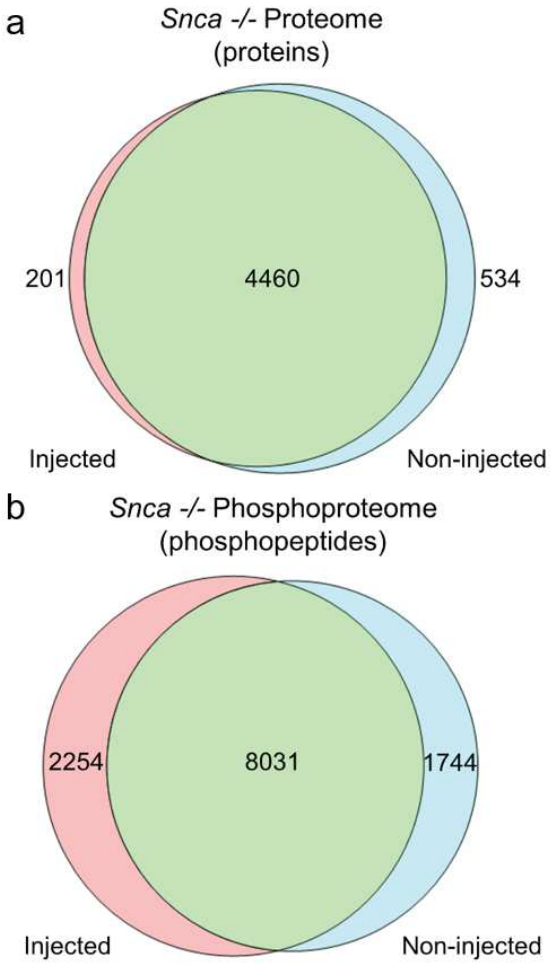

Figure 3.S4. Number of proteins and phosphopeptides quantified in of *Snca-/-* mice. Venn diagrams depict the number of proteins (a) and phosphopeptides (b) quantified in the injected side (red), non-injected side (blue), and in both sides (green) of the *Snca-/-* mouse brains (n=3).

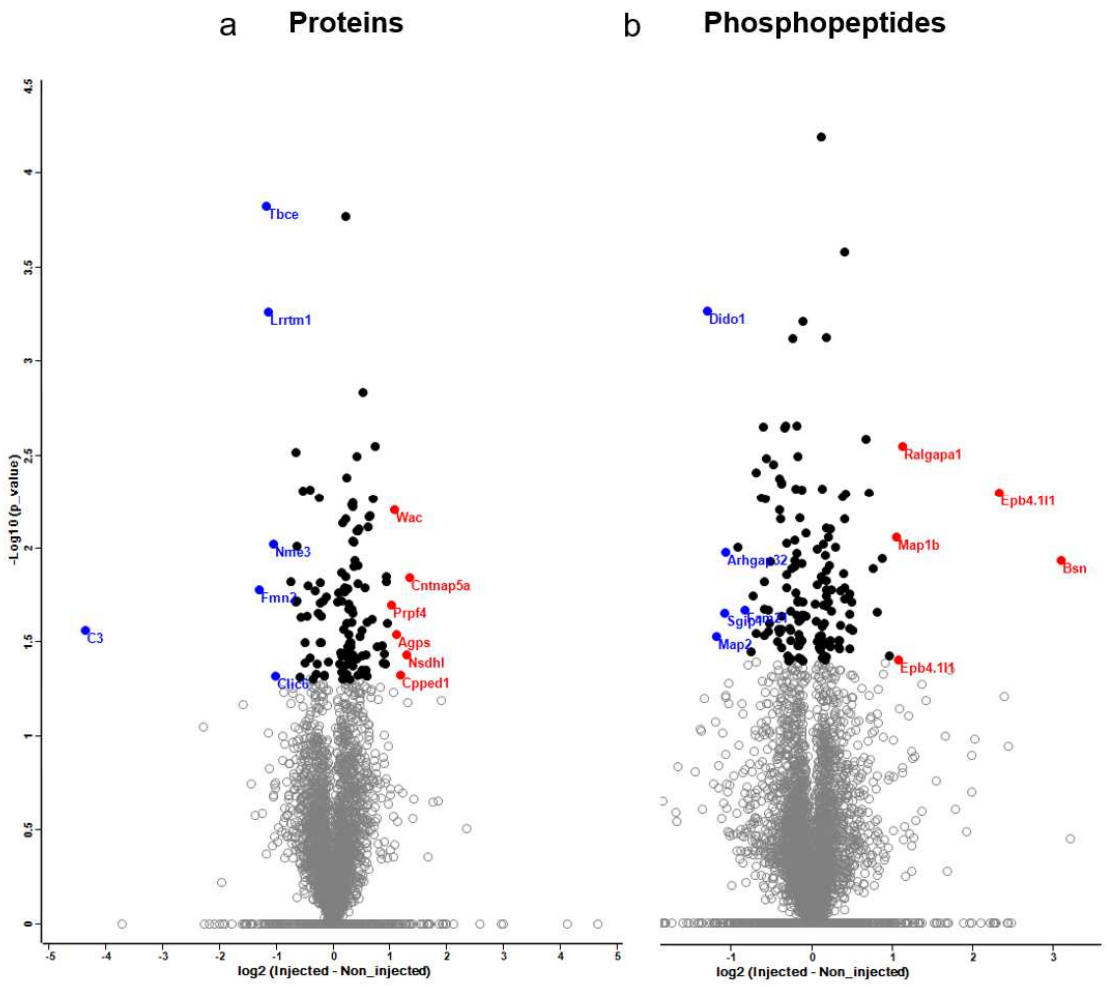

Figure 3.S5. Volcano Plot of proteins and phosphopeptides quantified in *Snca-/-* mice. (a) Volcano plot for proteins and (b) for phosphoproteins depicting the proteins (black circles) that changed significantly (P <0.05) in relative abundance in the inject side as compared to the contralateral non-injected midbrain. The red dots indicate the proteins with >2-fold increase and the blue dots the proteins with >2-fold decrease in relative abundance.

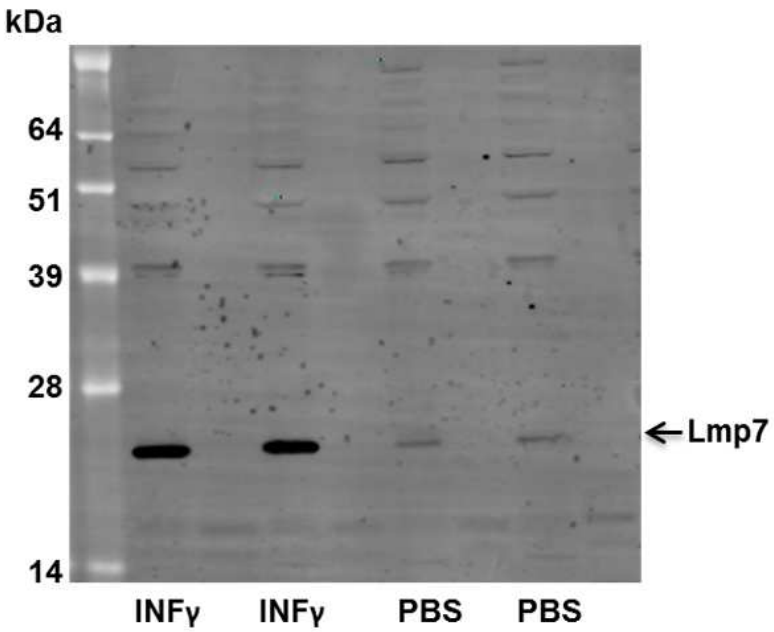

Figure 3.S6. Characterization of the Lmp7 antibody. Western blot image obtained by scanning the PVDF membrane on an Odyssey LC scanner. U-251 cells were treated with 2 µg of interferon gamma (INFγ) or PBS for 24 hours and cell homogenates were analyzed on a 12% Bis-Tris gel, transferred to PVDF membrane, and probed with anti-proteasome 20S LMP7 antibody (ab3329).

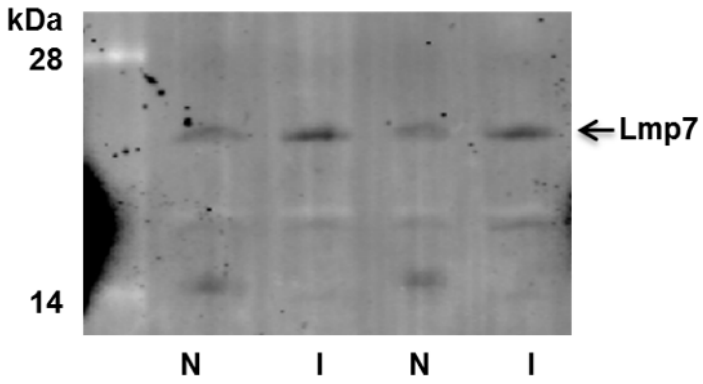

Figure 3.S7. Western blot detection of lmp7 in the mouse brain. Representative western blot image for Lmp7 obtained by scanning the PVDF membrane on an Odyssey LC scanner. Two biological replicates of combined midbrain and striatum homogenates from non-injected (N) and PFF-injected (I) wild type mice were separated on a 12% Bis-Tris gel, transferred to PVDF membrane and probed with anti-proteasome 20S LMP7 antibody (ab3329). Quantification of Lmp7 by densitometry confirmed the mass spectrometry-based increase in the injected side compared to the non-injected side. Lmp7 was not detected in *Snca -/-* mice by either western blot or mass spectrometry-based proteomics.

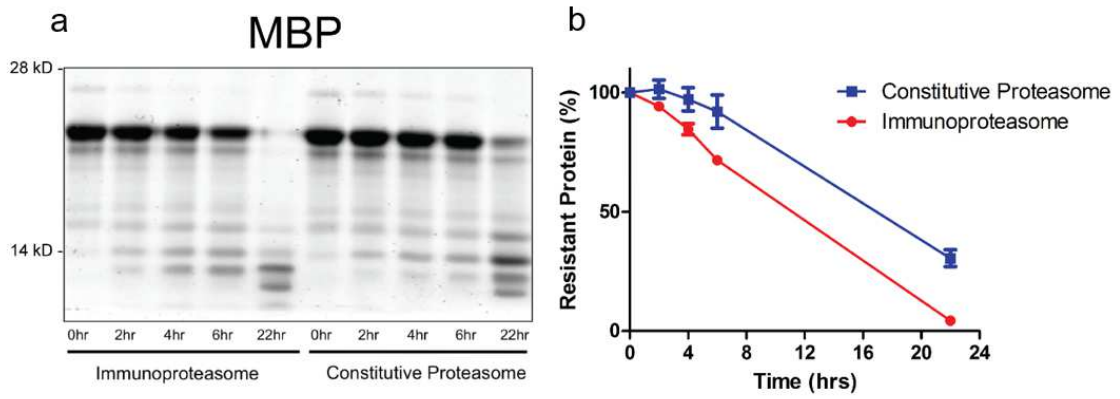

Figure 3.S8. Degradation of Myelin Basic Protein (MBP) by the 20S constitutive proteasome and the 20S immunoproteasome. (a) Representative immunoblot for BMP after incubation with purified 20S constitutive proteasome or 20S immunoproteasome. The 20S proteasome does not require ubiquitin tagging or the presence of the 19S regulatory particle for protein degradation. At the indicated time points, aliquots were removed and analyzed by SDS-PAGE. (b) Quantification of the monomeric band of MBP indicated that incubation with the immunoproteasome results in 96% degradation compared to 70% with the constitutive proteasome after 22 hours of incubation; n=3.

CHAPTER 4: CYCLIZED NDGA MODIFIES DYNAMIC ALPHA-SYNCULEIN MONOMERS, PREVENTING AGGREGATION AND TOXICITY

Malcolm J. Daniels[1], J. Brucker Nourse Jr.[2], Hanna Kim[2], Valerio Sainati[3], Marco Schiavina[3], Maria Grazia Murrali[3], Buyan Pan[4], John J. Ferrie[4], Conor M. Haney[4], Rani Moons[5], Antonino Natalello[6], Rita Grandori[6], Frank Sobott[7], E. James Petersson[4], Elizabeth Rhoades[4], Roberta Pierattelli[3], Isabella Felli[3], Kim A. Caldwell[2], Guy A. Caldwell[2], Edward S. Krol[8] and Harry Ischiropoulos[1,9]

[1]Pharmacology Graduate Group, Raymond and Ruth Perelman School of Medicine at the University of Pennsylvania
[2]Department of Biological Sciences at the University of Alabama
[3]Department of Chemistry at the University of Florence, Italy
[4]Department of Chemistry at the University of Pennsylvania
[5]Department of Chemistry at the University of Antwerp, Belgium
[6]Department of Biotechnology and Biosciences at the University of Milan-Bicocca, Italy
[7]School of Molecular and Cellular Biology at the University of Leeds, United Kingdom
[8]College of Pharmacy & Nutrition at the University of Saskatchewan, Canada
[9]Department of Pediatrics at the Children's Hospital of Philadelphia and Systems Pharmacology and Translational Therapeutics, the Raymond and Ruth Perelman School of Medicine at the University of Pennsylvania

(Manuscript in preparation)

4.1 Abstract

Parkinson's disease (PD) is a neurodegenerative disorder characterized by loss of dopaminergic neurons and the presence of Lewy bodies, proteinaceous inclusions containing aggregated α-synuclein. A growing body of evidence suggests α-synuclein aggregation is a key driver of neurodegeneration in PD. Several classes of small molecules, many containing phenolic ring structures, have shown promise in altering aggregation of α-synuclein. Herein, novel analogs of nordihydroguaiaretic acid (NDGA), a phenolic dibenzenediol lignin, were shown to induce modest, progressive compaction of monomeric α-synuclein without preventing the dynamic adoption of α-helical conformations. The structural alteration of monomeric α-synuclein prevented the primary and secondary nucleation-dependent formation of amyloid-like fibrils. The NDGA analog-mediated inhibition of fibril formation persisted for 14 days and NDGA analog-pretreated α-synuclein did not aggregate even in the absence of molecules in the aggregation mixture. Strikingly, NDGA-preatreated α-synuclein suppressed aggregation of naïve untreated monomeric α-synuclein. Further, cyclized NDGA reduced α-synuclein-driven neurodegeneration in *Caenorhabditis elegans*. NDGA analogs that stabilize aggregation-resistant α-synuclein monomers, without interfering with their ability to adopt functional conformations, might yield therapies to prevent or slow neurodegeneration in PD.

4.2 Introduction

Parkinson's disease (PD) is an age-related neurodegenerative disorder characterized by a progressive motor phenotype including tremors, rigidity, and bradykinesia. These symptoms are driven primarily by loss of dopamine-producing neurons in the substantia nigra pars compacta. Lewy bodies, intracellular proteinaceous inclusions, are the histopathological hallmark of PD. Immunohistochemical analysis of Lewy bodies revealed aggregated forms of α-synuclein, a 140 amino acid neuronally-expressed protein, as a major component (Baba et al., 1998; Spillantini et al., 1997). Mutations, duplications, and triplications of the gene encoding α-synuclein cause dominantly-inherited familial forms of PD (Chartier-Harlin et al., 2004; Krüger et al., 1998; Polymeropoulos et al., 1997; Singleton et al., 2003). The pathological and genetic evidence implicating α-synuclein in PD has sparked numerous studies of the normal function of α-synuclein and its role in PD pathogenesis. α-Synuclein has been implicated in synaptic function (Abeliovich et al., 2000). It preferentially binds lipid membranes with high curvature (Middleton and Rhoades, 2010) and may modulate neurotransmitter release and synaptic function by affecting vesicular fusion (Greten-Harrison et al., 2010; Larsen et al., 2006; Murphy et al., 2000; Nemani et al., 2010).

Repeated studies across various animal models have shown that expression of mutant α-synuclein with altered aggregation kinetics causes neurodegeneration (Giasson et al., 2002; Yang et al., 2015). Likewise, induction of α-synuclein aggregation in wildtype animals by seeding with α-synuclein aggregates—isolated from PD Lewy bodies (Recasens et al., 2014) or generated *in vitro* (Luk et al., 2012a; Sacino et al., 2014a; Shimozawa et al., 2017)—produces progressive neurodegeneration. α-Synuclein aggregation also occurs in animal models of dopamine neuron degeneration induced by oxidative chemical insult (Betarbet et al., 2000; Kowall et al., 2000).

The implication of α-synuclein in PD pathogenesis stimulated several screens for small molecules that alter its aggregation. Dopamine and related catecholamines were among the first molecules found to prevent α-synuclein fibril formation (Conway et al., 2001). Oxidation of vicinal hydroxyls in dopamine, and related phenols, induces formation of soluble α-synuclein oligomers that do not incorporate into fibrils (Mazzulli et al., 2006; Meng et al., 2009; Norris et al., 2005). Recently, dopamine-induced α-synuclein oligomers were shown to contribute to neurodegeneration in mice (Mor et al., 2017), but the precise mechanism of oligomer toxicity remains a subject of debate (Danzer et al., 2007).

Ongoing research has identified many other inhibitors of α-synuclein aggregation. Many of these inhibitors stabilize multimers or oligomers through direct interaction with α-synuclein (e.g. various phenols, catechols, and flavonoids (Ehrnhoefer et al., 2008; Fernandes et al., 2017; Di Giovanni et al., 2010; Lorenzen et al., 2014; Masuda et al., 2006; Meng et al., 2009, 2010; Ono and Yamada, 2006), Anle138b (Deeg et al., 2015; Wagner et al., 2013), rifampicin (Li et al., 2004)). One well studied member of this groups is epigallocatechin gallate (EGCG), a polyphenol sharing the vicinal hydroxyls implicated in dopamine's interaction with α-synuclein. Despite their chemical similarities, dopamine and EGCG have divergent effects on the structure of α-synuclein (Konijnenberg et al., 2016). In fact, while dopamine may induce toxic oligomers, adding EGCG during cell-free α-synuclein aggregation produces species less toxic to cells (Ehrnhoefer et al., 2008). Other aggregation inhibitors alter α-synuclein-protein or -lipid interactions to prevent aggregation (e.g. NPT100-18A (Wrasidlo et al., 2016), squalamine (Perni et al., 2017), PcTS (Fonseca-Ornelas et al., 2014; Lee et al., 2004), Hsp70 (Danzer et al., 2011)). Recent studies have examined small molecules that directly stabilize α-synuclein monomers (e.g. BIOD303 (Moree et al., 2015), nortriptyline (Collier et al., 2017), CLR01 (Acharya et al., 2014; Prabhudesai et al., 2012)). However, it remains unknown whether these small molecules perturb α-synuclein's lipid interactions, which are directly implicated in its role in neurotransmitter release (Burré et al., 2014; Dettmer et al., 2017; Lou et al., 2017).

In this study we employed nordihydroguaiaretic acid (NDGA), a phenolic dibenzenediol lignan that inhibits α-synuclein aggregation (Caruana et al., 2011; Ono and Yamada, 2006). Recent work has exhaustively characterized the products and kinetics of the oxidation of NDGA and several novel analogs (Asiamah et al., 2015). We provide evidence that cyclized NDGA, formed during oxidation, interacts with α-synuclein to produce modified monomers. We demonstrate that these aggregation-resistant monomers retain their capacity to interact with phospholipid membranes and that they inhibit aggregation of untreated α-synuclein. Further, we demonstrate for the first time that cyclized NDGA reduces α-synuclein-driven neurodegeneration in a relevant animal model. Generating α-synuclein species that undergo native structural dynamics while exerting a dominant-negative effect of α-synuclein aggregation and neurotoxicity represents a new paradigm for intervening in PD and related disorders.

4.3 Results

NDGA inhibits both primary and secondary nucleation-mediated α-synuclein aggregation

Two established assays, measurement of insoluble protein and Thioflavin-T binding, quantified the effect of NDGA on the aggregation of monomeric α-synuclein. NDGA caused concentration-dependent inhibition of insoluble α-synuclein accumulation and amyloid-like aggregate formation (Fig. 4.1a and b). Maximal inhibition was achieved at stoichiometric, equimolar concentrations of NDGA to monomeric α-synuclein. To confirm the Thioflavin-T findings, the secondary structure of aggregates was quantified by circular dichroism (CD). NDGA caused a dose-dependent decrease in the β-sheet content of the α-synuclein aggregates, as indicated by molar ellipticity decreases at 200nm and increases at 220nm (Fig. 4.1c). Finally, transmission electron microscopy was used to image the α-synuclein aggregates produced in the presence or absence of NDGA. Typical α-synuclein fibrils were observed in the absence of NDGA, but not after aggregation with equimolar NDGA (Fig. 4.1d). These data demonstrate that stoichiometric concentrations of NDGA inhibit the formation of amyloid-like α-synuclein fibrils.

The preceding experiments examined the effect of NDGA on a typical α-synuclein aggregation assay, in which primary nucleation is the rate-limiting step for the formation of fibrils. Aggregation of α-synuclein can also proceed by a secondary nucleation surface-catalyzed formation of fibrils. To test the effect of NDGA on secondary nucleation-dependent aggregation, α-synuclein fibrils (representing 5% of total α-synuclein) were added with monomeric α-synuclein. Equimolar NDGA (molecule to monomeric α-synuclein) inhibited the formation of insoluble α-synuclein aggregates in the presence of fibril seeds (Fig. 4.1e). Together, these findings demonstrate that stoichiometric NDGA prevents both primary and secondary nucleation dependent aggregation of α-synuclein.

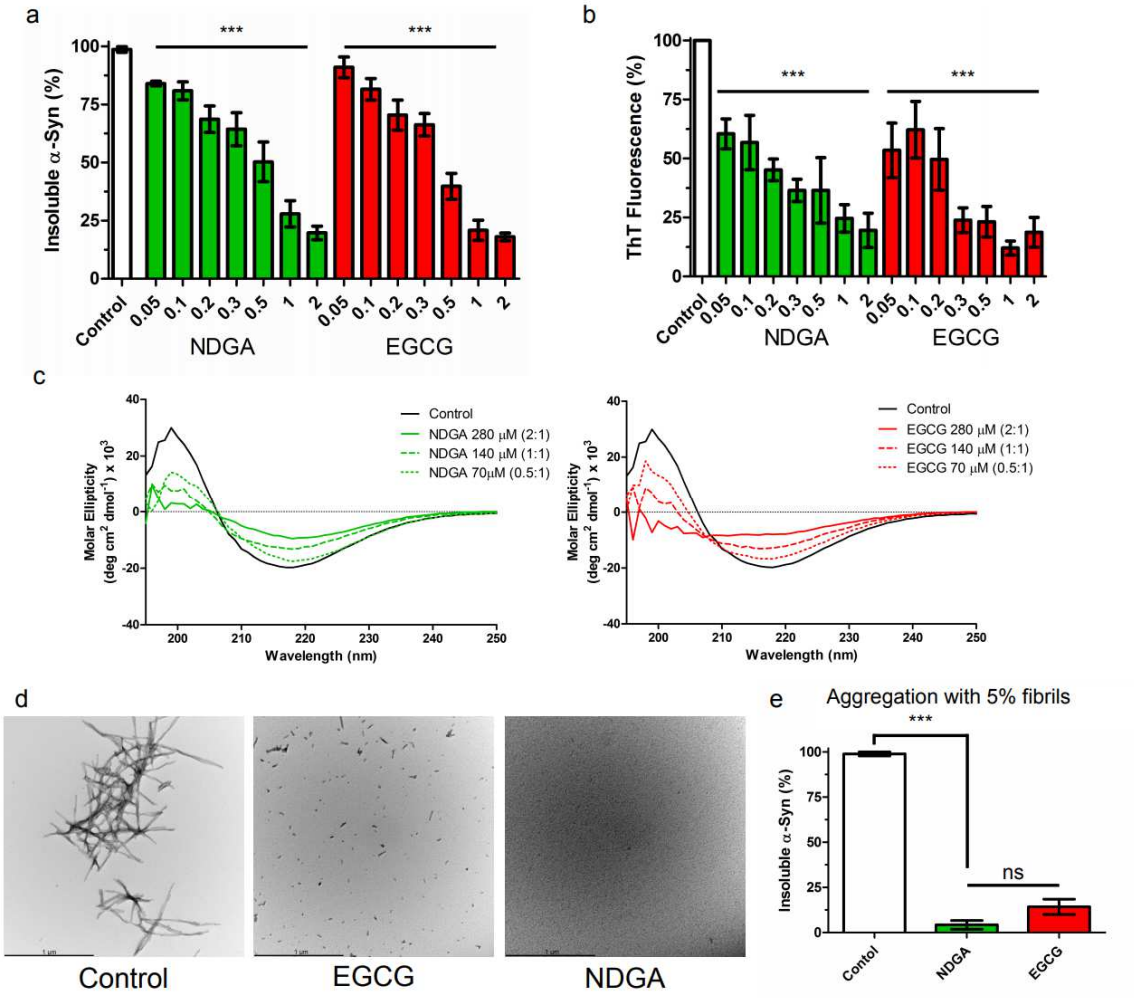

Figure 4.1: NDGA inhibits recombinant human α-synuclein aggregation. (a) Insoluble α-synuclein present after 7 days aggregation was reduced by NDGA and EGCG in a dose-dependent fashion as compared to solvent control. Recombinant human wildtype α-synuclein (138 μM) was aggregated for 7 days in the presence of EGCG or NDGA at the indicated molar ratios. After aggregation, PBS-insoluble α-synuclein was separated by centrifugation (21k g for 10 min). Soluble and insoluble fractions were boiled in SDS, run by SDS-PAGE, and colloidal stained. α-Synuclein in each fraction was quantified by in-gel densitometry. (n = 3-5). **(b)** Formation of amyloid α-synuclein fibrils quantified by ThioT was reduced by NDGA and EGCG in a dose-dependent fashion as compared to control after 7 days aggregation. (n = 3-5). **(c)** α-Synuclein beta-sheet secondary structure was reduced by EGCG and NDGA in a dose dependent fashion. Recombinant human wildtype α-synuclein (138 μM) was aggregated for 7 days in the presence of EGCG or NDGA at the indicated molar ratios. Secondary structure was quantified by circular dichroism. **(d)** Transmission electron microscopy images of α-synuclein aggregates after 3 days aggregation with small molecules at 1:1 molar ratio. **(e)** Insoluble α-synuclein present after 7 days aggregation in the presence of a 5% fibril seed was reduced by EGCG and NDGA. EGCG or NDGA were present at a 1:1 molar ratio. After aggregation, PBS-insoluble α-synuclein was separated by centrifugation (21k g for 10 min). Soluble and insoluble fractions were boiled in SDS, run by SDS-PAGE, and colloidal stained. α-Synuclein in each fraction was quantified by in-gel densitometry. (n = 3).

Interaction with α-synuclein requires oxidation and cyclization of NDGA

We used N-acetylcysteine (NAC), an electron donor, to inhibit NDGA oxidation in the presence of α-synuclein. NAC was included in a typical α-synuclein aggregation mixture at 20:1 molar excess to NDGA. After aggregation for 3 days, levels of α-synuclein aggregation were measured by the established solubility assay. mNDGA, a NDGA analog incapable of oxidation and cyclization was included as a negative control (Supplemental Fig. 4.S1). The addition of NAC allowed α-synuclein to aggregate in the presence of NDGA, suggesting that oxidation is necessary (Fig. 4.2a and b). The inclusion of NAC also reduced levels of quinone-containing NDGA oxidation products detected by near-infrared fluorescence (nIRF), a technique developed to study the oxidation-dependent interaction between α-synuclein and dopamine (Mazzulli et al., 2016) (Fig. 4.2c). The correlation of increased aggregation and decreased quinone nIRF suggests a relationship between NDGA oxidation and inhibition of α-synuclein aggregation. Separately, catalase, which rapidly converts H_2O_2 to water and hydrogen gas, was included in the aggregation assay to determine whether H_2O_2 that might be produced during NDGA oxidation mediated the effects on aggregation. Inclusion of catalase had no effect on α-synuclein aggregation in the presence of NDGA nor on quinone nIRF, indicating that the effect is not H_2O_2-dependent (Fig. 4.2a, Supplemental Fig. 4.S2). These data indicate that NDGA interaction with α-synuclein is oxidation-dependent but not mediated by peroxide chemistry.

Previous work has identified the majority product of NDGA oxidation as a cyclized form (Asiamah et al., 2015). During that study, novel NDGA analogs with defined oxidation pathways were generated. Here, these analogs were used to examine of the role of cyclization in NDGA's oxidation-dependent inhibition of α-synuclein aggregation. We employed NDGA and two such analogs: NDGA-1, which oxidizes with comparable kinetics but does not cyclize due to unilateral hydroxyl substitution, and NDGA-5, which cyclizes more readily than NDGA due to reduced steric hindrance in the crosslinking region (Supplemental Fig. 4.S1). α-Synuclein was aggregated for 3 days in the presence of equimolar NDGA analogs, and aggregation was quantified by the

solubility assay. Both cyclizing analogs, NDGA and NDGA-5, inhibited α-synuclein aggregation, while non-cyclizing NDGA-1 did not (Fig. 4.2d). The products of the above experiment where also analyzed by nIRF. NDGA and NDGA-5-treated α-synuclein exhibited quinone nIRF signals, while NDGA-1-treated α-synuclein did not (Supplemental Fig. 4.S3). These results indicate that cyclized forms of NDGA, or the process of cyclization, are required for interaction with α-synuclein and inhibition of aggregation. To address this uncertainty, α-synuclein was aggregated in the presence of cNDGA and cNDGA-5, the purified cyclized forms of NDGA and NDGA-5, respectively (Supplemental Fig. 4.S1). Using the solubility assay, both cNDGA and cNDGA-5 inhibited α-synuclein aggregation as potently as NDGA (Fig. 4.2e, Supplemental Fig. 4.S4). This indicates that NDGA's inhibition of α-synuclein aggregation is mediated by cyclized oxidation products.

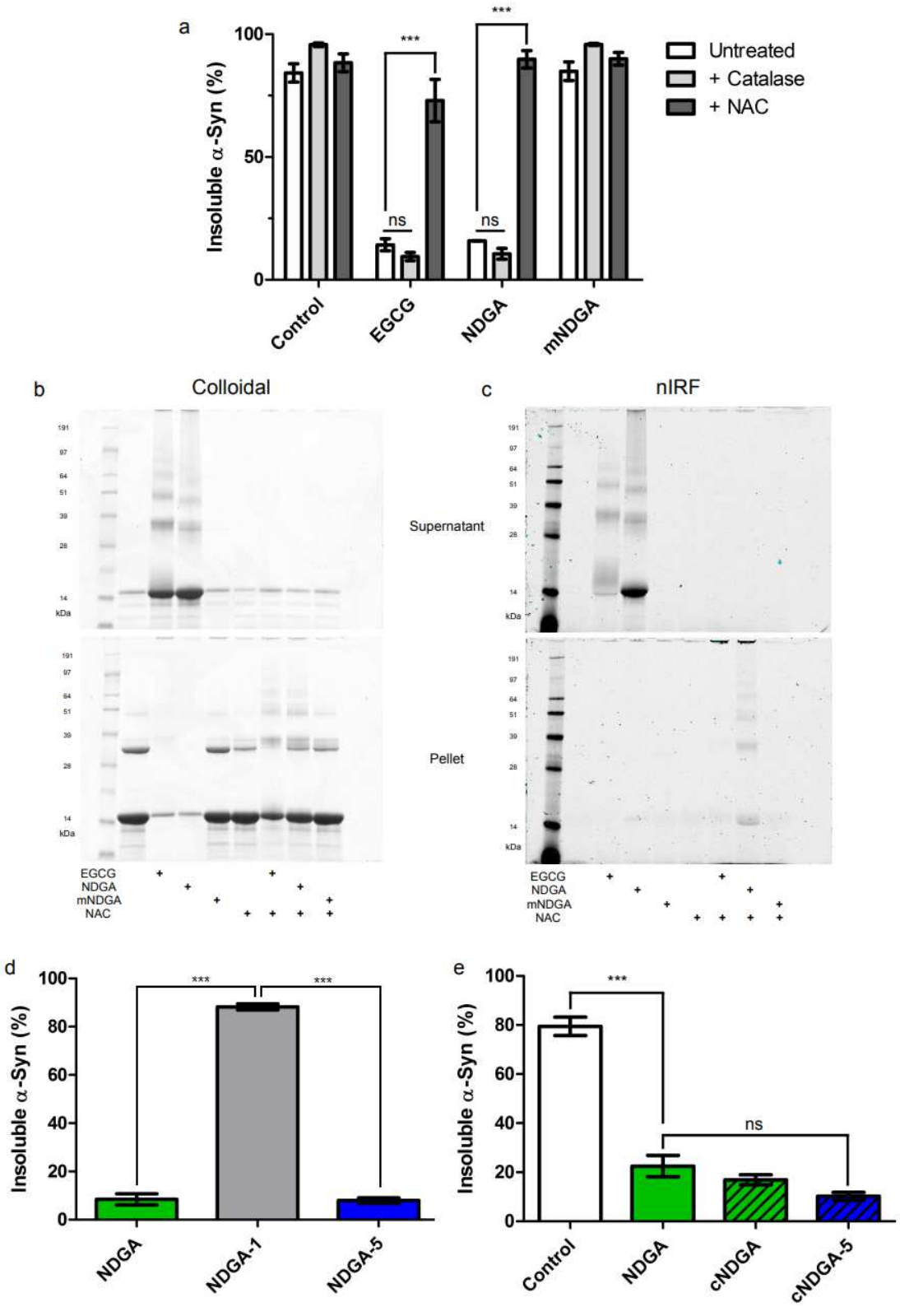
a
Insoluble α-Syn (%)
100
50
0
***
***
ns
ns
Untreated
+ Catalase
+ NAC
Control
EGCG
NDGA
mNDGA
b
Colloidal
c
nIRF
Supernatant
Pellet
191
97
64
51
39
28
14
kDa
EGCG
NDGA
mNDGA
NAC
d
Insoluble α-Syn (%)
100
80
60
40
20
0
***
***
NDGA
NDGA-1
NDGA-5
e
Insoluble α-Syn (%)
100
80
60
40
20
0
***
ns
Control
NDGA
cNDGA
cNDGA-5

Figure 4.2: Interaction between NDGA and α-synuclein requires NDGA oxidation and cyclization. (a) NDGA treatment did not affect α-synuclein aggregation in the presence of N-acetylcysteine. α-Synuclein was aggregated for 3 days in the presence of 1:1 small molecules. After aggregation, PBS-insoluble α-synuclein was separated by centrifugation (21k g for 10 min). Soluble and insoluble fractions were boiled in SDS, run by SDS-PAGE, and colloidal stained. α-Synuclein in each fraction was quantified by in-gel densitometry. NAC was added at 20x molar excess to small molecule and catalase was added equal to 5% of protein, providing excess hydrogen peroxide decomposition capacity. **(b)** Colloidal staining of representative gels showed the formation of insoluble α-synuclein aggregates in the presence of NDGA and NAC. **(c)** Near-infrared fluorescent imaging of the same gels before colloidal staining showed a reduction of quinone-dependent fluorescence in the presence of NAC. **(d)** α-Synuclein did not aggregate in the presence of cyclizable analogs, NDGA and NDGA-5, but did with non-cyclizable NDGA-1. (n = 3). **(e)** α-synuclein did not aggregate in the presence of cyclized cNDGA and cNDGA-5. (n = 3). α-Synuclein was aggregated for 3 days in the presence of 1:1 small molecules. After aggregation, PBS-insoluble α-synuclein was separated by centrifugation (21k g for 10 min). Soluble and insoluble fractions were boiled in SDS, run by SDS-PAGE, and colloidal stained. α-Synuclein in each fraction was quantified by in-gel densitometry.

NDGA induces modest, progressive α-synuclein compaction without preventing dynamic adoption of α-helical conformation

During analysis of the interaction between NDGA and α-synuclein, equimolar incubation consistently produced nIRF-positive quinone-modified α-synuclein (Supplemental Fig. 4.S5). Based on this observation, NDGA-treated α-synuclein was further analyzed to determine any structural effects of the interaction. Native nano-ESI mass spectra (ESI-MS), collected following 10 minute incubations of the protein-ligand mixtures, detected α-synuclein-NDGA complexes with masses matching the theoretical values of the unmodified protein and ligand (Natalello et al., 2017). Masses indicative of α-synuclein modifications such as oxidation or nitrosylation were not detected. Complexes were observed with higher relative intensities at low protein charge states, suggesting a preferential binding to the more compact α-synuclein conformations as previously observed with EGCG. However, levels of α-synuclein binding were much lower for NDGA than previously observed with EGCG (Konijnenberg et al., 2016) (Supplemental Fig. 4.S6).

Ion-mobility mass spectrometry (IM-MS) allows for highly sensitive detection of changes in ion compactness, mass, and charge. Of note, this allows ions of identical mass and charge to be distinguished by compactness. This attribute of IM-MS has previously been employed to show the differential effects of EGCG and dopamine on α-synuclein compaction (Konijnenberg et al., 2016). IM-MS revealed that incubation with NDGA, but not mNDGA, resulted in α-synuclein assuming slightly more compact conformations (Fig. 4.3a). This compaction was more pronounced in lower charge states (+5 through +7) in which distinct populations of conformers with differing compaction can be observed. These data indirectly indicate complex formation with conformational memory, although the complexes are likely lost under these experimental conditions. The previous IM-MS study of EGCG-treated α-synuclein found increased pool of compact conformations, as well as mass-shifts consistent with EGCG binding (Konijnenberg et al., 2016). As with ESI-MS, IM-MS did not detect substantial amounts of α-synuclein with mass-

shifts indicative of covalent adduction by NDGA. Mass spectrometry indicates that NDGA causes subtle structural remodeling of α-synuclein, without forming covalent adducts.

NMR allowed for localization of NDGA's structural effects within the sequence of α-synuclein. After 24 hours incubation with 1:1 NDGA small variations in peak positions were observed in the N-terminus – Val 3, Met 4, Phe 5 – as well as His 50 (Fig. 4.3b). cNGDA and NDGA-1-treatment caused similar changes in the spectra. Incubation with 3:1 NDGA resulted in more pronounced shifts in the same set of peaks.

These samples were followed for several days through NMR revealing a progressive variation of the peak shifts. After several days, additional changes occurred in the signals of several peaks. These peaks showed a second set of signals, indicative of a subset of the α-synuclein population with altered conformation at these residues (Supplemental Fig. 4.S7).

Förster resonance energy transfer (FRET) analysis of α-synuclein provided further insight into the regions altered by NDGA treatment. This examination employed several synthetic α-synuclein proteins with varying fluorescent label pairs spread throughout the amino acid sequence. Based on this methodology, FRET signal from an individual label pair can be converted to an intramolecular distance within α-synuclein and, when taken together, the multiple label pairs provided eight partially overlapped measurements covering the amino acid sequence from residue 9 to 136 (Ferrie et al., 2018). FRET revealed progressive changes in α-synuclein conformation when treated with EGCG, while NDGA, cNDGA, and mNDGA did not induce changes, even after 24 hours (Fig. 4.3c and d). As with IM-MS and NMR, NDGA-treatment was found to induce minimal changes in α-synuclein conformation, while EGCG showed more marked effects.

NDGA-treated α-synuclein secondary structure was examined using circular dichroism (CD). CD failed to detect any changes in the secondary structure of pretreated, dialyzed α-synuclein, further confirming the IM-MS and NMR analyses (Fig. 4.3e). Despite observing limited effects of NDGA on α-synuclein structure in aqueous solution, we also examined whether NDGA-

treatment alters the capacity of α-synuclein to interact with hydrophobic membranes. Membrane interaction induces the N-terminus of α-synuclein to assume an α-helical secondary structure (Davidson et al., 1998; George et al., 1995; Ulmer and Bax, 2005). Capacity for membrane interaction is necessary for α-synuclein's putative biological functions in the synapse (Abeliovich et al., 2000; Murphy et al., 2000; Nemani et al., 2010). Neither NDGA nor mNDGA treatment prevented α-synuclein from assuming α-helical conformations in the presence of SDS, just as occurred under control conditions (Fig. 4.3f). This indicates that the structural changes induced by NDGA do not restrict α-synuclein's dynamic flexibility.

The ability of NDGA-treated α-synuclein to interact with membranes was further examined by fluorescence correlation spectroscopy (FCS), which has been used extensively to study the interaction of α-synuclein with lipid vesicles (Middleton and Rhoades, 2010; Rhoades et al., 2006). The binding of fluorescently labelled recombinant human α-synuclein to various concentrations of phospholipid vesicles (1:1, POPS:POPC) was compared following α-synuclein incubation for 24 hours with equimolar NDGA analogs or solvent alone. NDGA, cNDGA, and mNDGA did not alter phospholipid affinity as indicated by similar protein binding affinity at each vesicle concentration, regardless of treatment condition (Fig. 4.3g). FCS was also used to determine whether the addition of NDGA would displace α-synuclein already bound to phospholipid vesicles. The fraction of α-synuclein bound to vesicles was not altered by the addition of NDGA as compared to the addition of solvent alone (Fig. 4.3h). These data further indicate that NDGA treatment does not perturb α-synuclein interaction with hydrophobic membranes. Collectively, these results show that NDGA causes α-synuclein compaction across the sequence, without altering secondary structure or preventing structural remodeling involved in physiological function.

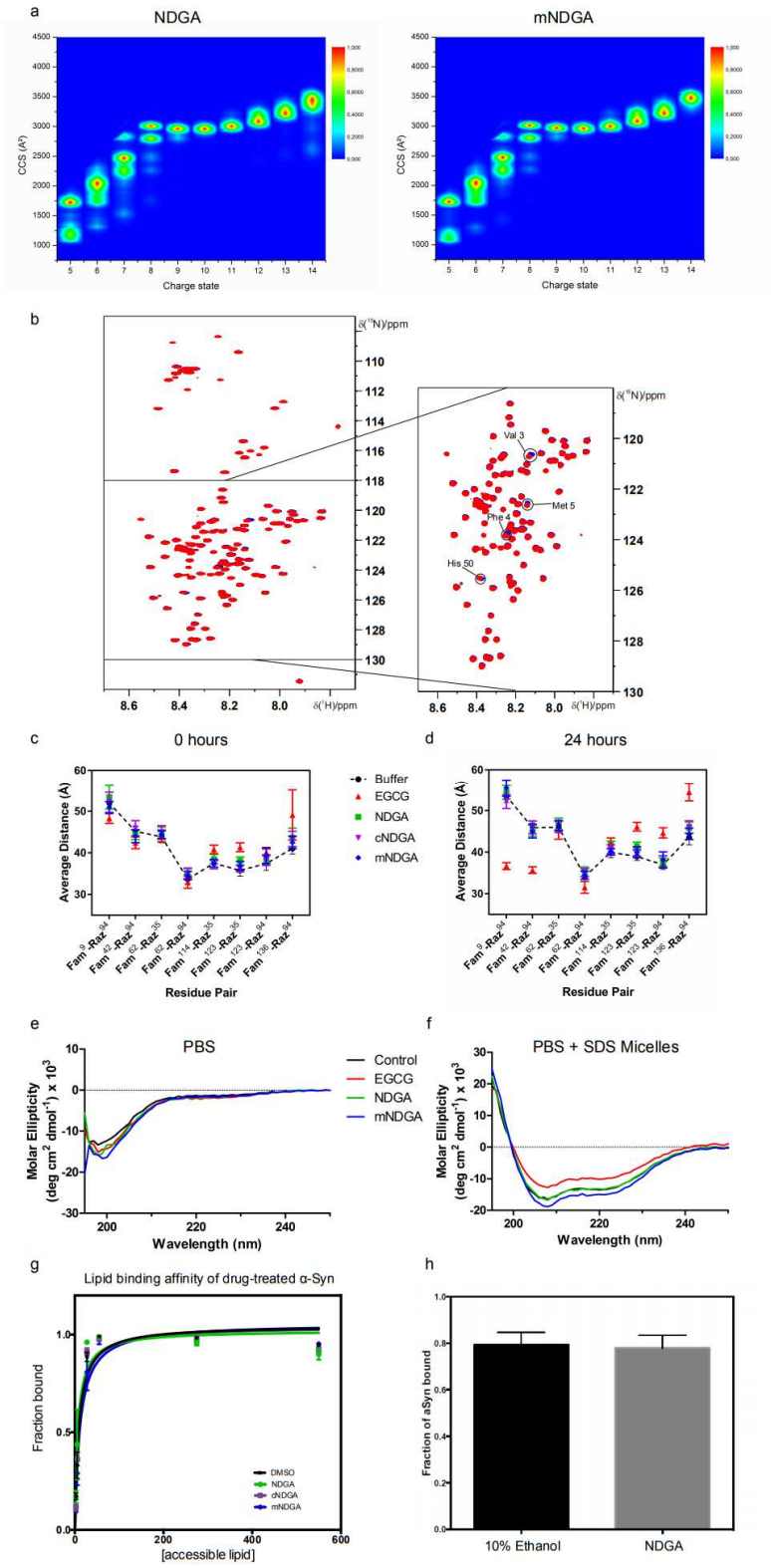
a
NDGA
mNDGA
CCS (Å²)
Charge state
b
δ(¹⁵N)/ppm
δ(¹H)/ppm
Val 3
Met 5
Phe 4
His 50
c
0 hours
d
24 hours
Average Distance (Å)
Residue Pair
Buffer
EGCG
NDGA
cNDGA
mNDGA
e
PBS
f
PBS + SDS Micelles
Molar Ellipticity (deg cm² dmol⁻¹) x 10³
Wavelength (nm)
Control
EGCG
NDGA
mNDGA
g
Lipid binding affinity of drug-treated α-Syn
Fraction bound
[accessible lipid]
DMSO
NDGA
cNDGA
mNDGA
h
Fraction of aSyn bound
10% Ethanol
NDGA

Figure 4.3: NDGA induces compaction of α-synuclein without preventing structural remodeling. (a) NDGA treatment induced compaction of monomeric α-synuclein relative to mNDGA treatment. Ion-mobility mass spectrometry detected increased abundance of α-synuclein species with lower collisional cross section after α-synuclein was incubated with NDGA at 5:1 excess for 10 minutes. **(b)** NDGA treatment of α-synuclein did not induce extensive shifts in 2D NMR spectra. α-Synuclein was incubated 1:1 with NDGA for 24 hours before spectra were collected. NDGA-treated α-synuclein spectra (blue) was overlaid on solvent-treated α-synuclein (red). FRET measurement of **(c)** 0 hour and **(d)** 24 hour small molecule treatments showed progressive alteration of α-synuclein intramolecular distances by EGCG, but not NDGA, cNDGA, or mNDGA. The dashed line depicts 1 μM α-synuclein treated with buffer (1x PBS). Treatments were 5 μM NDGA (green square), EGCG (red triangle), cNDGA (purple inverted triangle), and mNDGA (blue diamond). (n = 3). **(e)** α-Synuclein secondary structure was not altered by pretreatment with NDGA. **(f)** NDGA pretreatment did not prevent α-synuclein assuming α-helical secondary structure in the presence of SDS micelles. α-Synuclein was incubated 1:1 with NDGA, mNDGA, or solvent alone for 24 hours and then dialyzed against PBS for 24 hours. 40 mM SDS micelles were added 5 minutes before analysis. Secondary structure was quantified by circular dichroism. **(g)** NDGA treatment did not alter α-synuclein phospholipid binding. α-Synuclein was incubated 1:1 with NDGA analogs or solvent alone for 24 hours before fluorescence correlation spectroscopy in the presence of POPS:POPC vesicles at the indicated concentrations. (n = 3). **(h)** Addition of NDGA did not displace fluorescently labeled α-synuclein from POPS:POPC vesicles. (n = 3).

NGDA pretreated α-synuclein stably resists seeded aggregation

Based on the progressive remodeling of α-synuclein treated with NDGA, we analyzed the capacity of NDGA-pretreated α-synuclein to aggregate into fibrils. α-Synuclein was incubated with equimolar NDGA (as well as mNDGA and EGCG controls) for 24 hours before dialysis against excess PBS for 24 hours. This pretreated, dialyzed α-synuclein was then aggregated for 3 days before undergoing the solubility assay (as depicted in Supplemental Fig. 4.S8). NDGA, but not mNDGA, pretreatment prevented α-synuclein aggregation (Fig. 4.4a). Further, pretreated, dialyzed α-synuclein was aggregated for 14 days to test the duration of the effect. Again, NDGA but not mNDGA pretreatment prevented α-synuclein aggregation (Supplemental Fig. 4.S9). Consistent with previous data, we found that pretreatment with cyclizing (NDGA and NDGA-5) and cyclized (cNDGA and cNDGA-5) analogs prevented α-synuclein aggregation, while non-cyclizing analogs (NDGA-1 and SECO-1) did not (Supplemental Fig. 4.S10 and 4.S11). We also examined the soluble species that remained following aggregation of pretreated, dialyzed α-synuclein using native state SEC and found that monomeric species are the majority product (Supplemental Fig. 4.S12). Collectively, these findings demonstrate the NDGA pretreatment renders α-synuclein monomers resistant to aggregation. This effect was not observed with non-oxidizable and non-cyclizing analogs of NDGA.

Native-state SEC fractionation found that pretreatment with either NDGA or EGCG produces both monomeric and oligomeric α-synuclein species (Supplemental Fig. 4.S5). We compared the aggregation of these two pools of α-synuclein species. α-Synuclein was incubated with equimolar small molecules for 24 hours before oligomeric (≥51Å) and monomeric (<51Å) species were separated using native state SEC. The resulting fractions were then aggregated for 3 days before analysis by the solubility assay. Both monomers and oligomers produced upon NDGA and EGCG pretreatment resisted aggregation, while the majority of mNDGA treatment products formed insoluble aggregates (Fig. 4.4b). This indicates that while aggregation-resistant

α-synuclein oligomers do form after NDGA treatment, resulting monomers are also aggregation-resistant, even in the absence of oligomers.

Next, we explored whether NDGA can prevent surface-catalyzed, secondary nucleation-dependent, aggregation of α-synuclein. Pretreated, dialyzed α-synuclein was aggregated for 3 days in the presence of α-synuclein fibril seeds (equal to 5% of total α-synuclein in solution) before aggregation was quantified by the solubility assay. Again, NDGA but not mNDGA pretreatment reduced α-synuclein aggregation (Fig. 4.4c). This demonstrates that NDGA-pretreated, dialyzed α-synuclein does not readily undergo secondary nucleation to form species capable of incorporating into existing fibrils.

Based on the observation that NDGA treatment prevents α-synuclein aggregation, we conducted a novel analysis to determine whether aggregation of untreated α-synuclein is altered by the presence of NDGA-pretreated α-synuclein. Pretreated, dialyzed α-synuclein was generated as before, then mixed with untreated α-synuclein at varying ratios and the resulting mixtures were aggregated for 3 days before undergoing the solubility assay (as depicted in Supplemental Fig. 4.S12). The addition of pretreated, dialyzed α-synuclein caused a super-stoichiometric reduction in insoluble α-synuclein, demonstrating that aggregation of untreated α-synuclein was reduced (Fig. 4.4d). This effect is demonstrated in the 20% condition wherein NDGA pretreated, dialyzed α-synuclein represents only 20% of total α-synuclein, but insoluble α-synuclein is reduced from 88% in control conditions to 37%. These data, taken in totality, indicate that pretreatment with NDGA produces α-synuclein monomers that are not only resistant to aggregation, but reduce aggregation of α-synuclein never exposed to NDGA.

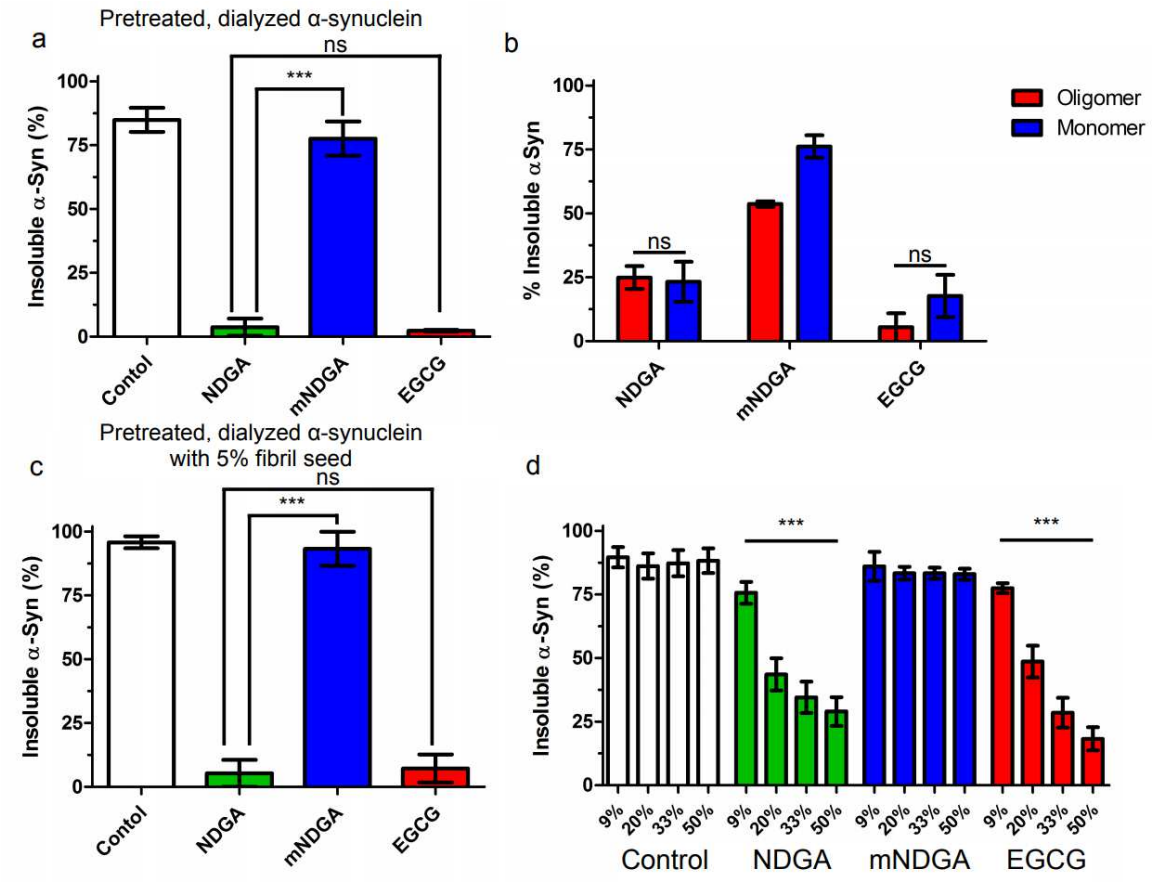

Figure 4.4: NDGA pretreatment prevents α-synuclein aggregation. (a) α-Synuclein did not aggregate after pretreatment with NDGA. α-Synuclein was incubated 1:1 with small molecules for 24 hours then dialyzed against PBS for 24 hours. After aggregation for 3 days, PBS-insoluble α-synuclein was separated by centrifugation (21k g for 10 min). Soluble and insoluble fractions were boiled in SDS, run by SDS-PAGE, and colloidal stained. α-Synuclein in each fraction was quantified by in-gel densitometry. (n = 3). **(b)** Both oligomeric and monomeric α-synuclein species induced by NDGA treatment resist aggregation. α-Synuclein was incubated 1:1 with small molecules for 24 hours then subjected to native state size exclusion chromatography. Oligomeric (≥51Å) and Monomeric (<51Å) α-synuclein fractions were collected and aggregated separately for 3 days. Soluble and insoluble species were separated and quantified as above. (n = 3). **(c)** NDGA-treated α-synuclein resisted fibrillization in the presence of 5% fibril seed. α-Synuclein was incubated 1:1 with small molecules for 24 hours then dialyzed against excess PBS for 24 hours. Untreated α-synuclein fibrils equal to 5% total protein was added immediately before mixtures were aggregated for 3 days. Soluble and insoluble species were separated and quantified as above. (n = 3). **(d)** NDGA pretreated, dialyzed α-synuclein inhibited aggregation of untreated α-synuclein. α-Synuclein was incubated 1:1 with small molecules for 24 hours then dialyzed against excess PBS for 24 hours. Pretreated, dialyzed α-synuclein was then mixed with untreated monomeric α-synuclein at the indicated ratios. Mixtures were aggregated for 3 days. Soluble and insoluble species were separated and quantified as above. (n = 3).

cNDGA reduces α-synuclein-driven dopamine neurodegeneration in animals

We examined the effect of NDGA and cNDGA treatment on α-synuclein-driven neurodegeneration. We employed a widely used *C. elegans* model in which expression of human wildtype α-synuclein in dopaminergic neurons leads to progressive neurodegeneration. Animals were treated with varying doses of NDGA or cNDGA from hatching until the day before scoring on either day 6 or day 8. NDGA did not have a statistically significant effect on the number of animals undergoing neurodegeneration. However, cNGDA caused a significant reduction in the number of animals with degenerating dopamine neurons across all doses at day 8 (Fig. 4.5a). Representative images of animals scored during this experiment show the loss of fluorescent dopamine neuron processes and bodies in solvent and NDGA-treated animals (Fig. 4.5b). This demonstrates, for the first time, that cNDGA can reduce neurodegeneration caused by α-synuclein.

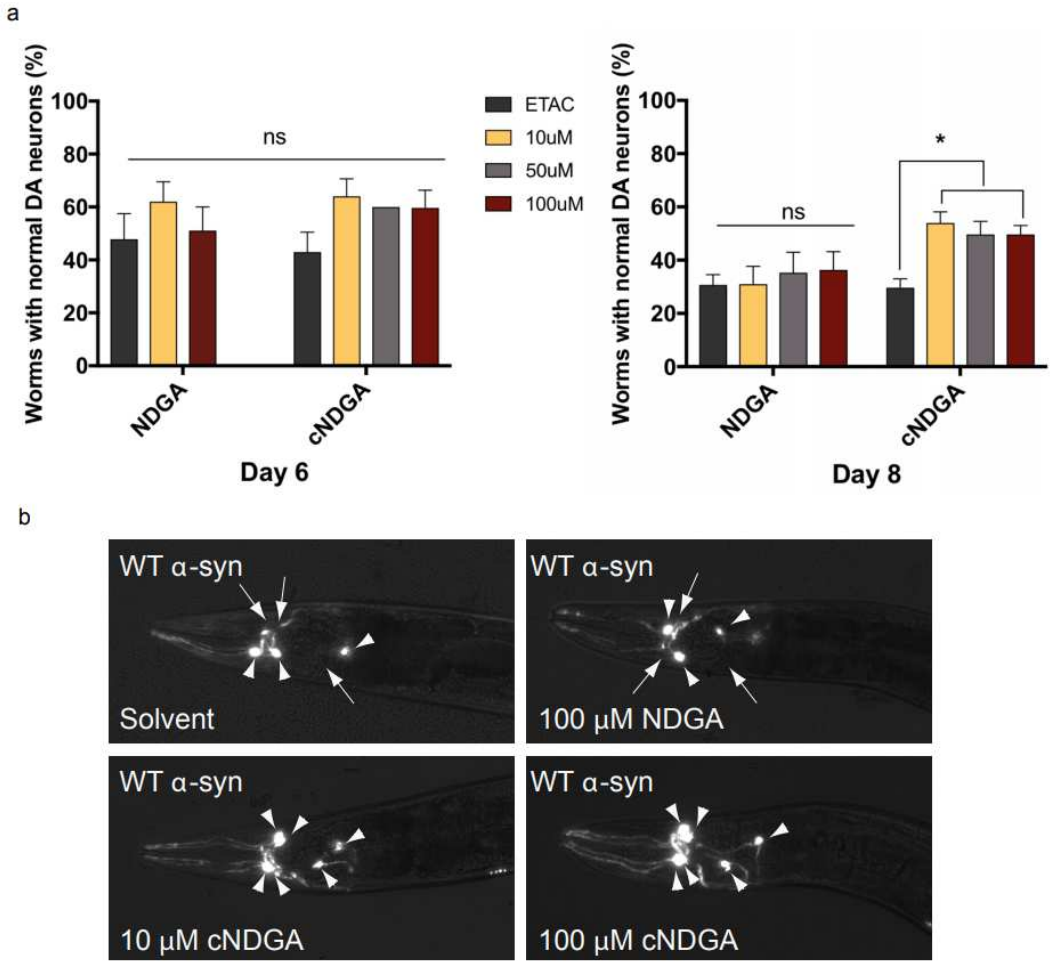

Figure 4.5: cNDGA reduces α-synuclein-driven neurodegeneration. (a) cNDGA, but not NDGA reduces dopaminergic neurodegeneration in *C. elegans* expressing wildtype α-synuclein. Animals were exposed to each concentration of the drugs on days 0-3, 5, and 7 post-hatching. Animals were scored on days 6 and 8 post-hatching for dopaminergic neurodegeneration. The data are represented as mean ± SEM; one-way ANOVA with Tukey's *post hoc* test for multiple comparisons. (n = 3; 30 animals per replicate; * $p < 0.05$; ns, not significant). **(b)** Representative images from day 8 post-hatching. Arrowheads indicate intact neurons while arrows indicate degenerating or missing neurons. Scale bar represents 10 µm.

4.4 Discussion

α-Synuclein aggregation remains a promising target for therapeutic development. Using NDGA and novel analogs, we uncovered that NDGA oxidation and cyclization was required for interaction with monomeric α-synuclein. This interaction caused slight compaction throughout the α-synuclein sequence and prevented α-synuclein aggregation into fibrils. Indeed, NDGA-treated monomers not only resisted aggregation, but prevented aggregation of naïve untreated α-synuclein. Treatment with cNDGA reduced neurodegeneration in an animal model of α-synuclein neurotoxicity. Taken together, these findings suggest that NDGA and related molecules that prevent α-synuclein aggregation without perturbing native structure and associations may be promising targets for PD and related disorders characterized by α-synuclein aggregation.

Attempts to develop therapeutic strategies targeting α-synuclein have included decreasing levels by altering expression (Zharikov et al., 2015b) and clearance (Dehay et al., 2010; Lee, 2004), immunological targeting (Masliah et al., 2005, 2011), and altering aggregation. Many aggregation inhibitors were identified through chemical library screens before being subjected to mechanistic analysis (Conway et al., 2001; Masuda et al., 2006; Ono and Yamada, 2006). The neurotransmitter dopamine, and molecules that share structural and chemical similarities, were the first inhibitors identified and are among the most potent inhibitors of α-synuclein aggregation (Conway et al., 2001).

Identification of dopamine and related phenols as inhibitors of α-synuclein aggregation has led to many studies of phenolic compounds as potentially neuroprotective inhibitors. The most studied of these is EGCG, which is currently undergoing clinical trials in multiple system atrophy, a synucleinopathy characterized by microglial inclusions (Levin et al., 2016). EGCG was found to be neuroprotective in animals treated with MPTP, which induces α-synuclein-dependent dopaminergic neurodegeneration (Chen et al., 2015; Reznichenko et al., 2010). Adding EGCG during *in vitro* α-synuclein aggregation results in less toxic products (Ehrnhoefer et al., 2008). Given the structural differences between EGCG and NDGA, as well as the existing knowledge

about NDGA oxidation and the availability of analogs, we hope that studying NDGA as an α-synuclein aggregation inhibitor will provide new insight into the neuroprotective potential of inhibiting α-synuclein aggregation.

Our analysis revealed some substantial departures between the effects of NDGA and EGCG on α-synuclein. Konijnenberg et al. found, using IM-MS, that EGCG induces α-synuclein compaction (Konijnenberg et al., 2016), while analysis conducted by the same group for this study showed that NDGA and cNDGA cause a more subtle effect (Fig. 4.3a). Likewise, FRET found that EGCG causes substantial α-synuclein remodeling, while NDGA and cNDGA have no measurable effect on intramolecular distances (Fig. 4.3b). We also observed consistent differences in the patterns of SDS-stable multimers present after α-synuclein was treated with EGCG and NDGA (Fig. 4.2b and Supplemental Fig. 4.S2, 4.S5, and 4.S12). This trend of subtle, but measurable, differences between the effect of the two molecules leaves open the possibility of different mechanisms of interaction with α-synuclein and differing biophysical properties of the resulting species.

Previous studies of EGCG have focused on the oligomers formed when α-synuclein is aggregated in the presence of EGCG (Bieschke et al., 2010; Ehrnhoefer et al., 2008; Yang et al., 2017). In this study, we found that α-synuclein aggregation in the presence of EGCG and NDGA does produce oligomers, but that monomers are the predominant product, representing more than 75% of soluble protein (Supplemental Fig. 4.S12). Further, we found that α-synuclein monomers and oligomers induced by pretreatment with EGCG and NDGA both resisted aggregation (Fig. 4.4b). This aggregation was conducted after separation by size-exclusion chromatography, which removed from solution any EGCG or NDGA not interacting with α-synuclein, suggesting a stable interaction or modification of α-synuclein itself. Most strikingly, pretreated species inhibited aggregation of untreated α-synuclein, suggesting a dominant-negative effect on aggregation. This effect, not previously described for EGCG or any other exogenous phenolic inhibitors, may contribute to their neuroprotective effects. The combination of

a durable modification of α-synuclein and a dominant negative effect on aggregation are very desirable given concerns over polyphenol bioavailability in the brain (Pogačnik et al., 2016) and the hepatotoxic side effects seen with EGCG (Lambert et al., 2010; Levin et al., 2016).

Lipid-bound α-synuclein is resistant to aggregation (Zhu and Fink, 2003), and appropriate membrane interactions are implicated in its physiological function (Burré et al., 2014; Dettmer et al., 2017). As such, an ideal therapeutic targeting α-synuclein aggregation would allow normal lipid interaction. Interestingly, both CD and FCS showed that the membrane interactions of α-synuclein were not perturbed by NDGA-treatment (Fig. 4.3f, g, and h). Preservation of α-synuclein membrane interaction may help explain the divergent effects of NDGA and dopamine on neuron viability. Indeed, α-synuclein oligomers induce membrane destabilization and dopamine-induced oligomers may contribute to neurodegeneration in synucleinopathies (Danzer et al., 2007; Mor et al., 2017). Future studies aimed at identifying neuroprotective α-synuclein aggregation inhibitors would be well served by incorporating methods to determine whether membrane interactions are maintained, as is the case with NDGA.

NDGA pretreatment induced an NMR peak shift at His 50 (Fig. 4.3b). His 50 falls within the second α-helical region during α-synuclein interaction with curved lipid membranes, falling in sequence just after the fourth lysine-rich repeat (George et al., 1995; Ulmer and Bax, 2005). His 50 also mediates oligomer-stabilizing interaction between α-synuclein and divalent metal ions, particularly Cu(II) (Binolfi et al., 2006; Rasia et al., 2005). Additionally, His 50 to Gln mutation causes autosomal dominant familial PD and accelerates α-synuclein aggregation *in vitro* (Appel-Cresswell et al., 2013; Ghosh et al., 2013; Proukakis et al., 2013). This suggests that interaction with His 50 could alter α-synuclein aggregation kinetics. Further investigation of the interaction between NDGA and His 50 might provide insight into NDGA's inhibition of α-synuclein aggregation.

The chemistry underpinning dopamine and related small molecule modulators of α-synuclein aggregation includes the capacity for auto-oxidation and the presence of vicinal

hydroxyl (catechol) moieties (Meng et al., 2009; Norris et al., 2005). In this study, we have expanded the previous observations and documented many new mechanistic insights for the biochemistry of catechol structures to inhibit the aggregation of α-synuclein. We found that NDGA-analogs require two pairs of vicinal hydroxyls to interact with α-synuclein. NDGA-1, which contains only one pair of vicinal hydroxyl groups, did not modify α-synuclein or inhibit aggregation. This indicates that NDGA cyclization, which is enabled by its two pairs of vicinal hydroxyls, is required for inhibition of α-synuclein aggregation (Asiamah et al., 2015). Indeed, cNDGA and cNDGA-5, two cyclized analogs of NDGA, were found to inhibit α-synuclein aggregation. The finding that NDGA's cyclized oxidation products are responsible for its effects on α-synuclein aggregation presents the dual opportunities to study NDGA as a prodrug, converted by oxidation-dependent cyclization to active cNDGA, and to examine novel molecules based on the cNDGA structure in hopes of identifying inhibitors of α-synuclein aggregation.

The importance of NDGA cyclization is reinforced by the finding that cNDGA, but not NDGA, treatment reduces neurodegeneration caused by expression of human α-synuclein in dopamine neurons in *C. elegans* (Fig. 4.5). There are many potential explanations for the divergent effects of the two molecules, including differences in stability, uptake, metabolism, and excretion. One possibility is that NDGA does not form cNDGA under these conditions. Oxidation of NDGA likely occurs less frequently in the reducing environment of the cell (Back et al., 2012), and yield of cNDGA may be lower than previously observed. While the cyclization of NDGA has been precisely described under controlled conditions in buffer (Asiamah et al., 2015), it has never been examined in a complex milieu or within a living cell, where other chemistry may occur.

Collectively, these findings change our understanding of the mechanisms of phenolic α-synuclein aggregation inhibitors. We demonstrate, for the first time, that NDGA's interaction with α-synuclein requires oxidation-dependent cyclization, reframing NDGA as a prodrug. Additionally, we show that both NDGA and EGCG stably modify α-synuclein monomers, rendering them aggregation incompetent. In the case of NDGA, this is achieved without altering the structure of

α-synuclein in solution, nor perturbing membrane interactions. This combination of attributes has not been previously observed in other inhibitors of α-synuclein aggregation. Further examination is certainly warranted to determine whether NDGA analogs might provide the basis for novel neuroprotective therapies for PD and related synucleinopathies.

4.5 Methods

In vitro α-synuclein aggregation analyses

Recombinant human wildtype α-synuclein was expressed and purified from *E. coli* as previously described (Winner et al., 2011). Purified α-synuclein was used at at 2 mg/ml (138 μM) with or without small molecules at various molar ratios in PBS with 1% DMSO. Mixtures were aggregated for 3 or 7 days at 37°C shaking at 1400 rpm. Alternatively, purified α-synuclein was incubated for 24 hours with or with equimolar small molecules in PBS with 1% DMSO. Resulting mixtures were then dialyzed against excess PBS for 24 hours at 4°C (using mini-dialysis tubes, Thermo Fisher 69572). Mixtures were aggregated for 3 or 14 days shaking at 1400 rpm.

α-Synuclein solubility analysis and densitometric quantification

Sedimentation was performed by centrifugation at 21,000 g for 15 minutes. Supernatants were removed, and pellets were resuspended in an equal volume. Pellets and supernatants were boiled in SDS sample buffer for 3 minutes at 95°C. α-Synuclein species were resolved by SDS-PAGE in 12% Bis/Tris gels and stained in-gel with colloidal blue (Invitrogen LC6025). Stained gels were imaged at 700 nm using LI-COR Odyssey Infrared Imaging System and densitometric quantification was conducted using LI-COR Odyssey software suite 3.0.

Near infrared fluorescence

SDS-PAGE gels were imaged as previously described (Mazzulli et al., 2016). Briefly, gels were imaged immediately after electrophoresis at 700 nm with intensity 10 on LI-COR Odyssey Infrared Imaging System.

Size-exclusion chromatography

For size exclusion chromatography 200μL recombinant α-synuclein (2mg/ml) was injected onto a Superdex 200 10/300 GL (GE Healthcare) connected to an Agilent 1100 series HPLC system and fraction collector controlled by ChemStation software version 1.04 (Agilent). Mobile phase consisted of 25mM HEPES and 150 mM NaCl, pH 7.25 with a 0.3 ml/min flow rate. Fractions

corresponding to 140-100, 100-85, 85-75, 75-68, 68-61.5, 61.5-56, 56-51, 51-47, 47-43, 43-39, 39, 39-36, 36-32, 32-29, 29-26 Å were combined and concentrated using 3kDa NMWL ultracel microcon filters (Millipore UFC5003). SEC column elution time was calibrated to Å size using globular protein standards (GE Healthcare).

Circular dichroism

Circular dichroism spectra were obtained on a Jasco-810 spectropolarimeter maintained in the Children's Hospital of Philadelphia Protein Core facility. Protein in PBS was diluted to 20 μM in 0.05 M KH_2PO_4 pH 7.8. Spectra were corrected for baseline measurement of an equivalent volume of PBS diluted in KH_2PO_4 buffer. Spectra were collected with a scanning width of 1 nm, at 5 nm/min with 2 accumulations per run.

Transmission electron microscopy

Transmission electron microscopy was conducted on a JEOL1010 maintained in the University of Pennsylvania Electron Microscopy Resource Laboratory. Protein solutions were diluted to 0.5 mg/ml (34.5 μM) before mounting to carbon-coated 300 grids and negative staining with 2% uranium acetate. Images were collected with at HV = 80.0 kV, Magnification 50,000x. Contrast was automatically adjusted during capture for each image, and not altered after capture. 1 μm scale bars were included for each image presented.

Nuclear magnetic resonance spectroscopy

To provide atomic resolution information on α-synuclein, 2D ^{1}H-^{15}N NMR spectra were acquired through a series of BEST-TROSY HSQC (Favier and Brutscher, 2011), a fast and common experiment used to evaluate if there is an effect of the different molecules on some amino acids, each of them represented by a H^N-N correlation (a cross-peak in the 2D spectrum).

All the NMR experiments were recorded on a Bruker Avance III spectrometer operating at 900 MHz ^{1}H frequency (21.14 T) equipped with a cryogenically cooled probehead for triple resonance experiments (TCI). The pulses involved in this pulse sequence were the standard ones used to investigate bio-molecules(Brutscher et al., 2015). The ^{15}N hard pulses were applied at the center

of the region (117.02 ppm) and the ^{1}H band selective pulses were applied at the center of the amide proton region at 8.70 ppm. A spectral width of 10822.511 Hz in the direct ^{1}H dimension and 3647.991 Hz in the indirect ^{15}N dimension was used. All the spectra were recorded with 8 scans per increment, 4096 and 2048 points in the direct dimension and in the indirect dimension respectively and a recycle delay of 500 ms.

The experiments were recorded at 288.0 K on a 165 μM uniformly ^{15}N labeled α-synuclein sample, prepared as previously described (Huang et al., 2005), in buffer (10 mM KPi, 140 mM NaCl, 0.25 mM EDTA + Roche protease inhibitors, pH 7.5). 5% D_2O was added for the lock signal. The different drugs (described above) were added as DMSO solutions at 1:1 stoichiometric ratio and left at room temperature 24 hours to incubate before NMR measurements. The same experiments were acquired on a sample containing 3 equivalents of NDGA. Care was taken to minimize the volume of the DMSO solution added and to keep it constant for all the samples investigated. All the samples were analyzed again in the following days (outlined in Supplementary Table 1) to evaluate thermodynamic and kinetic effects.

Native nano-electrospray ionization mass spectrometry

ESI-MS experiments were conducted as previously described (Konijnenberg et al., 2016). The only methodological departure was the inclusion of DMSO to solubilize the ligands. Briefly, MS spectra were collected after 10 minute incubation of protein-ligand mixtures in 7.4 pH 10 mM ammonium acetate. Spectra were collected using a hybrid quadrupole-time-of-flight mass spectrometer (QSTAR-Elite, Biosystems, Foster City, CA) equipped with a nano-ESI sample source.

Ion mobility mass spectrometry

IM-MS experiments were conducted as previously described (Konijnenberg et al., 2016). The only methodological departure was the inclusion of DMSO to solubilize the ligands. Briefly, MS spectra were collected after 10 minute incubation of protein-ligand mixtures in 7.4 pH 10 mM ammonium acetate. α-Synuclein was present in the mixtures at 20 μM, ligand at 100 μM. Ion mobility-mass

spectrometry (IM-MS) was performed on a Synapt G2 HDMS (Waters, Manchester, U.K.) using nano-ESI with homemade gold-coated borosilicate capillaries.

Fluorescence correlation spectroscopy

Expression of fluorescently-labeled α-synuclein

α-Synuclein protein labeled at residue S9C with Alexa Fluor 488 was produced via recombinant protein production. Plasmid containing α-synuclein S9C fused to a polyhistidine-tagged GyrA intein from Mycobacterium xenopi (Mxe) was transformed into BL21 DE3 competent cells by heat shocking at 42°C. Single colonies grown on Ampicillin (Amp) plates were picked to inoculate primary cultures in LB supplemented with 1μg/mL Amp. Primary cultures were combined into secondary cultures, which were grown at 37°C in a shaker-incubator until optical density (OD) reached ~0.6. Expression of the gene of interest was induced with Isopropyl β-D-1-thiogalactopyranoside (IPTG). Cells were then grown in the shaker-incubator at 18°C overnight. After centrifugation (5000 rpm, 20 min, 4°C), cell pellets were re-suspended in re-suspension buffer (20 mM Tris, 1 mM PMSF, 1 Roche protease inhibitor tablet, pH 8.3) and sonicated in a cup in an ice bath (5 min, 1 s ON, 1 s OFF). The resulting lysate was centrifuged (14,000 rpm, 25 min, 4°C), and supernatant containing the protein of interest (POI) was purified over Ni-NTA affinity column. Intein cleavage was carried out by incubation with 200 mM β-mercaptoethanol (βME) on a rotisserie over night at room temperature. Cleaved POI was dialyzed into 20 mM Tris pH 8 before purification over a second Ni-NTA column to remove the free intein from the sample. Flow-through containing the POI was kept, dialyzed into 20 mM Tris pH 8, and spin concentrated. Labeling with Alexa Fluor 488 (AF488) maleimide was done by adding 4 equivalents (eq.) of fluorophore dissolved in DMSO. The reaction tube was wrapped in aluminum foil and incubated at 37°C for ~6 hrs. Formation of the product α-synuclein C9-AF488 was checked by matrix-assisted laser desorption ionization mass spectrometry (MALDI-MS) and polyacrylamide gel electrophoresis (SDS-PAGE). Labeled protein was purified by fast-protein liquid chromatography (FPLC) using a Hi-Trap Q 5 mL column and by reverse-phase high-performance liquid

chromatography (RP-HPLC) using a C18 preparatory column. Purified protein was spin concentrated into buffer (20 mM Tris, 100 mM NaCl), and aliquots were stored at -80°C.

Treating α-synuclein with drug molecules

The concentration of α-synuclein aliquots was determined by UV-Vis at 488 nm. The drug molecules NDGA, mNDGA, and cNDGA were dissolved in DMSO and diluted 10-fold into buffer (20 mM Tris, 100 mM NaCl). A control of 10% DMSO in buffer was also made. Each aliquot of α-synuclein was respectively treated with 1eq. of NDGA, mNDGA, and cNDGA, and DMSO-buffer. Treatment samples were incubated at room temperature for 8 hours, then dialyzed against 10 mM Tris, 100 mM NaCl overnight.

Preparation of lipid vesicles

Synthetic lipid vesicles were prepared for use in binding experiments. A mixture in 50:50 molar ratio of 1-palmitoyl-2-oleoyl-sn-glycero-3-phosphoserine (POPS) and 1-palmitoyl-2-oleoyl-sn-glycero-3-phosphocholine (POPC) were drawn from chloroform stock and dried under nitrogen gas to form a film inside a glass vial. Films were desiccated under vacuum and re-hydrated in 3-(N-morpholino)propanesulfonic acid (MOPS) buffer. 10 Freeze-thaw cycles consisting of cooling in liquid nitrogen for 40 s and warming in a 60°C water bath for 2 min were performed to aid the formation of uniformly sized vesicles. Using syringes fitted onto an extruder, vesicles were pushed 31 times through 50 nm pore membranes. Vesicles were determined by Dynamic Light Scattering (DLS) to be monodisperse and distributed uniformly around 80 nm in diameter, consistent across different concentrations of all samples. All lipid vesicles were prepared fresh and used within 48 hours of extrusion.

Fluorescence correlation spectroscopy

Eight-well chambered coverglasses (Nunc, Rochester, NY) were prepared by plasma cleaning followed by incubation over night with polylysine-conjugated polyethylene glycol (PEG-PLL), prepared using a modified Pierce PEGylation protocol (Pierce, Rockford, IL). PEG-PLL coated Chambers were rinsed with and stored in Milli-Q water until use. FCS measurements were done

on a lab-built instrument based on an Olympus IX71 microscope with a continuous emission 488 nm DPSS 50 mW laser (Spectra-Physics, Santa Clara, CA). All measurements were done at 20°C. The laser power entering the microscope was adjusted to 4.5 μW. Fluorescence emission collected through the objective was separated from the excitation signal through a Z488rdc long pass dichroic and an HQ600/200m bandpass filter (Chroma, Bellows Falls, VT). Emission signal was focused through a 50 μm optical fiber. Signal was amplified by an avalanche photodiode (Perkin Elmer, Waltham, MA) coupled to the fiber. A digital autocorrelator (Flex03Q-12, correlator.com, Bridgewater, NJ) was used to collect 30 autocorrelation curves of 30 seconds for each measurement. Fitting was done using MATLAB (The MathWorks, Natick, MA).

Binding assay of drug-treated α-synuclein to lipid vesicles

FCS was used to examine the binding affinity of drug-treated α-synuclein to lipid vesicles. Each drug-treated α-synuclein labeled with AF488 was examined in the presence of varying concentrations of lipid vesicles, and each autocorrelation curve was fit to a 2-component equation to extract the fraction of bound α-syn at each concentration. From these data, a binding curve was generated and fit to an exponential to determine the dissociation constant Kd, i.e. the concentration at which half of the protein is bound. In fitting the autocorrelation curves for α-syn in the presence of lipid vesicles, the diffusion time (τ) of bound and unbound α-syn were respectively fixed to experimentally determined values. The diffusion time of unbound protein, ταS, was determined by measurements of the protein in buffer without lipids. Since bound protein diffuses with the vesicles to which they are bound, the diffusion time of the vesicles, τvesicle, was determined by measurements of BODIPY-labeled 50:50 POPS/POPC. The diffusion time of our unlabeled vesicles were also deduced from a calibration curve generated from the diffusion times of commercial fluorescent bead standards of 50 nm and 100 nm in diameter.

To generate a vesicle-binding curve, FCS was performed on α-syn C9-AF488 in the presence of varying concentrations (0.005 mM to 1 mM lipid) of 50:50 POPS/POPC. The accessible surface lipid concentration was calculated based on the characteristic bilayer thickness of POPS and

POPC. The fraction of bound protein was extracted from the fit to each autocorrelation curve by fixing ταS and globally fitting τvesicle to the same value across all concentrations.

$$G(\tau) = \frac{1}{N}\left(F_F * \frac{1}{1+\frac{\tau}{\tau_{\alpha S}}} * \left(\frac{1}{1+\frac{s^2\tau}{\tau_{\alpha S}}}\right)^{1/2} + (1-F_F) * \frac{1}{1+\frac{\tau}{\tau_{vesicle}}} * \left(\frac{1}{1+\frac{s^2\tau}{\tau_{vesicle}}}\right)^{1/2}\right)$$

The fraction bound was plotted against accessible lipid concentration and fit to an exponential, from which the Kd was determined.

$$F_B = \frac{B_{max}x}{K_{d,app}+x}$$

Assay for effect of NDGA on lipid-bound α-synuclein

Untreated α-synuclein C9-AF488 (final concentration 20 μM) was added to 250 μL of 0.05 mM POPS/PC in a microscope chamber well. The sample was incubated for 15 minutes to ensure maximum binding interactions. NDGA stock was made by dissolving the drug in ethanol and diluting 10-fold into buffer (20 mM Tris, 100 mM NaCl). NDGA was added at 20 μM final concentration to the vesicle-bound α-synuclein sample, and fraction of protein bound was determined using the fitting described above. A control treatment was made of 10% ethanol in buffer, and fraction of protein bound was determined in the same manner.

Förster resonance energy transfer anaylsis

Small molecule stock solutions containing either NDGA, EGCG, cNDGA or mNDGA were prepared in DMSO. Labeled proteins constructs, including new constructs not previously described, were prepared using methods previously described (Ferrie et al., 2018). Labeled positions not previously reported were confirmed by mass spectrometry of both the full-length protein and fragments from trypsin digestion using MALDI. The concentration of each protein stock was assessed by UV-Vis absorbance of the attached fluorescein-maleimide [Fam] (ε_{494} = 68,000 $M^{-1}cm^{-1}$) and/or tetramethylrhodamide azide [Raz] (ε_{555} = 87,000 $M^{-1}cm^{-1}$) dyes. Fluorescence assays were performed in a black, clear bottom half-diameter Greiner 96-well plate and measurements were taken on a Tecan M1000 plate reader. Each well of the plate contained

a single protein sample, containing either one or both fluorescent labels, and one of the small molecules of interest. Protein samples were also measured in the absence of small molecules as a control. Each sample was prepared in 1X PBS with a final concentration of 1 μM protein. Samples containing NDGA, EGCG, cNDGA and mNDGA were prepared with a 5-fold excess of small molecules relative to the protein concentration. Small molecule stocks were prepared just prior to performing the assay. Each assay was performed by diluting the protein in buffer in each well and adding the small molecule solution, using a multichannel pipette, just prior to measuring the fluorescence. Each sample was excited at 494 nm and the emission spectrum was measured from 502 - 700 nm with a 1 nm step size. Each step consisted of 50 flashes at a frequency of 400 Hz with a 20 μs integration time and the gain was set to 135. The Z-position of the plate was optimized prior to the first measurement and was maintained at 21728 μm for all measurements. All measurements were performed at room temperature. After measuring the emission spectrum from each well immediately after the introduction of small molecule, the plates were sealed with parafilm and covered in aluminum foil and left at room temperature for 24 hrs. After 24 hrs the fluorescence of each sample was measured again as detailed above. The FRET between Fam and Raz probes attached to a single protein was assessed by computing the fluorescence quenching of the donor Fam fluorophore induced by the presence of the Raz acceptor as previously described (Ferrie et al., 2018). FRET efficiencies were converted to average interresidue distances using the Förster equation and a gaussian chain polymer model.

Analysis of dopaminergic neurodegeneration in *C. elegans*

Generation of transgenic nematodes

Transgenic *C. elegans* lines were generated by microinjection using previously described methods (Berkowitz et al., 2008). The strain UA294 (*baEx175 a,b,c* [P_{dat-1}::WT a-syn, P_{unc-54}::tdTomato]; *vtIs7*[P_{dat-1}::GFP]) was generated by injecting with a solution of 50 ng/μl plasmid with either P_{dat-1}::WT a-syn with a phenotypic marker (P_{unc-54}::tdTomato, 50 ng/μl, for body wall muscle expression). Three distinct stable lines (*a, b, c*) were generated.

Analysis of dopaminergic neurodegeneration and NDGA analog treatments in C. elegans

NDGA and cNDGA were used at final concentrations of 10μM, 50μM, or 100μM in ethyl acetate (EtAc). Three resulting independent transgenic lines (*a, b, c*) were synchronized, and exposed to corresponding concentration of NDGA, cNDGA, or solvent (EtAc) from hatching to day 3, then were transferred and maintained on NGM plates until the day of analysis. Animals on NGM plates were treated with additional NDGA, cNDGA, or solvent on days 5 and 7. For dopaminergic neurodegeneration analyses, the transgenic animals were scored as described previously (Hamamichi et al., 2008). Briefly, on the day of analysis, the six anterior dopaminergic neurons (four CEP (cephalic) and two ADE (anterior deirid)) were examined in 30 randomly selected nematodes with the marker transgene (tdTomato) in the body wall muscle cells. Worms were considered normal when all six anterior neurons were present without any signs of degeneration, such as broken dendritic process, cell body loss, dendritic blebbing, or a missing neuron. In total, at least 90 adult worms were analyzed for each treatment condition, at least 30 for each independent transgenic line. An average of total percentage of worms with normal neurons was reported in the study.

Reagents

Nordihydroguaiaretic acid, NDGA 74540 Aldrich; (−)- Epigallocatechin gallate, EGCG E4143 Sigma; Terameprocol/mNDGA, T3455 Sigma; Catalase, C9322 Sigma; NDGA analogs NDGA-1, SECO-1, NDGA-5, cNDGA, and cNDGA-5 were generated, purified, and validated by Krol et al. at the University of Saskatchewan as previously described (Asiamah et al., 2015).

Statistical analysis

Statistical analysis was conducted using Prism 5 software (GraphPad). Unpaired students *t* test was used for comparisons between two groups. Comparisons between multiple independent groups used one-way ANOVA with Tukey's *post hoc* test for multiple comparisons. Comparisons involving multiple groups, such as molecule and dose comparisons, used two-way ANOVA with

Tukey's *post hoc* test for multiple comparisons. In all cases $p < 0.05$ was considered statically significant.

4.6 Supplemental Figures

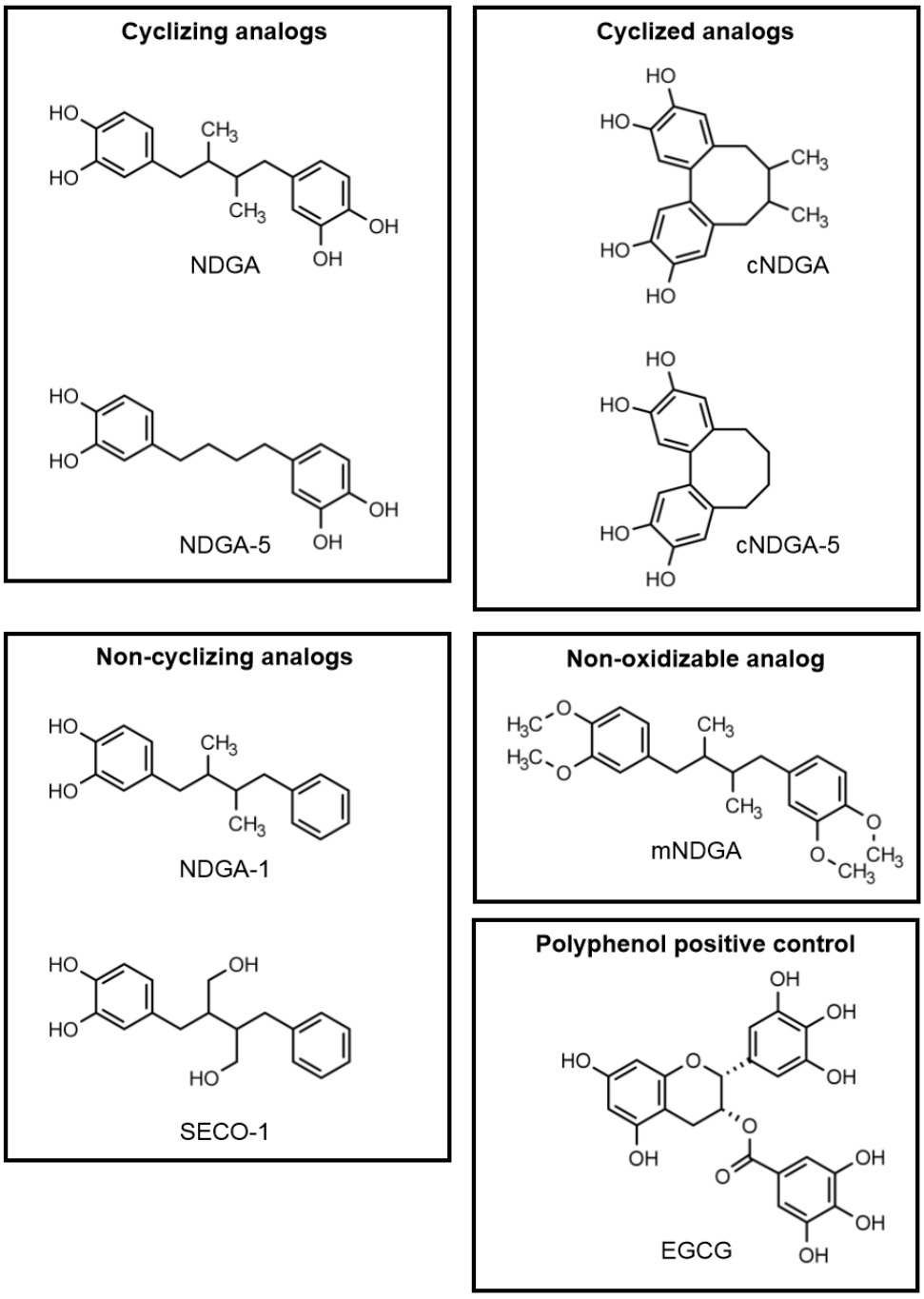

Figure 4.S1. Structures of EGCG, NDGA, and NDGA analogs employed in this study.

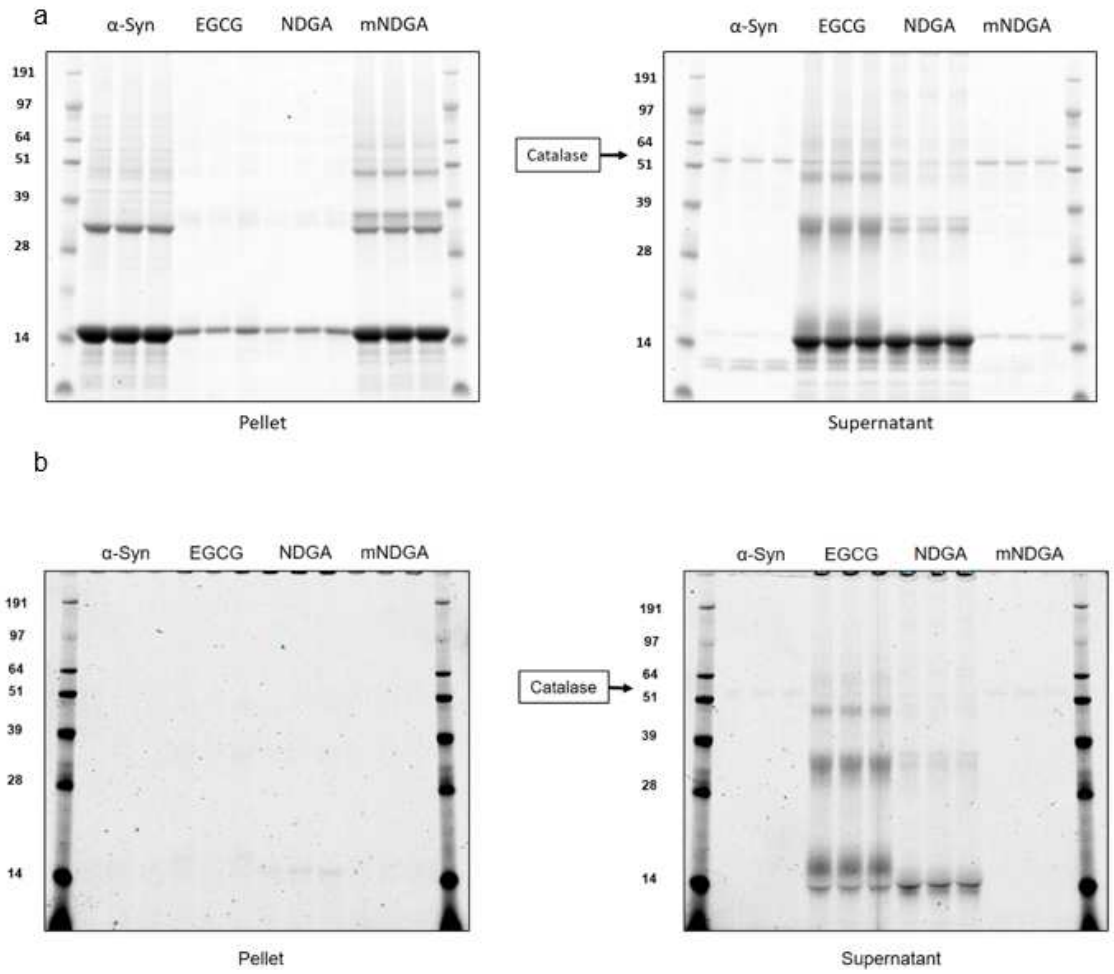

Figure 4.S2: Colloidal and nIRF images of α-synuclein aggregation in the presence of 5% catalase. (a) Colloidal stained gel **(b)** nIRF image of the same gel before colloidal staining

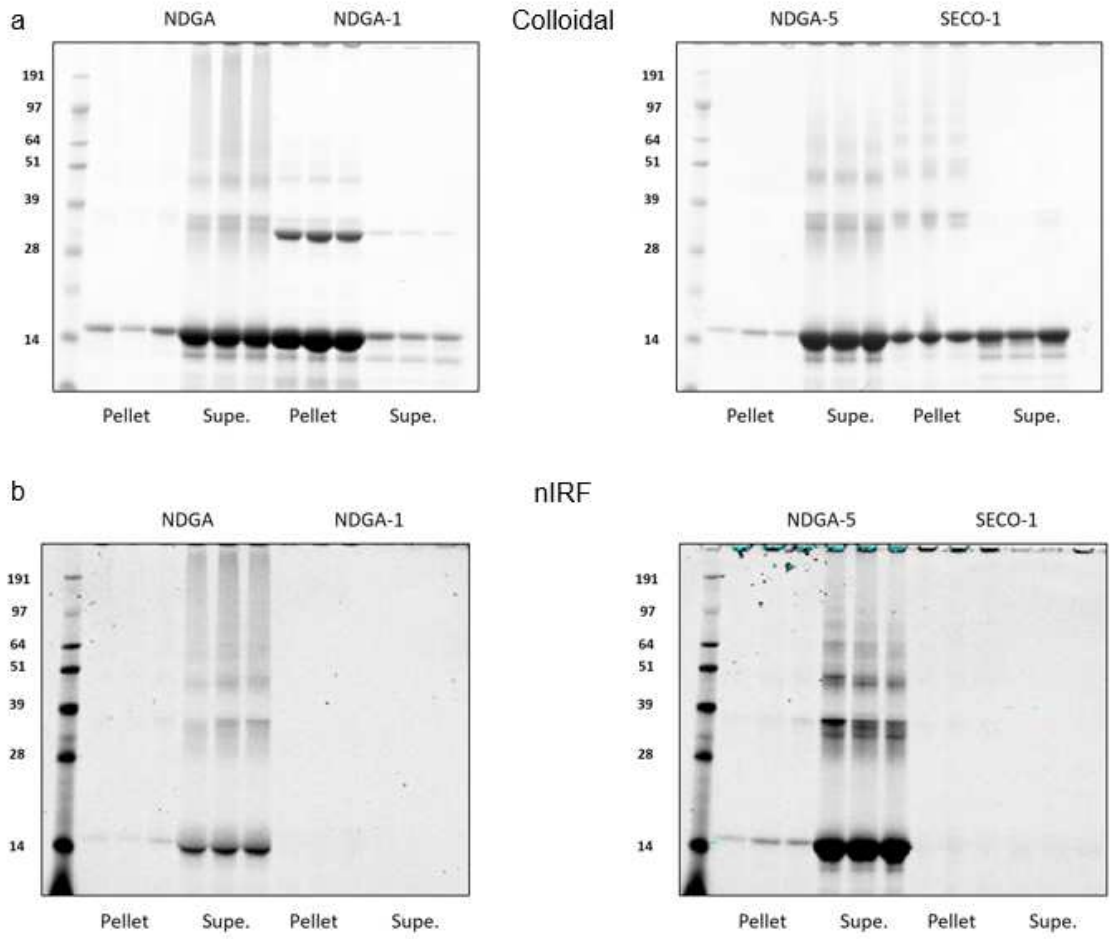

Figure 4.S3: Colloidal and nIRF images of α-synuclein aggregation in the presence of NDGA analogs. (a) Colloidal images of gels after separation by centrifugation. **(b)** Near-infrared images of the same gels before colloidal staining.

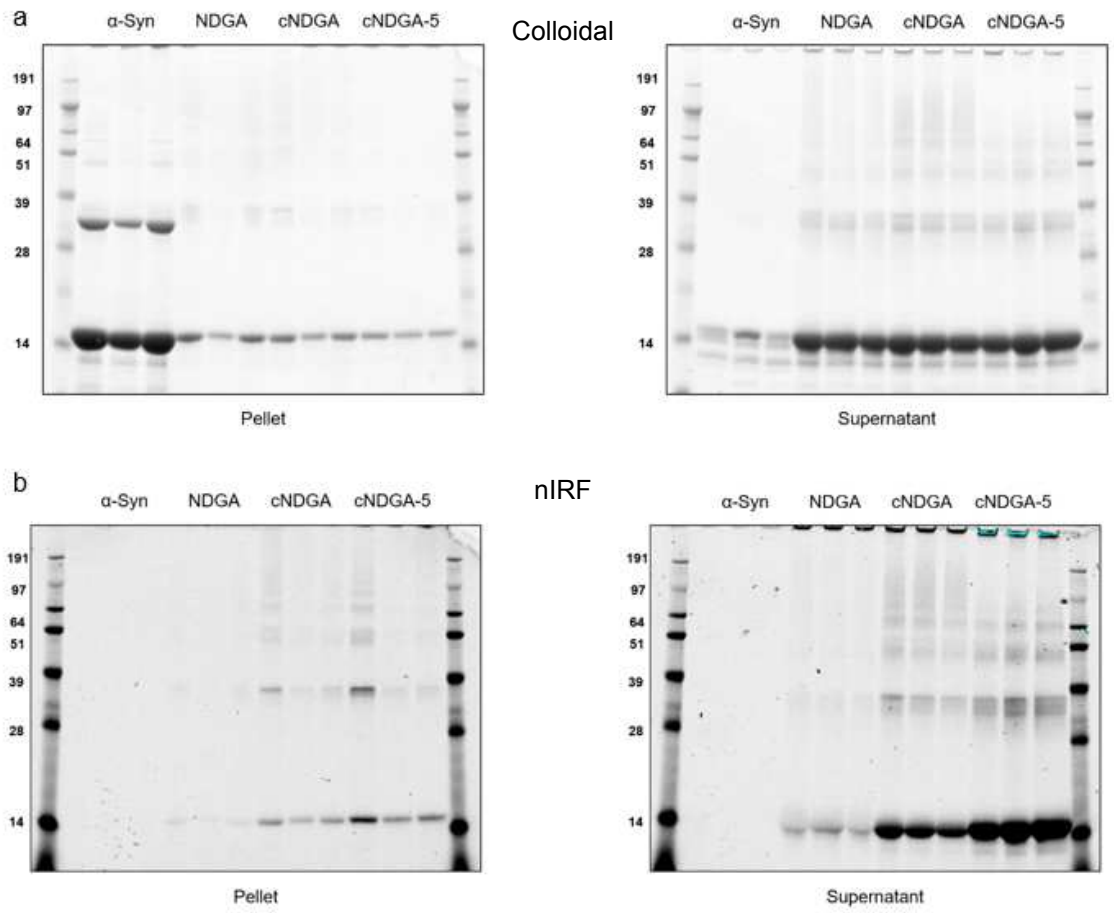

Figure 4.S4: Colloidal and nIRF images of α-synuclein aggregation in the presence of cyclized NDGA analogs. (a) Colloidal images of gels after separation by centrifugation. **(b)** Near-infrared images of the same gels before colloidal staining.

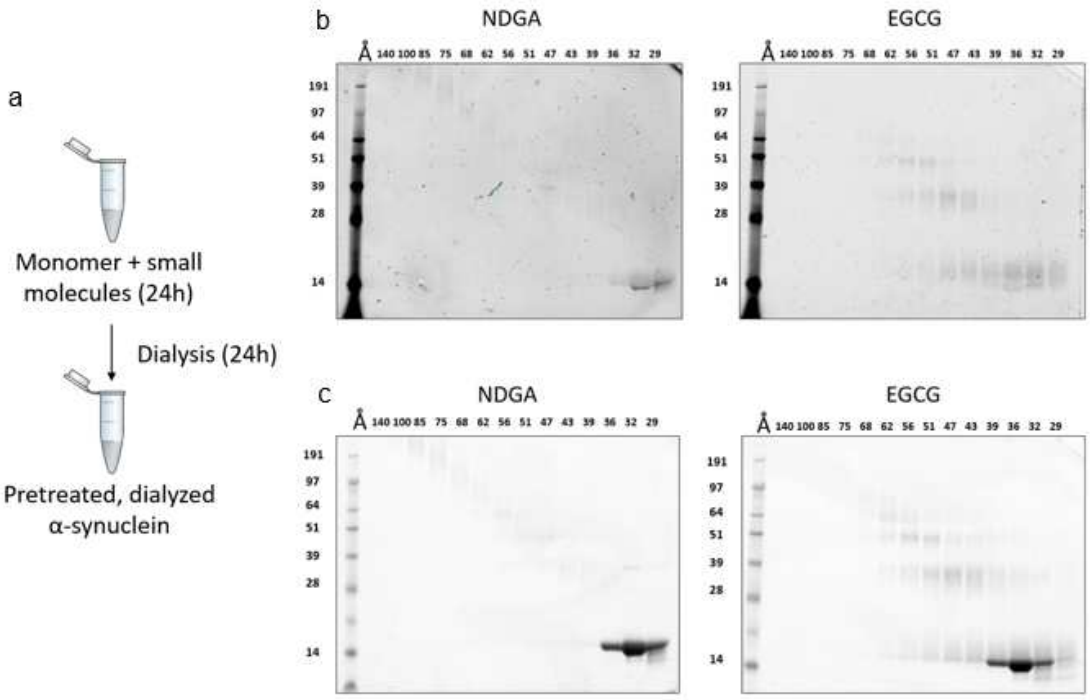

Figure 4.S5: NDGA pretreatment produces nIRF positive α-synuclein monomers. (a) Workflow for CD analysis and aggregation. **(b)** Near-infrared fluorescence images of NDGA and EGCG pretreated, dialyzed α-synuclein separated by native-state size-exclusion chromatography. **(c)** Colloidal staining of the same gels shown in panel b.

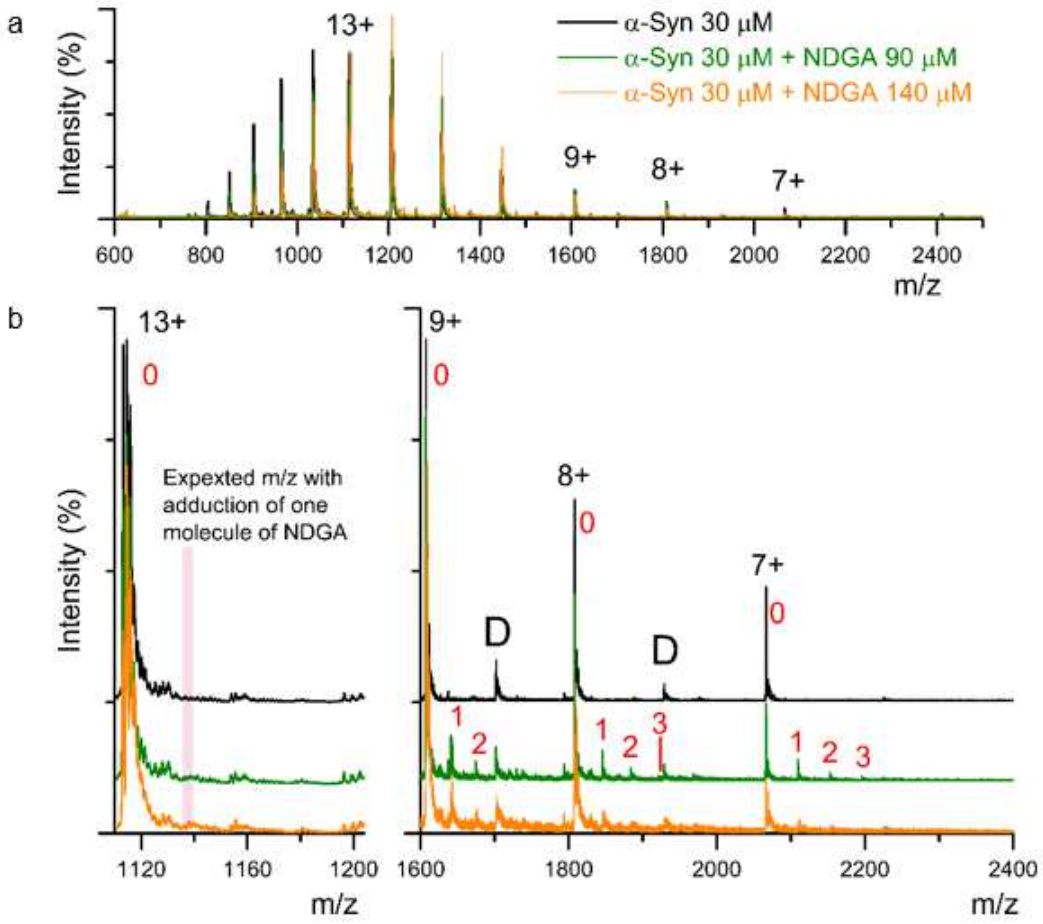

Figure 4.S6: Electrospray mass spectrometry characterization of α-synuclein-NDGA interaction. (a) Nano-ESI-MS spectra in positive-ion mode of 30 μM α-synuclein in the absence and presence of NDGA at 90 μM and 140 μM. **(b)** Magnification of the spectra in the Upper panel. The number of NDGA molecules bound to α-synuclein monomers is indicated by red numbers. Dimer-specific peaks of α-synuclein are labeled as "D". Charge states are indicated by black numbers.
Nano-ESI-MS spectra were collected as described in Konijnenberg et al., 2016.

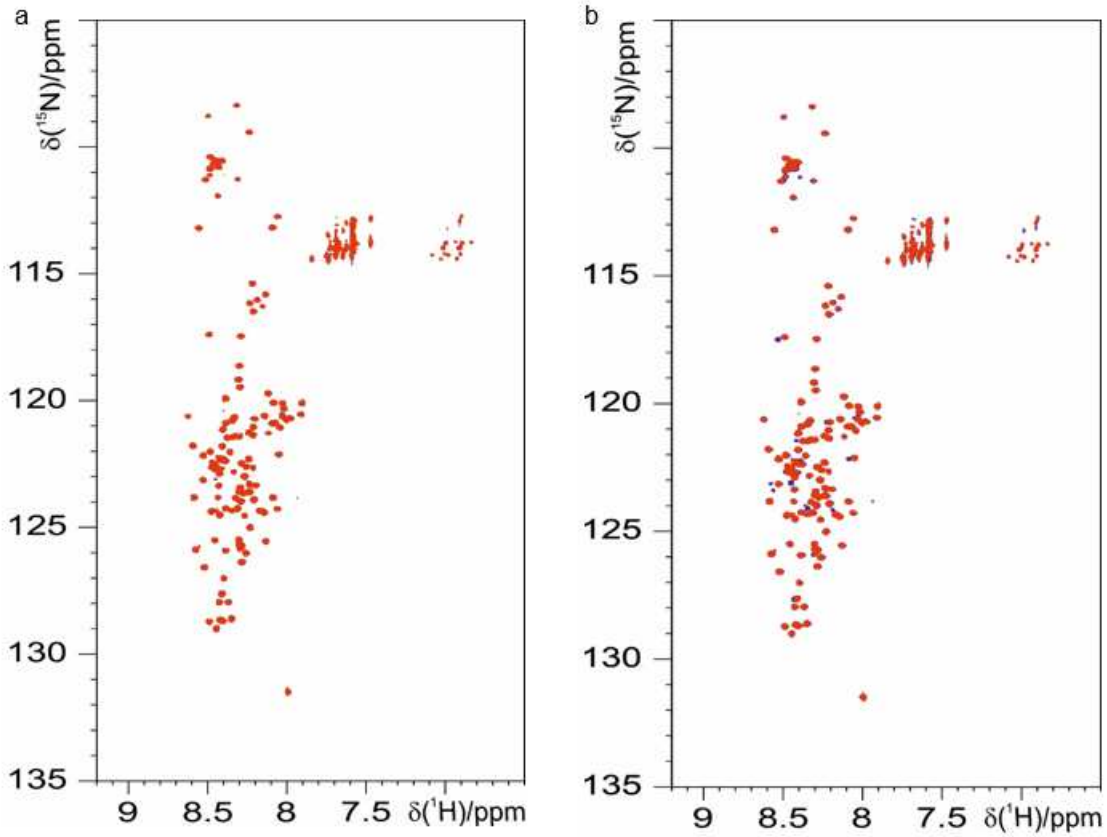

Figure 4.S7: 2D NMR spectra comparing α-synuclein treated with 1:1 NDGA for 24 hours (red), with **(a)** α-synuclein treated with 3:1 NDGA for 24 hours (blue), and **(b)** α-synuclein treated with 1:1 NDGA for 10 days (blue).

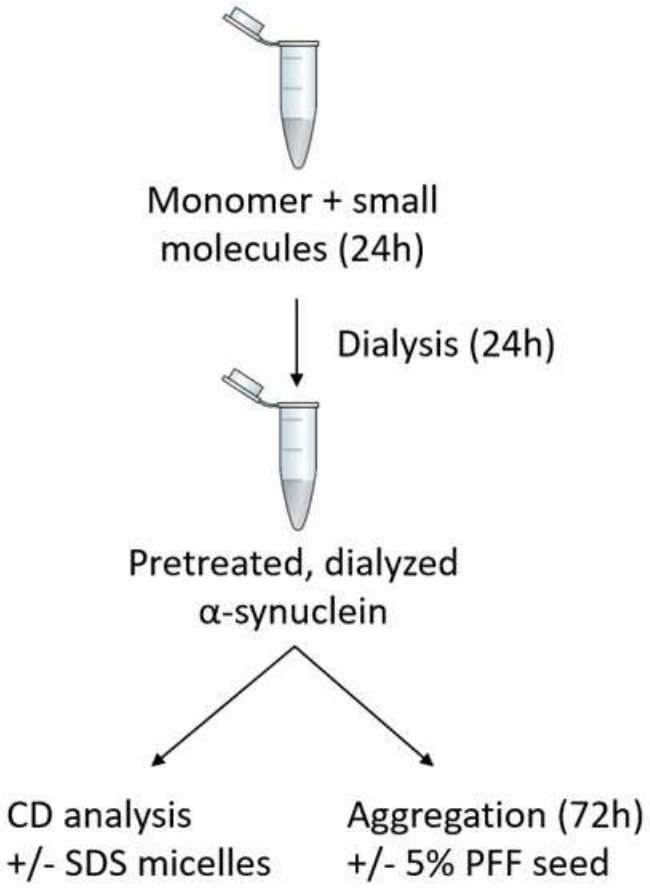

Figure 4.S8: Workflow for analysis of pretreated, dialyzed α-synuclein

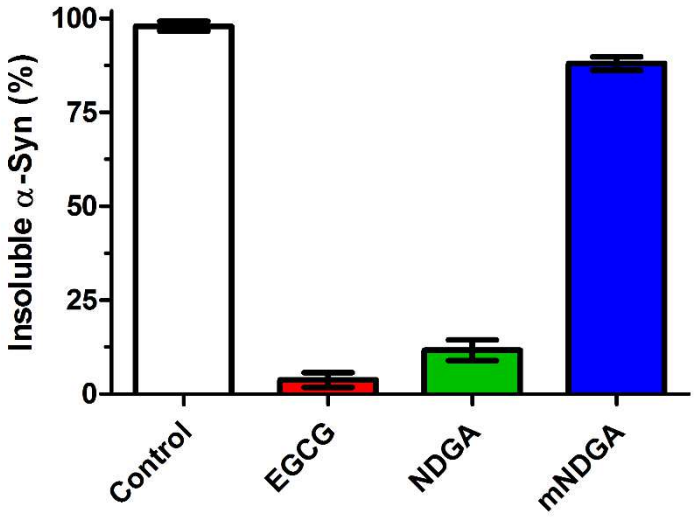

Figure 4.S9: NDGA pretreatment inhibits α-synuclein aggregation despite 14 days under aggregation conditions.

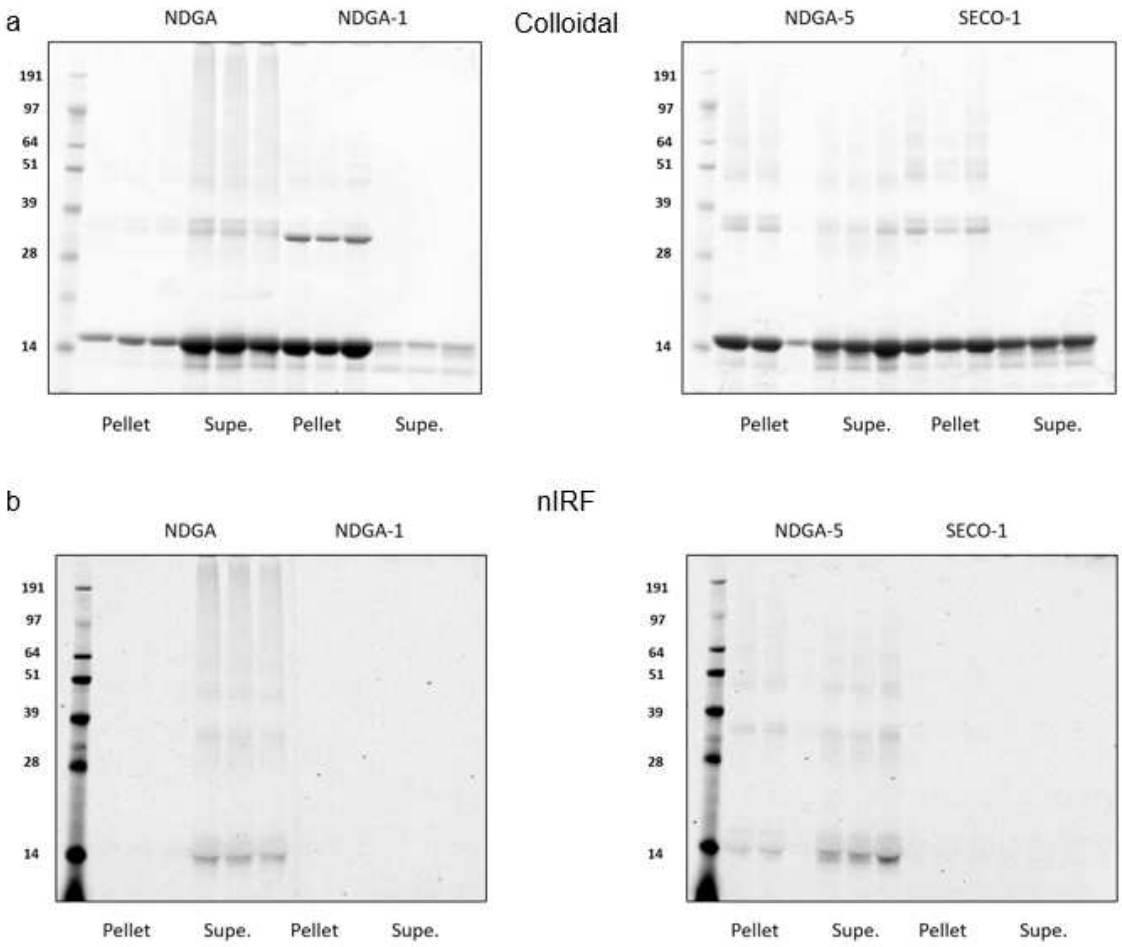

Figure 4.S10: Colloidal and nIRF images of NDGA analog pretreated, dialyzed α-synuclein aggregation (a) Colloidal images of gels after separation by centrifugation. **(b)** Near-infrared images of the same gels before colloidal staining.

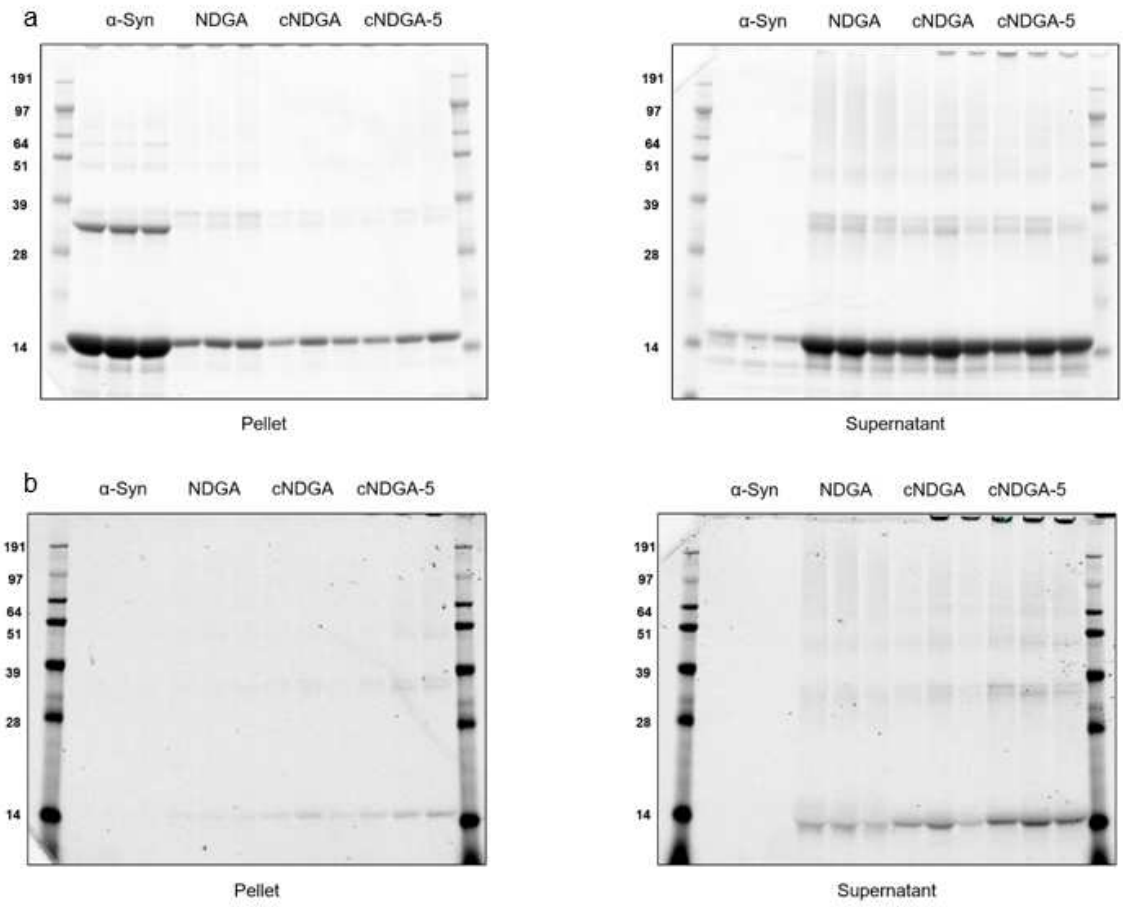

Figure 4.S11: Colloidal and nIRF images of cyclized NDGA analog pretreated, dialyzed α-synuclein aggregation (a) Colloidal images of gels after separation by centrifugation. **(b)** Near-infrared images of the same gels before colloidal staining.

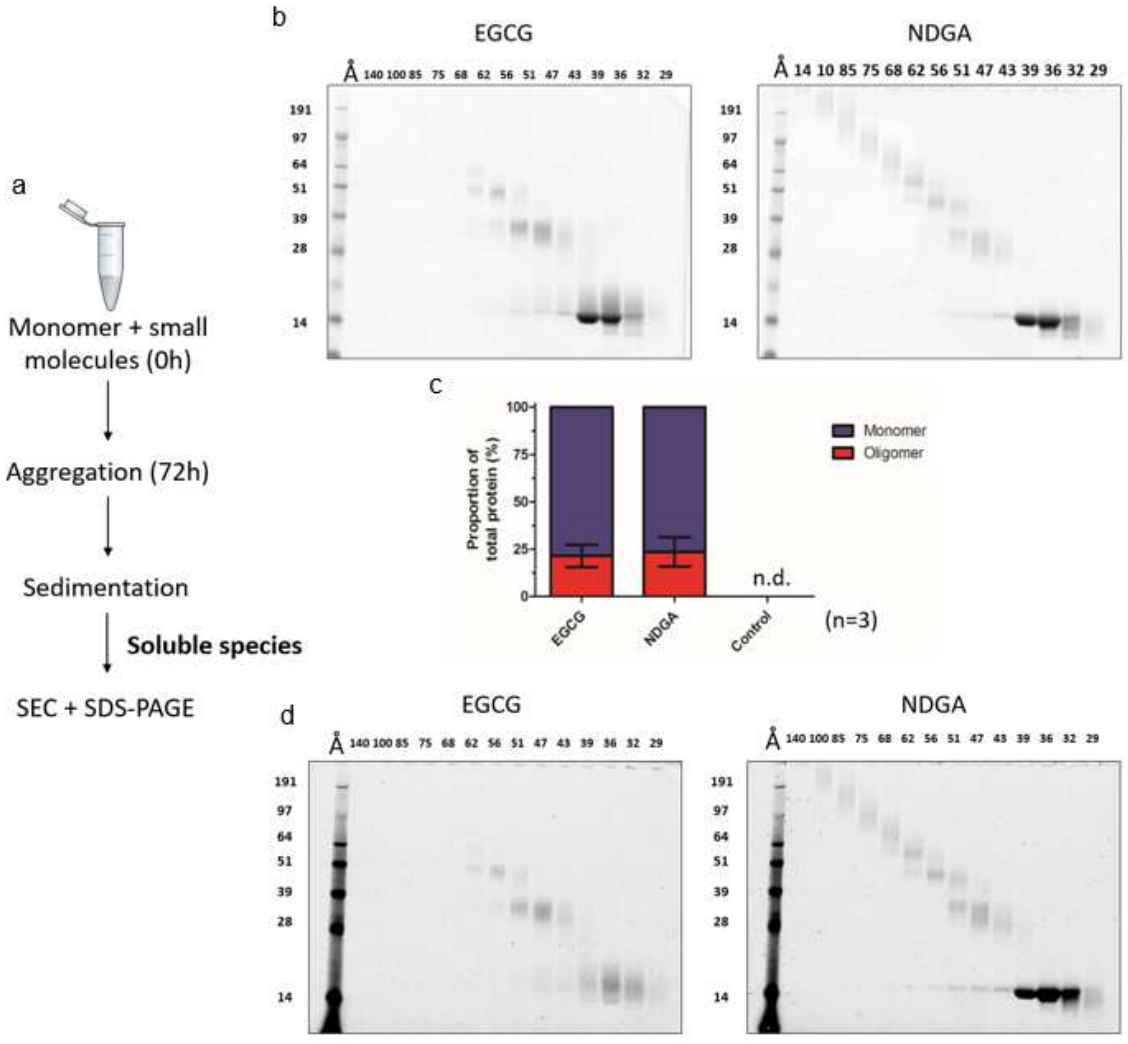

Figure 4.S12: nIRF positive monomers are the predominant product of α-synuclein aggregation in the presence of EGCG and NDGA. (a) Workflow **(b)** Colloidal **(c)** Densitometry **(d)** nIRF

CHAPTER 5: SUMMARY AND CONCLUSION

Lewy bodies serve as the histopathological hallmark of sporadic PD. Their presence correlates with disease progression and, more roughly, with dysfunction in the regions containing pathology (Braak et al., 2003; Emre, 2003). However, this correlation is imperfect, as highlighted by the presence of Lewy bodies in some non-parkinsonian patients and the lack of Lewy pathology in certain forms of PD (Ding et al., 2006; Gaig et al., 2007). Despite the uncertainty surrounding the relationship between Lewy pathology and neurodegeneration in sporadic PD, results from familial forms of PD and animal models strongly imply that α-synuclein aggregation drives neuron dysfunction and eventual death. All of the SNCA gene mutations that drive familial forms of PD cause alterations in α-synuclein aggregation kinetics (Appel-Cresswell et al., 2013; Krüger et al., 1998; Lesage et al., 2013; Pasanen et al., 2014; Polymeropoulos et al., 1997; Proukakis et al., 2013; Zarranz et al., 2004). Likewise, transgenic animals expressing these mutants show both pathology and neurodegeneration, though none perfectly recapitulates human disease caused by the same mutation (Emmer et al., 2011; Giasson et al., 2002; Gomez-Isla et al., 2003; Lee et al., 2002; van der Putten et al., 2000).

Compelling evidence for the neurotoxicity of α-synuclein aggregation can been found in animal models driven by PFF injection. In these models, injection of α-synuclein aggregates into wildtype mice gives rise to progressive α-synuclein aggregation and concomitant neurodegeneration (Luk et al., 2012b, 2012a). Notably, this phenotype is dependent on the aggregation of endogenous α-synuclein and does not occur in SNCA knockout mice. α-Synuclein aggregate injection has been shown to induce pathology and neurodegeneration in several mammals (Manfredsson et al., 2018; Shimozawa et al., 2017) and similar results are induced by injection of Lewy body extracts from PD patients (Holmqvist et al., 2014; Recasens et al., 2014). Considered alongside the evidence from sporadic and familial PD, these data further strengthen the arguments that some unknown form or forms (Peng et al., 2018) of aggregated α-synuclein act as pathogenic seeds, leading to the propagation of pathology throughout the brain (a feature

that may be shared by other neurodegenerative diseases (Guo and Lee, 2014)), and that the aggregation of α-synuclein drives neurodegeneration.

The later conclusion begs the question of which processes during α-synuclein aggregation, or products thereof, cause neurotoxicity. This study aimed to provide tools and understanding to address this deficit. We reviewed how the dynamic structure of α-synuclein affects its physiological functions and roles in pathology. We endeavored to untangle the cellular processes involved by examining the changes in the mouse brain proteome and phosphoproteome during α-synuclein aggregation. We deepened understanding of the products of aggregation by evaluating the chemistry and products of the interaction between α-synuclein and NDGA, a putatively neuroprotective α-synuclein aggregation inhibitor.

Chapter 2 underscores how much of α-synuclein function and pathology can be traced to its remarkable structural dynamism. α-Synuclein's role in the synapse is made possible by interactions with lipids, other α-synuclein monomers, and lipid-bound V-SNAREs (Burré et al., 2010, 2014; Davidson et al., 1998; Wang et al., 2014; Zhu et al., 2003b). Identifying the native state of α-synuclein remains difficult, and it seems increasingly unlikely that there is one single cytosolic conformation of α-synuclein. Native states may include lipid-containing conformations, multimers, and monomeric conformers (Bartels et al., 2011; Gould et al., 2014; Wang et al., 2011). Despite this complexity, many studies have found that disturbance of native α-synuclein structure increases its propensity to aggregate. In fact, all SNCA mutations linked to early onset PD fall in the α-synuclein N-terminal domain involved in lipid and protein interaction. Indeed, these mutations perturb native multimers/conformers (Dettmer et al., 2015a). Further, mutations designed to interrupt native structure also alter vesicular trafficking (Dettmer et al., 2017). Taken together, existing research shows that complex dynamics link α-synuclein's native state, its interactions with vesicular function, and its propensity for pathological aggregation. When considered through the lens of therapeutic development, this demonstrates the importance of examining the effect of any intervention on the native structure of α-synuclein.

The findings presented in Chapter 3 represent the first proteomic analysis of the mouse brain undergoing neurodegeneration due to endogenous α-synuclein aggregation. Our analysis was able to quantify relative abundance (between healthy and diseased hemispheres) of more than 6,000 proteins and 8,000 phosphopeptides. Among these, only 6% of proteins and 1.6% of phosphopeptides changed in relative abundance during α-synuclein aggregation. This demonstrates that proteomic changes were limited to a small subset of proteins. This result does not support the hypothesis that widespread proteostatic disruption mediates α-synuclein neurotoxicity (Balch et al., 2008; Douglas and Dillin, 2010). Significant changes were observed in the relative abundance of several proteins involved in dopamine biosynthesis and neurotransmission, consistent with localized dysfunction of dopamine neuron synapses. Ontological analysis of proteins with significant changes in relative abundance showed marked changes in the areas of mRNA processing, mRNA binding, protein translation, and protein folding, suggesting adaptive proteostatic responses to α-synuclein aggregation and neurodegeneration.

Of particular interest, Lmp7—a component of the immunoproteasome—increased in hemispheres undergoing α-synuclein aggregation. Strikingly, this result was observed in each of the varying statistical workflows evaluated during the preparation of the manuscript. The immunoproteasome is induced in other neurodegenerative diseases, but had never been studied in synucleinopathies (Aso et al., 2012; Díaz-Hernández et al., 2003; Mishto et al., 2006; Orre et al., 2013). We found increases in Lmp7 levels and immunoproteasome function in brain tissue from patients with PD and DLB. *In vitro,* the immunoproteasome degraded α-synuclein aggregates, producing potentially antigenic peptide fragments (Sulzer et al., 2017). In totality, these data demonstrate that the immunoproteasome is induced in response to α-synuclein aggregation and directly digests α-synuclein fibrils. The data further suggest that Lmp7 may modulate inclusion formation, propagation, and neuroinflammation.

Functional immunoproteasome knockout mice exist (Kincaid et al., 2011) and PFF injection of these mice could provide an excellent model in which to test whether induction of the immunoproteasome during α-synuclein aggregation is protective or deleterious. Activity of the immunoproteasome can also be manipulated pharmacologically (Muchamuel et al., 2009), raising the possibility of the immunoproteasome as a druggable target in human disease. However, it is difficult to predict the downstream effects of genetic or pharmacological reduction of immunoproteasome activity during α-synuclein aggregation. If immunoproteasome induction in the brain produces α-synuclein peptide fragments that cause T-cell activation, the induction may contribute to the neuroinflammation that occurs prior to neurodegeneration driven by α-synuclein aggregation (Duffy et al., 2018; Sulzer et al., 2017). Indeed, dopaminergic neurons in the SNpc express MHC-I and MHC-I-induced T-cell activation leads to neuron death (Cebrián et al., 2014). Additionally, partial degradation of α-synuclein fibrils might increase the number of seeding-competent α-synuclein species in the brain, accelerating the spread of pathology (Luk et al., 2012b; Tran et al., 2014). This uncertainty underscores the value of investigating the effect of Lmp7 induction on α-synuclein aggregation pathology and neurodegeneration.

The study of NGDA, presented in Chapter 4, first sought to elucidate the chemistry of the interaction between NDGA and α-synuclein. NDGA shares the vicinal hydroxyl substitution responsible for the interaction between α-synuclein and dopamine (Conway et al., 2001). As with dopamine, and related catecholamines (Mazzulli et al., 2007; Norris et al., 2005), NDGA must undergo oxidation to interact with α-synuclein. NDGA analogs allowed for further insight into the interaction between NDGA and α-synuclein. Oxidation-dependent cyclization of NDGA was required for interaction with α-synuclein and inhibition of aggregation. As mentioned in Section 4.4, this recasts NDGA as a prodrug that can be oxidized to form α-synuclein-interaction competent cNDGA. As such, if future studies employ NDGA and related analogs, careful consideration should be given how rates of oxidation and cyclization might impact bioavailability and side-effects. Particular attention should be given to hepatotoxic side-effects which are

common in studies evaluating aggregation-inhibiting polyphenols, such as EGCG and exifone (Lambert et al., 2010; Levin et al., 2016; Ouzan et al., 1990). Promisingly, rates of NDGA cyclization have already been manipulated though rational chemical modification of the crosslinker connecting the two aromatic rings. Reducing steric hindrance in the region increases kinetics and yield of NDGA cyclization (Asiamah et al., 2015).

Given the importance of α-synuclein conformation—reviewed in Chapter 2—we also analyzed the conformational effects of NDGA. Independent analysis by IM-MS, NMR, and FRET found that NDGA and cNDGA induced only subtle conformational changes. Both compounds caused slight compaction of monomeric α-synuclein, which progressed with incubation time. These effects were much less profound than those caused by EGCG in previous studies employing IM-MS and NMR (Ehrnhoefer et al., 2008; Konijnenberg et al., 2016). Likewise, FRET analysis showed that EGCG induced significant changes in α-synuclein conformation after 24 hours, while NDGA was indistinguishable from negative controls. As α-synuclein physiological function requires membrane interaction (Burré et al., 2010; Lou et al., 2017), we also measured the effect of NDGA treatment on phospholipid binding affinity using FCS. FCS found that treatment with NDGA and cNDGA did not alter phospholipid binding affinity, nor did NDGA displace lipid-bound α-synuclein. This result demonstrates that while interaction with cNDGA prevents α-synuclein aggregation, it does not alter native α-synuclein conformational dynamics essential for physiological function.

Maintaining the dynamic structure of monomeric α-synuclein suggests two potential advantages when considering NDGA analogs as potential neuroprotective anti-aggregation therapies. First, this attribute might preserve α-synuclein's function in the presynapse. Membrane-bound α-synuclein mediates SNARE function and vesicular fusion (Burré et al., 2010; Lou et al., 2017). α-Synuclein multimerization has also been implicated during this process (Burré et al., 2014; Wang et al., 2014), highlighting the importance of complex interactions. Disruption of α-synuclein function in the synapse does not cause profound neurological dysfunction (Abeliovich

et al., 2000; Dettmer et al., 2017; Vargas et al., 2014), but prolonging typical neurotransmission should be paramount during neurodegeneration. Second, membrane binding may enhance aggregation resistance of NDGA-treated α-synuclein. During *in vitro* aggregation of α-synuclein, levels of lipid binding directly correlate with lag time to fibril formation (Zhu and Fink, 2003). Likewise, native multimers/conformers are more resistant to aggregation (Bartels et al., 2011) and mutation of the lysine-rich repeats implicated in lipid binding and multimerization leads to inclusion formation (Dettmer et al., 2015b). Indeed, using small molecules to stabilize α-synuclein-lipid interactions both reduces inclusion formation and cytotoxicity (Fonseca-Ornelas et al., 2014).

It is important to note that there is some controversy around the role of lipids in α-synuclein aggregation. Lipids may enhance fibril nucleation (Galvagnion et al., 2015) and one small molecule has been shown to displace α-synuclein from lipids while reducing aggregation (Perni et al., 2017). However, given the physiological role of lipid-bound α-synuclein and the importance of native multimerization in reducing aggregation, the preponderance of evidence supports the conclusion that disrupting native conformations increases the likelihood that α-synuclein will form pathological aggregates.

Ultimately, our study of NDGA was motivated by its potential to reduce α-synuclein aggregation. As expected, its presence during aggregation prevented α-synuclein fibril formation (Ono and Yamada, 2006). Remarkably, however, pretreatment with either NDGA or EGCG rendered α-synuclein resistant to aggregation, even after dialysis or native-state SEC was used to remove unbound NDGA or EGCG from the aggregation mixture. This effect persisted during a two week aggregation of pretreated α-synuclein, suggesting the modification is highly stable. Adding fibril seeds to the aggregation mixture did not induce aggregation of pretreated α-synuclein, demonstrating that the effect does not simply prevent fibril nucleation, but that pretreated α-synuclein is resistant to incorporation into existing fibrils. One potential explanation of these effects is that the slight conformational changes induced by NDGA treatment might

prevent α-synuclein aggregation. Another is that the SDS-stable, dialysis-resistant interaction that occurs between NDGA oxidation products and α-synuclein (observed by near-infrared fluorescence) results in a chemical change, or direct steric hindrance, that prevents incorporation into α-synuclein fibrils.

Most strikingly, the presence of pretreated α-synuclein inhibited aggregation of naïve, untreated α-synuclein. To the best of our knowledge, this dominant-negative effect has not previously been documented with EGCG nor any other neuroprotective inhibitor of α-synuclein aggregation. Our study does not explore the mechanism by which this effect occurs. It is possible that pretreated α-synuclein interacts with and transforms untreated α-synuclein monomers, or recruits untreated α-synuclein into aggregation-resistant multimers. This seems unlikely given the random coil structure exhibited by pretreated recombinant α-synuclein in solution, which is inconsistent with the α-helical structure exhibited by aggregation-resistant α-synuclein multimers extracted from cells (Bartels et al., 2011; Wang et al., 2011). Likewise, given the slight conformational changes observed, there is no ready explanation for why untreated α-synuclein would adopt the same conformation in solution. Instead, it seems more likely that incorporation of pretreated α-synuclein into fibrils or oligomers composed of untreated α-synuclein renders them aggregation incompetent. This hypothesis provides an explanation for the dominant-negative effect without having to propose that structural changes propagate between pretreated and untreated monomers. It is also consistent with our observation of α-synuclein oligomers after α-synuclein aggregation in the presence of both EGCG and NDGA (Fig 4.S12), as well as previous reports of EGCG-stabilized oligomers (Ehrnhoefer et al., 2008).

Results from *C. elegans* reinforced the potential for neuroprotective therapies based on NDGA analogs and the importance of cyclization in NDGA's interaction with α-synuclein. Expression of α-synuclein in *C. elegans* dopamine neurons leads to age-related progressive degeneration that can be altered by direct interaction between α-synuclein and small molecules (Mor et al., 2017). NDGA treatment of these animals failed to alter the neurodegenerative

phenotype. However, treatment with cNDGA reduced the number of animals experiencing neurodegeneration. This divergence is striking given the similarity of the effects of NDGA and cNDGA on α-synuclein conformation and aggregation *in vitro*. Potential explanations for this difference are discussed in Section 4.4, though no conclusion can be reached based on the current study. Regardless, the finding that cNDGA, but not NDGA, affords protection against α-synuclein-driven neurodegeneration powerfully underscores the importance of considering NDGA cyclization in subsequent studies of its interaction with α-synuclein. Pending further study, our findings suggest that cNDGA should be considered the active form of NDGA with regard to inhibiting α-synuclein aggregation and reducing neurotoxicity caused by α-synuclein.

Overall, this thesis provides three novel findings. First, inhibition of α-synuclein aggregation by NDGA requires oxidation-dependent cyclization. Second, phenolic molecules inhibit α-synuclein aggregation by remodeling α-synuclein monomers, rendering them stably resistant to aggregation. Third, modified α-synuclein monomers exhibit a dominant-negative effect on α-synuclein aggregation. Consequently, small molecule induction of dominant-negative, aggregation-preventing α-synuclein monomers may represent a new paradigm for therapeutic development in PD and related synucleinopathies.

BIBLIOGRAPHY

Abeliovich, A., Schmitz, Y., Fariñas, I., Choi-Lundberg, D., Ho, W.H., Castillo, P.E., Shinsky, N., Verdugo, J.M., Armanini, M., Ryan, A., et al. (2000). Mice lacking alpha-synuclein display functional deficits in the nigrostriatal dopamine system. Neuron *25*, 239–252.

Acharya, S., Safaie, B.M., Wongkongkathep, P., Ivanova, M.I., Attar, A., Klärner, F.G., Schrader, T., Loo, J.A., Bitan, G., and Lapidus, L.J. (2014). Molecular basis for preventing α-synuclein aggregation by a molecular tweezer. J. Biol. Chem. *289*, 10727–10737.

Aflaki, E., Borger, D.K., Moaven, N., Stubblefield, B.K., Rogers, S.A., Patnaik, S., Schoenen, F.J., Westbroek, W., Zheng, W., Sullivan, P., et al. (2016). A New Glucocerebrosidase Chaperone Reduces α-Synuclein and Glycolipid Levels in iPSC-Derived Dopaminergic Neurons from Patients with Gaucher Disease and Parkinsonism. J. Neurosci. *36*, 7441–7452.

Aki, M., Shimbara, N., Takashina, M., Akiyama, K., Kagawa, S., Tamura, T., Tanahashi, N., Yoshimura, T., Tanaka, K., and Ichihara, A. (1994). Interferon-gamma induces different subunit organizations and functional diversity of proteasomes. J. Biochem. *115*, 257–269.

Alarcón-Arís, D., Recasens, A., Galofré, M., Carballo-Carbajal, I., Zacchi, N., Ruiz-Bronchal, E., Pavia-Collado, R., Chica, R., Ferrés-Coy, A., Santos, M., et al. (2018). Selective α-Synuclein Knockdown in Monoamine Neurons by Intranasal Oligonucleotide Delivery: Potential Therapy for Parkinson's Disease. Mol. Ther. *26*, 550–567.

Anderson, J.P., Walker, D.E., Goldstein, J.M., De Laat, R., Banducci, K., Caccavello, R.J., Barbour, R., Huang, J., Kling, K., Lee, M., et al. (2006). Phosphorylation of Ser-129 is the dominant pathological modification of α-synuclein in familial and sporadic lewy body disease. J. Biol. Chem. *281*, 29739–29752.

Anwar, S., Peters, O., Millership, S., Ninkina, N., Doig, N., Connor-Robson, N., Threlfell, S., Kooner, G., Deacon, R.M., Bannerman, D.M., et al. (2011). Functional Alterations to the Nigrostriatal System in Mice Lacking All Three Members of the Synuclein Family. J. Neurosci. *31*, 7264–7274.

Appel-Cresswell, S., Vilarino-Guell, C., Encarnacion, M., Sherman, H., Yu, I., Shah, B., Weir, D., Thompson, C., Szu-Tu, C., Trinh, J., et al. (2013). Alpha-synuclein p.H50Q, a novel pathogenic mutation for Parkinson's disease. Mov. Disord. *28*, 811–813.

Ara, J., Przedborski, S., Naini, a B., Jackson-Lewis, V., Trifiletti, R.R., Horwitz, J., and Ischiropoulos, H. (1998). Inactivation of tyrosine hydroxylase by nitration following exposure to peroxynitrite and 1-methyl-4-phenyl-1,2,3,6-tetrahydropyridine (MPTP). Proc. Natl. Acad. Sci. U. S. A. *95*, 7659–7663.

Asiamah, I., Hodgson, H.L., Maloney, K., Allen, K.J.H., and Krol, E.S. (2015). Ring substitution influences oxidative cyclisation and reactive metabolite formation of nordihydroguaiaretic acid analogues. Bioorganic Med. Chem. *23*, 7007–7014.

Aso, E., Lomoio, S., Lõpez-González, I., Joda, L., Carmona, M., Fernández-Yagüe, N., Moreno, J., Juvés, S., Pujol, A., Pamplona, R., et al. (2012). Amyloid generation and dysfunctional immunoproteasome activation with disease progression in animal model of familial Alzheimer's disease. Brain Pathol. *22*, 636–653.

Auluck, P.K., Chan, H.Y.E., Trojanowski, J.Q., Lee, V.M.Y., and Bonini, N.M. (2002). Chaperone suppression of alpha-synuclein toxicity in a Drosophila model for Parkinson's disease. Science *295*, 865–868.

Baba, M., Nakajo, S., Tu, P.H., Tomita, T., Nakaya, K., Lee, V.M., Trojanowski, J.Q., and Iwatsubo, T. (1998). Aggregation of alpha-synuclein in Lewy bodies of sporadic Parkinson's disease and dementia with Lewy bodies. Am. J. Pathol. *152*, 879–884.

Back, P., De Vos, W.H., Depuydt, G.G., Matthijssens, F., Vanfleteren, J.R., and Braeckman, B.P. (2012). Exploring real-time in vivo redox biology of developing and aging Caenorhabditis elegans. Free Radic. Biol. Med. *52*, 850–859.

Bae, E.-J., Lee, H.-J., Rockenstein, E., Ho, D.-H., Park, E.-B., Yang, N.-Y., Desplats, P., Masliah, E., and Lee, S.-J. (2012). Antibody-Aided Clearance of Extracellular α-Synuclein Prevents Cell-to-Cell Aggregate Transmission. J. Neurosci. *32*, 13454–13469.

Balch, W.E., Morimoto, R.I., Dillin, A., and Kelly, J.W. (2008). Adapting proteostasis for disease intervention. Science *319*, 916–919.

Barrett, P.J., and Greenamyre, J.T. (2015). Post-translational modification of α-synuclein in Parkinson's disease. Brain Res. *1628*, 247–253.

Bartels, T., Choi, J.G., and Selkoe, D.J. (2011). α-Synuclein occurs physiologically as a helically folded tetramer that resists aggregation. Nature *477*, 107–111.

Benskey, M.J., Sellnow, R.C., Sandoval, I.M., Sortwell, C.E., Lipton, J.W., and Manfredsson, F.P. (2018). Silencing Alpha Synuclein in Mature Nigral Neurons Results in Rapid Neuroinflammation and Subsequent Toxicity. Front. Mol. Neurosci. *11*, 36.

Berkowitz, L.A., Knight, A.L., Caldwell, G.A., and Caldwell, K.A. (2008). Generation of Stable Transgenic C. elegans Using Microinjection. J. Vis. Exp. 3–5.

Bertoncini, C.W., Jung, Y.-S., Fernandez, C.O., Hoyer, W., Griesinger, C., Jovin, T.M., and Zweckstetter, M. (2005a). Release of long-range tertiary interactions potentiates aggregation of natively unstructured α-synuclein. Proc. Natl. Acad. Sci. *102*, 1430–1435.

Bertoncini, C.W., Fernandez, C.O., Griesinger, C., Jovin, T.M., and Zweckstetter, M. (2005b). Familial mutants of α-synuclein with increased neurotoxicity have a destabilized conformation. J. Biol. Chem. *280*, 30649–30652.

Betarbet, R., Sherer, T.B., MacKenzie, G., Garcia-Osuna, M., Panov, A. V., and Greenamyre, J.T. (2000). Chronic systemic pesticide exposure reproduces features of Parkinson's disease. Nat. Neurosci. *3*, 1301–1306.

Lo Bianco, C., Ridet, J.-L., Schneider, B.L., Deglon, N., and Aebischer, P. (2002). alpha-Synucleinopathy and selective dopaminergic neuron loss in a rat lentiviral-based model of Parkinson's disease. Proc. Natl. Acad. Sci. U. S. A. *99*, 10813–10818.

Lo Bianco, C., Shorter, J., Régulier, E., Lashuel, H., Iwatsubo, T., Lindquist, S., and Aebischer, P. (2008). Hsp104 antagonizes α-synuclein aggregation and reduces dopaminergic degeneration in a rat model of Parkinson disease. J. Clin. Invest. *118*, 3087–3097.

Bieschke, J., Russ, J., Friedrich, R.P., Ehrnhoefer, D.E., Wobst, H., Neugebauer, K., and Wanker, E.E. (2010). EGCG remodels mature α-synuclein and amyloid-β fibrils and reduces cellular toxicity. Proc. Natl. Acad. Sci. *107*, 7710–7715.

Binolfi, A., Rasia, R.M., Bertoncini, C.W., Ceolin, M., Zweckstetter, M., Griesinger, C., Jovin, T.M., and Fernández, C.O. (2006). Interaction of α-synuclein with divalent metal ions reveals key differences: A link between structure, binding specificity and fibrillation enhancement. J. Am. Chem. Soc. *128*, 9893–9901.

Binolfi, A., Theillet, F.-X., and Selenko, P. (2012). Bacterial in-cell NMR of human α-synuclein: a disordered monomer by nature? Biochem. Soc. Trans. *40*, 950–954.

Bonifati, V., Rizzu, P., Squitieri, F., Krieger, E., Vanacore, N., van Swieten, J.C., Brice, A., van Duijn, C.M., Oostra, B., Meco, G., et al. (2003). DJ-1 (PARK7), a novel gene for autosomal recessive, early onset parkinsonism. Neurol. Sci. *24*, 159–160.

Braak, E., Sandmann-Keil, D., Rüb, U., Gai, W.P., de Vos, R.A.I., Jansen Steur, E.N.H., Arai, K., and Braak, H. (2001). α-Synuclein immunopositive Parkinson's disease-related inclusion bodies in lower brain stem nuclei. Acta Neuropathol. *101*, 195–201.

Braak, H., Braak, E., Yilmazer, D., de Vos, R.A., Jansen, E.N., Bohl, J., and Jellinger, K. (1994). Amygdala pathology in Parkinson's disease. Acta Neuropathol. *88*, 493–500.

Braak, H., Del Tredici, K., Rüb, U., De Vos, R.A.I., Jansen Steur, E.N.H., and Braak, E. (2003). Staging of brain pathology related to sporadic Parkinson's disease. Neurobiol. Aging *24*, 197–211.

Brutscher, B., Felli, I.C., Gil-Caballero, S., Hošek, T., Kümmerle, R., Piai, A., Pierattelli, R., and Sólyom, Z. (2015). NMR Methods for the Study of Instrinsically Disordered Proteins Structure, Dynamics, and Interactions: General Overview and Practical Guidelines. Adv. Exp. Med. Biol. *870*, 49–122.

Burré, J., Sharma, M., Tsetsenis, T., Buchman, V., Etherton, M.R., and Südhof, T.C. (2010). α-Synuclein promotes SNARE-complex assembly in vivo and in vitro. Science *329*, 1663–1667.

Burré, J., Sharma, M., and Sudhof, T.C. (2012). Systematic Mutagenesis of α-Synuclein Reveals Distinct Sequence Requirements for Physiological and Pathological Activities. J. Neurosci. *32*, 15227–15242.

Burré, J., Vivona, S., Diao, J., Sharma, M., Brunger, A.T., and Südhof, T.C. (2013). Properties of native brain α-synuclein. Nature *498*, E4–E6.

Burré, J., Sharma, M., and Südhof, T.C. (2014). α-Synuclein assembles into higher-order multimers upon membrane binding to promote SNARE complex formation. Proc. Natl. Acad. Sci. *111*, E4274–E4283.

Burré, J., Sharma, M., and Sudhof, T.C. (2015). Definition of a Molecular Pathway Mediating α-Synuclein Neurotoxicity. J. Neurosci. *35*, 5221–5232.

Cabin, D.E., Shimazu, K., Murphy, D., Cole, N.B., Gottschalk, W., McIlwain, K.L., Orrison, B., Chen, A., Ellis, C.E., Paylor, R., et al. (2002). Synaptic vesicle depletion correlates with

attenuated synaptic responses to prolonged repetitive stimulation in mice lacking alpha-synuclein. J. Neurosci. *22*, 8797–8807.

Cao, P., Yuan, Y., Pehek, E.A., Moise, A.R., Huang, Y., Palczewski, K., and Feng, Z. (2010). Alpha-synuclein disrupted dopamine homeostasis leads to dopaminergic neuron degeneration in Caenorhabditis elegans. PLoS One *5*, e9312.

Caruana, M., Högen, T., Levin, J., Hillmer, A., Giese, A., and Vassallo, N. (2011). Inhibition and disaggregation of α-synuclein oligomers by natural polyphenolic compounds. FEBS Lett. *585*, 1113–1120.

Cascio, P., Hilton, C., Kisselev, A.F., Rock, K.L., and Goldberg, A.L. (2001). 26S proteasomes and immunoproteasomes produce mainly N-extended versions of an antigenic peptide. EMBO J. *20*, 2357–2366.

Cebrián, C., Zucca, F.A., Mauri, P., Steinbeck, J.A., Studer, L., Scherzer, C.R., Kanter, E., Budhu, S., Mandelbaum, J., Vonsattel, J.P., et al. (2014). MHC-I expression renders catecholaminergic neurons susceptible to T-cell-mediated degeneration. Nat. Commun. *5*, 3633.

Chandra, S., Fornai, F., Kwon, H.-B., Yazdani, U., Atasoy, D., Liu, X., Hammer, R.E., Battaglia, G., German, D.C., Castillo, P.E., et al. (2004). Double-knockout mice for α- and β-synucleins: Effect on synaptic functions. Proc. Natl. Acad. Sci. *101*, 14966–14971.

Chandra, S., Gallardo, G., Fernández-Chacón, R., Schlüter, O.M., and Südhof, T.C. (2005). α-Synuclein cooperates with CSPα in preventing neurodegeneration. Cell *123*, 383–396.

Chartier-Harlin, M.C., Kachergus, J., Roumier, C., Mouroux, V., Douay, X., Lincoln, S., Levecque, C., Larvor, L., Andrieux, J., Hulihan, M., et al. (2004). α-synuclein locus duplication as a cause of familial Parkinson's disease. Lancet *364*, 1167–1169.

Chen, L., Periquet, M., Wang, X., Negro, A., McLean, P.J., Hyman, B.T., and Feany, M.B. (2009). Tyrosine and serine phosphorylation of alpha-synuclein have opposing effects on neurotoxicity and soluble oligomer formation. J. Clin. Invest. *119*, 3257–3265.

Chen, M., Margittai, M., Chen, J., and Langen, R. (2007). Investigation of alpha-synuclein fibril structure by site-directed spin labeling. J. Biol. Chem. *282*, 24970–24979.

Chen, M., Wang, T., Yue, F., Li, X., Wang, P., Li, Y., Chan, P., and Yu, S. (2015). Tea polyphenols alleviate motor impairments, dopaminergic neuronal injury, and cerebral α-synuclein aggregation in MPTP-intoxicated parkinsonian monkeys. Neuroscience *286*, 383–392.

Choi, B.-K., Choi, M.-G., Kim, J.-Y., Yang, Y., Lai, Y., Kweon, D.-H., Lee, N.K., and Shin, Y.-K. (2013). Large α-synuclein oligomers inhibit neuronal SNARE-mediated vesicle docking. Proc. Natl. Acad. Sci. U. S. A. *110*, 4087–4092.

Chung, C.Y., Koprich, J.B., Siddiqi, H., and Isacson, O. (2009). Dynamic changes in presynaptic and axonal transport proteins combined with striatal neuroinflammation precede dopaminergic neuronal loss in a rat model of AAV alpha-synucleinopathy. J. Neurosci. *29*, 3365–3373.

Chung, C.Y., Khurana, V., Yi, S., Sahni, N., Loh, K.H., Auluck, P.K., Baru, V., Udeshi, N.D., Freyzon, Y., Carr, S.A., et al. (2017). In Situ Peroxidase Labeling and Mass-Spectrometry

Connects Alpha-Synuclein Directly to Endocytic Trafficking and mRNA Metabolism in Neurons. Cell Syst. *4*, 242–250.e4.

Cole, N.B., Murphy, D.D., Grider, T., Rueter, S., Brasaemle, D., and Nussbaum, R.L. (2002). Lipid droplet binding and oligomerization properties of the Parkinson's disease protein α-synuclein. J. Biol. Chem. *277*, 6344–6352.

Collier, T.J., Srivastava, K.R., Justman, C., Grammatopoulous, T., Hutter-Paier, B., Prokesch, M., Havas, D., Rochet, J.-C., Liu, F., Jock, K., et al. (2017). Nortriptyline inhibits aggregation and neurotoxicity of alpha-synuclein by enhancing reconfiguration of the monomeric form. Neurobiol. Dis. *106*, 191–204.

Colom-Cadena, M., Pegueroles, J., Herrmann, A.G., Henstridge, C.M., Muñoz, L., Querol-Vilaseca, M., Martín-Paniello, C.S., Luque-Cabecerans, J., Clarimon, J., Belbin, O., et al. (2017). Synaptic phosphorylated α-synuclein in dementia with Lewy bodies. Brain *140*, 3204–3214.

Conway, K.A., Lee, S.-J., Rochet, J.-C., Ding, T.T., Williamson, R.E., and Lansbury, P.T. (2000). Acceleration of oligomerization, not fibrillization, is a shared property of both α-synuclein mutations linked to early-onset Parkinson's disease: Implications for pathogenesis and therapy. Proc. Natl. Acad. Sci. *97*, 571–576.

Conway, K.A., Rochet, J.C., Bieganski, R.M., and Lansbury, J. (2001). Kinetic stabilization of the α-synuclein protofibril by a dopamine-α-synuclein adduct. Science *294*, 1346–1349.

Cooper, J.M., Wiklander, P.B.O., Nordin, J.Z., Al-Shawi, R., Wood, M.J., Vithlani, M., Schapira, A.H. V, Simons, J.P., El-Andaloussi, S., and Alvarez-Erviti, L. (2014). Systemic exosomal siRNA delivery reduced alpha-synuclein aggregates in brains of transgenic mice. Mov. Disord. *29*, 1476–1485.

Coskuner, O., and Wise-Scira, O. (2013). Structures and free energy landscapes of the A53T mutant-type α-synuclein protein and impact of A53T mutation on the structures of the wild-type α-synuclein protein with dynamics. ACS Chem. Neurosci. *4*, 1101–1113.

Danzer, K.M., Haasen, D., Karow, A.R., Moussaud, S., Habeck, M., Giese, A., Kretzschmar, H., Hengerer, B., and Kostka, M. (2007). Different Species of α-Synuclein Oligomers Induce Calcium Influx and Seeding. J. Neurosci. *27*, 9220–9232.

Danzer, K.M., Ruf, W.P., Putcha, P., Joyner, D., Hashimoto, T., Glabe, C., Hyman, B.T., and McLean, P.J. (2011). Heat-shock protein 70 modulates toxic extracellular α-synuclein oligomers and rescues trans-synaptic toxicity. FASEB J. *25*, 326–336.

Danzer, K.M., Kranich, L.R., Ruf, W.P., Cagsal-Getkin, O., Winslow, A.R., Zhu, L., Vanderburg, C.R., and McLean, P.J. (2012). Exosomal cell-to-cell transmission of alpha synuclein oligomers. Mol. Neurodegener. *7*, 1–18.

Dauer, W., Kholodilov, N., Vila, M., Trillat, A.-C., Goodchild, R., Larsen, K.E., Staal, R., Tieu, K., Schmitz, Y., Yuan, C.A., et al. (2002). Resistance of alpha-synuclein null mice to the parkinsonian neurotoxin MPTP. Proc. Natl. Acad. Sci. U. S. A. *99*, 14524–14529.

Davidson, W.S., Jonas, A., Clayton, D.F., and George, J.M. (1998). Stabilization of α-Synuclein secondary structure upon binding to synthetic membranes. J. Biol. Chem. *273*, 9443–9449.

Davies, P., Moualla, D., and Brown, D.R. (2011). Alpha-synuclein is a cellular ferrireductase. PLoS One *6*, e15814.

Decressac, M., Mattsson, B., Weikop, P., Lundblad, M., Jakobsson, J., and Björklund, A. (2013). TFEB-mediated autophagy rescues midbrain dopamine neurons from α-synuclein toxicity. Proc. Natl. Acad. Sci. U. S. A. *110*, E1817-26.

Dedmon, M.M., Lindorff-Larsen, K., Christodoulou, J., Vendruscolo, M., and Dobson, C.M. (2005). Mapping long-range interactions in α-synuclein using spin-label NMR and ensemble molecular dynamics simulations. J. Am. Chem. Soc. *127*, 476–477.

Deeg, A.A., Reiner, A.M., Schmidt, F., Schueder, F., Ryazanov, S., Ruf, V.C., Giller, K., Becker, S., Leonov, A., Griesinger, C., et al. (2015). Anle138b and related compounds are aggregation specific fluorescence markers and reveal high affinity binding to α-synuclein aggregates. Biochim. Biophys. Acta *1850*, 1884–1890.

Dehay, B., Bove, J., Rodriguez-Muela, N., Perier, C., Recasens, A., Boya, P., and Vila, M. (2010). Pathogenic Lysosomal Depletion in Parkinson's Disease. J. Neurosci. *30*, 12535–12544.

Dettmer, U., Newman, A.J., Soldner, F., Luth, E.S., Kim, N.C., Von Saucken, V.E., Sanderson, J.B., Jaenisch, R., Bartels, T., and Selkoe, D. (2015a). Parkinson-causing α-synuclein missense mutations shift native tetramers to monomers as a mechanism for disease initiation. Nat. Commun. *6*, 7314.

Dettmer, U., Newman, A.J., von Saucken, V.E., Bartels, T., and Selkoe, D. (2015b). KTKEGV repeat motifs are key mediators of normal α-synuclein tetramerization: Their mutation causes excess monomers and neurotoxicity. Proc. Natl. Acad. Sci. *112*, 9596–9601.

Dettmer, U., Ramalingam, N., von Saucken, V.E., Kim, T.E., Newman, A.J., Terry-Kantor, E., Nuber, S., Ericsson, M., Fanning, S., Bartels, T., et al. (2017). Loss of native α-synuclein multimerization by strategically mutating its amphipathic helix causes abnormal vesicle interactions in neuronal cells. Hum. Mol. Genet. *26*, 3466–3481.

Díaz-Hernández, M., Hernández, F., Martín-Aparicio, E., Gómez-Ramos, P., Morán, M. a, Castaño, J.G., Ferrer, I., Avila, J., and Lucas, J.J. (2003). Neuronal induction of the immunoproteasome in Huntington's disease. J. Neurosci. *23*, 11653–11661.

DiFiglia, M., Sapp, E., Chase, K.O., Davies, S.W., Bates, G.P., Vonsattel, J.P., and Aronin, N. (1997). Aggregation of huntingtin in neuronal intranuclear inclusions and dystrophic neurites in brain. Science *277*, 1990–1993.

Dikiy, I., and Eliezer, D. (2014). N-terminal Acetylation stabilizes N-terminal Helicity in Lipid- and Micelle-bound α-Synuclein and increases its affinity for Physiological Membranes. J. Biol. Chem. *289*, 3652–3665.

Ding, Z.T., Wang, Y., Jiang, Y.P., Hashizume, Y., Yoshida, M., Mimuro, M., Inagaki, T., and Iwase, T. (2006). Characteristics of alpha-synucleinopathy in centenarians. Acta Neuropathol. *111*, 450–458.

Douglas, P.M., and Dillin, A. (2010). Protein homeostasis and aging in neurodegeneration. J. Cell Biol. *190*, 719–729.

Driscoll, J., Brown, M.G., Finley, D., and Monaco, J.J. (1993). MHC-linked LMP gene products specifically alter peptidase activities of the proteasome. Nature *365*, 262–264.

Du, H.N., Tang, L., Luo, X.Y., Li, H.T., Hu, J., Zhou, J.W., and Hu, H.Y. (2003). A peptide motif consisting of glycine, alanine, and valine is required for the fibrillization and cytotoxicity of human α-synuclein. Biochemistry *42*, 8870–8878.

Duda, J.E., Giasson, B.I., Mabon, M.E., Lee, V.M.Y., and Trojanowski, J.Q. (2002). Novel antibodies to synuclein show abundant striatal pathology in Lewy body diseases. Ann. Neurol. *52*, 205–210.

Duffy, M.F., Collier, T.J., Patterson, J.R., Kemp, C.J., Luk, K.C., Tansey, M.G., Paumier, K.L., Kanaan, N.M., Fischer, L.D., Polinski, N.K., et al. (2018). Lewy body-like alpha-synuclein inclusions trigger reactive microgliosis prior to nigral degeneration. J. Neuroinflammation *15*, 129.

Ebrahimi-Fakhari, D., Cantuti-Castelvetri, I., Fan, Z., Rockenstein, E., Masliah, E., Hyman, B.T., McLean, P.J., and Unni, V.K. (2011). Distinct roles in vivo for the ubiquitin-proteasome system and the autophagy-lysosomal pathway in the degradation of α-synuclein. J. Neurosci. *31*, 14508–14520.

Ebstein, F., Voigt, A., Lange, N., Warnatsch, A., Schröter, F., Prozorovski, T., Kuckelkorn, U., Aktas, O., Seifert, U., Kloetzel, P.M., et al. (2013). Immunoproteasomes are important for proteostasis in immune responses. Cell *152*, 935–937.

Van Den Eeden, S.K., Tanner, C.M., Bernstein, A.L., Fross, R.D., Leimpeter, A., Bloch, D.A., and Nelson, L.M. (2003). Incidence of Parkinson's Disease: Variation by Age, Gender, and Race/Ethnicity. Am. J. Epidemiol. *157*, 1015–1022.

Ehringer, H., and Hornykiewicz, O. (1960). Distribution of noradrenaline and dopamine (3-hydroxytyramine) in the human brain and their behavior in diseases of the extrapyramidal system. Klin. Wochenschr. *15*, 1236–1239.

Ehrnhoefer, D.E., Bieschke, J., Boeddrich, A., Herbst, M., Masino, L., Lurz, R., Engemann, S., Pastore, A., and Wanker, E.E. (2008). EGCG redirects amyloidogenic polypeptides into unstructured, off-pathway oligomers. Nat. Struct. Mol. Biol. *15*, 558–566.

Emmanouilidou, E., Melachroinou, K., Roumeliotis, T., Garbis, S.D., Ntzouni, M., Margaritis, L.H., Stefanis, L., and Vekrellis, K. (2010). Cell-produced alpha-synuclein is secreted in a calcium-dependent manner by exosomes and impacts neuronal survival. J. Neurosci. *30*, 6838–6851.

Emmer, K.L., Waxman, E.A., Covy, J.P., and Giasson, B.I. (2011). E46K human alpha-synuclein transgenic mice develop Lewy-like and tau pathology associated with age-dependent, detrimental motor impairment. J. Biol. Chem. *286*, 35104–35118.

Emre, M. (2003). Dementia associated with Parkinson's disease. Lancet Neurol. *2*, 229–237.

Farrer, M., Kachergus, J., Forno, L., Lincoln, S., Wang, D.S., Hulihan, M., Maraganore, D., Gwinn-Hardy, K., Wszolek, Z., Dickson, D., et al. (2004). Comparison of Kindreds with Parkinsonism and α-Synuclein Genomic Multiplications. Ann. Neurol. *55*, 174–179.

Fauvet, B., Fares, M.B., Samuel, F., Dikiy, I., Tandon, A., Eliezer, D., and Lashuel, H.A. (2012).

Characterization of semisynthetic and naturally N α- acetylated α-synuclein in vitro and in intact cells: Implications for aggregation and cellular properties of α-synuclein. J. Biol. Chem. *287*, 28243–28262.

Favier, A., and Brutscher, B. (2011). Recovering lost magnetization: Polarization enhancement in biomolecular NMR. J. Biomol. NMR *49*, 9–15.

Feany, M.B., and Bender, W.W. (2000). A Drosophila model of Parkinson's disease. Nature *404*, 394–398.

Fearnley, J.M., and Lees, A.J. (1991). Ageing and Parkinson's disease: substantia nigra regional selectivity. Brain *114*, 2283–2301.

Ferese, R., Modugno, N., Campopiano, R., Santilli, M., Zampatti, S., Giardina, E., Nardone, A., Postorivo, D., Fornai, F., Novelli, G., et al. (2015). Four Copies of SNCA Responsible for Autosomal Dominant Parkinson's Disease in Two Italian Siblings. Parkinsons. Dis. *2015*.

Fernandes, L., Moraes, N., Sagrillo, F.S., Magalhães, A. V., de Moraes, M.C., Romão, L., Kelly, J.W., Foguel, D., Grimster, N.P., and Palhano, F.L. (2017). An ortho-Iminoquinone Compound Reacts with Lysine Inhibiting Aggregation while Remodeling Mature Amyloid Fibrils. ACS Chem. Neurosci. acschemneuro.7b00017.

Ferreon, A.C.M., Gambin, Y., Lemke, E.A., and Deniz, A.A. (2009). Interplay of α-synuclein binding and conformational switching probed by single-molecule fluorescence. Proc. Natl. Acad. Sci. *106*, 5645–5650.

Ferrer, I., Blanco, R., Carmona, M., Puig, B., Barrachina, M., Gómez, C., and Ambrosio, S. (2001). Active, phosphorylation-dependent mitogen-activated protein kinase (MAPK/ERK), stress-activated protein kinase/c-Jun N-terminal kinase (SAPK/JNK), and p38 kinase expression in Parkinson's disease and Dementia with Lewy bodies. J. Neural Transm. *108*, 1383–1396.

Ferrie, J.J., Haney, C.M., Yoon, J., Pan, B., Lin, Y.-C., Fakhraai, Z., Rhoades, E., Nath, A., and Petersson, E.J. (2018). Using a FRET Library with Multiple Probe Pairs To Drive Monte Carlo Simulations of α-Synuclein. Biophys. J. *114*, 53–64.

Fonseca-Ornelas, L., Eisbach, S.E., Paulat, M., Giller, K., Fernández, C.O., Outeiro, T.F., Becker, S., and Zweckstetter, M. (2014). Small molecule-mediated stabilization of vesicle-associated helical α-synuclein inhibits pathogenic misfolding and aggregation. Nat. Commun. *5*, 5857.

Fu, Y.H., Yuan, Y., Halliday, G., Rusznák, Z., Watson, C., and Paxinos, G. (2012). A cytoarchitectonic and chemoarchitectonic analysis of the dopamine cell groups in the substantia nigra, ventral tegmental area, and retrorubral field in the mouse. Brain Struct. Funct. *217*, 591–612.

Fujiwara, H., Hasegawa, M., Dohmae, N., Kawashima, A., Masliah, E., Goldberg, M.S., Shen, J., Takio, K., and Iwatsubo, T. (2002). A-Synuclein Is Phosphorylated in Synucleinopathy Lesions. Nat. Cell Biol. *4*, 160–164.

Gaczynska, M., Rock, K.L., Spies, T., and Goldberg, A.L. (1994). Peptidase activities of proteasomes are differentially regulated by the major histocompatibility complex-encoded genes for LMP2 and LMP7. Proc. Natl. Acad. Sci. U. S. A. *91*, 9213–9217.

Gaig, C., Martí, M.J., Ezquerra, M., Rey, M.J., Cardozo, A., and Tolosa, E. (2007). G2019S LRRK2 mutation causing Parkinson's disease without Lewy bodies. J. Neurol. Neurosurg. Psychiatry *78*, 626–628.

Galvagnion, C., Buell, A.K., Meisl, G., Michaels, T.C.T., Vendruscolo, M., Knowles, T.P.J., and Dobson, C.M. (2015). Lipid vesicles trigger α-synuclein aggregation by stimulating primary nucleation. Nat. Chem. Biol. *11*, 229–234.

Games, D., Valera, E., Spencer, B., Rockenstein, E., Mante, M., Adame, A., Patrick, C., Ubhi, K., Nuber, S., Sacayon, P., et al. (2014). Reducing C-Terminal-Truncated Alpha-Synuclein by Immunotherapy Attenuates Neurodegeneration and Propagation in Parkinson's Disease-Like Models. J. Neurosci. *34*, 9441–9454.

Garcia-Reitböck, P., Anichtchik, O., Bellucci, A., Iovino, M., Ballini, C., Fineberg, E., Ghetti, B., Della Corte, L., Spano, P., Tofaris, G.K., et al. (2010). SNARE protein redistribution and synaptic failure in a transgenic mouse model of Parkinson's disease. Brain *133*, 2032–2044.

George, J.M., Jin, H., Woods, W.S., and Clayton, D.F. (1995). Characterization of a novel protein regulated during the critical period for song learning in the zebra finch. Neuron *15*, 361–372.

Georgieva, E.R., Ramlall, T.F., Borbat, P.P., Freed, J.H., and Eliezer, D. (2010). The lipid-binding domain of wild type and mutant α-synuclein: Compactness and interconversion between the broken and extended helix forms. J. Biol. Chem. *285*, 28261–28274.

Ghosh, D., Mondal, M., Mohite, G.M., Singh, P.K., Ranjan, P., Anoop, A., Ghosh, S., Jha, N.N., Kumar, A., and Maji, S.K. (2013). The parkinson's disease-associated H50Q mutation accelerates α-synuclein aggregation in vitro. Biochemistry *52*, 6925–6927.

Ghosh, D., Sahay, S., Ranjan, P., Salot, S., Mohite, G.M., Singh, P.K., Dwivedi, S., Carvalho, E., Banerjee, R., Kumar, A., et al. (2014). The newly discovered Parkinsons disease associated finnish mutation (A53E) attenuates α-synuclein aggregation and membrane binding. Biochemistry *53*, 6419–6421.

Giasson, B.I., Uryu, K., Trojanowski, J.Q., and Lee, V.M.Y. (1999). Mutant and wild type human α-synucleins assemble into elongated filaments with distinct morphologies in vitro. J. Biol. Chem. *274*, 7619–7622.

Giasson, B.I., Duda, J.E., Murray, I.V.J., Chen, Q., Souza, J.M., Hurtig, H.I., Ischiropoulos, H., Trojanowski, J.Q., and Lee, V.M.Y. (2000). Oxidative damage linked to neurodegeneration by selective α-synuclein nitration in synucleinopathy lesions. Science *290*, 985–989.

Giasson, B.I., Murray, I. V, Trojanowski, J.Q., and Lee, V.M. (2001). A hydrophobic stretch of 12 amino acid residues in the middle of alpha-synuclein is essential for filament assembly. J. Biol. Chem. *276*, 2380–2386.

Giasson, B.I., Duda, J.E., Quinn, S.M., Zhang, B., Trojanowski, J.Q., and Lee, V.M.Y. (2002). Neuronal α-synucleinopathy with severe movement disorder in mice expressing A53T human α-synuclein. Neuron *34*, 521–533.

Di Giovanni, S., Eleuteri, S., Paleologou, K.E., Yin, G., Zweckstetter, M., Carrupt, P.A., and Lashuel, H.A. (2010). Entacapone and tolcapone, two catechol O-methyltransferase inhibitors,

block fibril formation of α-synuclein and β-amyloid and protect against amyloid-induced toxicity. J. Biol. Chem. *285*, 14941–14954.

Gitler, A.D., Bevis, B.J., Shorter, J., Strathearn, K.E., Hamamichi, S., Su, L.J., Caldwell, K.A., Caldwell, G.A., Rochet, J.-C., McCaffery, J.M., et al. (2008). The Parkinson's disease protein α-synuclein disrupts cellular Rab homeostasis. Proc. Natl. Acad. Sci. *105*, 145–150.

Glenner, G.G., and Wong, C.W. (1984). Alzheimer's disease: initial report of the purification and characterization of a novel cerebrovascular amyloid protein. Biochem. Biophys. Res. Commun. *120*, 885–890.

Goldman, J.E., Yen, S.H., Chiu, F.C., and Peress, N.S. (1983). Lewy bodies of Parkinson's disease contain neurofilament antigens. Science *221*, 1082–1084.

Gomez-Isla, T., Irizarry, M.C., Mariash, A., Cheung, B., Soto, O., Schrump, S., Sondel, J., Kotilinek, L., Day, J., Schwarzschild, M.A., et al. (2003). Motor dysfunction and gliosis with preserved dopaminergic markers in human α-synuclein A30P transgenic mice. Neurobiol. Aging *24*, 245–258.

Gorell, J.M., Johnson, C.C., Rybicki, B.A., Peterson, E.L., Kortsha, G.X., Brown, G.G., and Richardson, R.J. (1999). Occupational exposure to manganese, copper, lead, iron, mercury and zinc and the risk of Parkinson's disease. Neurotoxicology *20*, 239–247.

Gould, N., Mor, D.E., Lightfoot, R., Malkus, K., Giasson, B., and Ischiropoulos, H. (2014). Evidence of native α-synuclein conformers in the human brain. J. Biol. Chem. *289*, 7929–7934.

Greenbaum, E.A., Graves, C.L., Mishizen-Eberz, A.J., Lupoli, M.A., Lynch, D.R., Englander, S.W., Axelsen, P.H., and Giasson, B.I. (2005). The E46K mutation in α-synuclein increases amyloid fibril formation. J. Biol. Chem. *280*, 7800–7807.

Greten-Harrison, B., Polydoro, M., Morimoto-Tomita, M., Diao, L., Williams, A.M., Nie, E.H., Makani, S., Tian, N., Castillo, P.E., Buchman, V.L., et al. (2010). α-Synuclein triple knockout mice reveal age-dependent neuronal dysfunction. Proc. Natl. Acad. Sci. *107*, 19573–19578.

Guo, J.L., and Lee, V.M.Y. (2014). Cell-to-cell transmission of pathogenic proteins in neurodegenerative diseases. Nat. Med. *20*, 130–138.

Guo, J.L., Covell, D.J., Daniels, J.P., Iba, M., Stieber, A., Zhang, B., Riddle, D.M., Kwong, L.K., Xu, Y., Trojanowski, J.Q., et al. (2013). Distinct α-synuclein strains differentially promote tau inclusions in neurons. Cell *154*, 103–117.

Gurry, T., Ullman, O., Fisher, C.K., Perovic, I., Pochapsky, T., and Stultz, C.M. (2013). The dynamic structure of α-synuclein multimers. J. Am. Chem. Soc. *135*, 3865–3872.

Ha, Y., Yang, A., Lee, S., Kim, K., Liew, H., Lee, S.H., Lee, J.E., Lee, H.I., Suh, Y.H., Park, H.S., et al. (2014). Dopamine and Cu+/2+ can induce oligomerization of α-synuclein in the absence of oxygen: Two types of oligomerization mechanisms for α-synuclein and related cell toxicity studies. J. Neurosci. Res. *92*, 359–368.

Hamamichi, S., Rivas, R.N., Knight, A.L., Cao, S., Caldwell, K. a, and Caldwell, G. a (2008). Hypothesis-based RNAi screening identifies neuroprotective genes in a Parkinson's disease

model. Proc. Natl. Acad. Sci. U. S. A. *105*, 728–733.

Hasegawa, M., Fujiwara, H., Nonaka, T., Wakabayashi, K., Takahashi, H., Lee, V.M.Y., Trojanowski, J.Q., Mann, D., and Iwatsubo, T. (2002). Phosphorylated α-synuclein is ubiquitinated in α-synucleinopathy lesions. J. Biol. Chem. *277*, 49071–49076.

Heink, S., Ludwig, D., Kloetzel, P.-M., and Krüger, E. (2005). IFN-gamma-induced immune adaptation of the proteasome system is an accelerated and transient response. Proc. Natl. Acad. Sci. U. S. A. *102*, 9241–9246.

Heise, H., Hoyer, W., Becker, S., Andronesi, O.C., Riedel, D., and Baldus, M. (2005). Molecular-level secondary structure, polymorphism, and dynamics of full-length alpha-synuclein fibrils studied by solid-state NMR. Proc. Natl. Acad. Sci. U. S. A. *102*, 15871–15876.

Hernandez, D.G., Reed, X., and Singleton, A.B. (2016). Genetics in Parkinson disease: Mendelian versus non-Mendelian inheritance. J. Neurochem. *139*, 59–74.

Herrera, F.E., Chesi, A., Paleologou, K.E., Schmid, A., Munoz, A., Vendruscolo, M., Gustincich, S., Lashuel, H.A., and Carloni, P. (2008). Inhibition of α-synuclein fibrillization by dopamine is mediated by interactions with five C-terminal residues and with E83 in the NAC region. PLoS One *3*.

Hillmer, A.S., Putcha, P., Levin, J., Högen, T., Hyman, B.T., Kretzschmar, H., McLean, P.J., and Giese, A. (2010). Converse modulation of toxic alpha-synuclein oligomers in living cells by N'-benzylidene-benzohydrazide derivates and ferric iron. Biochem. Biophys. Res. Commun. *391*, 461–466.

Hirsch, E.C., Brandel, J.P., Galle, P., Javoy-Agid, F., and Agid, Y. (1991). Iron and aluminum increase in the substantia nigra of patients with Parkinson's disease: an X-ray microanalysis. J. Neurochem. *56*, 446–451.

Hodara, R., Norris, E.H., Giasson, B.I., Mishizen-Eberz, A.J., Lynch, D.R., Lee, V.M.Y., and Ischiropoulos, H. (2004). Functional consequences of α-synuclein tyrosine nitration: Diminished binding to lipid vesicles and increased fibril formation. J. Biol. Chem. *279*, 47746–47753.

Holmqvist, S., Chutna, O., Bousset, L., Aldrin-Kirk, P., Li, W., Björklund, T., Wang, Z.-Y., Roybon, L., Melki, R., and Li, J.-Y. (2014). Direct evidence of Parkinson pathology spread from the gastrointestinal tract to the brain in rats. Acta Neuropathol. *128*, 805–820.

Hoyer, W., Cherny, D., Subramaniam, V., and Jovin, T.M. (2004). Impact of the acidic C-terminal region comprising amino acids 109-140 on α-synuclein aggregation in vitro. Biochemistry *43*, 16233–16242.

Huang, C., Ren, G., Zhou, H., and Wang, C.C. (2005). A new method for purification of recombinant human α-synuclein in Escherichia coli. Protein Expr. Purif. *42*, 173–177.

Huber, E.M., Basler, M., Schwab, R., Heinemeyer, W., Kirk, C.J., Groettrup, M., and Groll, M. (2012). Immuno- and constitutive proteasome crystal structures reveal differences in substrate and inhibitor specificity. Cell *148*, 727–738.

Ischiropoulos, H., and Beckman, J.S. (2003). Oxidative stress and nitration in neurodegeneration:

Cause, effect, or association? J. Clin. Invest. *111*, 163–169.

Iwai, A., Masliah, E., Yoshimoto, M., Ge, N., Flanagan, L., Rohan de Silva, H.A., Kittel, A., and Saitoh, T. (1995). The precursor protein of non-Aβ component of Alzheimer's disease amyloid is a presynaptic protein of the central nervous system. Neuron *14*, 467–475.

Iwata, A., Maruyama, M., Kanazawa, I., and Nukina, N. (2001). alpha-Synuclein affects the MAPK pathway and accelerates cell death. J. Biol. Chem. *276*, 45320–45329.

Jackson-Lewis, V., Jakowec, M., Burke, R.E., and Przedborski, S. (1995). Time course and morphology of dopaminergic neuronal death caused by the neurotoxin 1-methyl-4-phenyl-1,2,3,6-tetrahydropyridine. Neurodegeneration *4*, 257–269.

Jakes, R., Spillantini, M.G., and Goedert, M. (1994). Identification of two distinct synucleins from human brain. FEBS Lett. *345*, 27–32.

Javitch, J.A., D'Amato, R.J., Strittmatter, S.M., and Snyder, S.H. (1985). Parkinsonism-inducing neurotoxin, N-methyl-4-phenyl-1,2,3,6 -tetrahydropyridine: uptake of the metabolite N-methyl-4-phenylpyridine by dopamine neurons explains selective toxicity. Proc. Natl. Acad. Sci. U. S. A. *82*, 2173–2177.

Jung, S.Y., Choi, J.M., Rousseaux, M.W.C., Malovannaya, A., Kim, J.J., Kutzera, J., Wang, Y., Huang, Y., Zhu, W., Maity, S., et al. (2017). An Anatomically Resolved Mouse Brain Proteome Reveals Parkinson Disease-relevant Pathways. Mol. Cell. Proteomics *16*, 581–593.

Karpowicz, R.J., Haney, C.M., Mihaila, T.S., Sandler, R.M., Petersson, E.J., and Lee, V.M.Y. (2017). Selective imaging of internalized proteopathic α-synuclein seeds in primary neurons reveals mechanistic insight into transmission of synucleinopathies. J. Biol. Chem. *292*, 13482–13497.

Kayed, R., Sokolov, Y., Edmonds, B., McIntire, T.M., Milton, S.C., Hall, J.E., and Glabe, C.G. (2004). Permeabilization of lipid bilayers is a common conformation-dependent activity of soluble amyloid oligomers in protein misfolding diseases. J. Biol. Chem. *279*, 46363–46366.

Kilpatrick, K., Novoa, J.A., Hancock, T., Guerriero, C.J., Wipf, P., Brodsky, J.L., and Segatori, L. (2013). Chemical induction of Hsp70 reduces α-synuclein aggregation in neuroglioma cells. ACS Chem. Biol. *8*, 1460–1468.

Kim, S., Yun, S.P., Lee, S., Umanah, G.E., Bandaru, V.V.R., Yin, X., Rhee, P., Karuppagounder, S.S., Kwon, S.-H., Lee, H., et al. (2018). GBA1 deficiency negatively affects physiological α-synuclein tetramers and related multimers. Proc. Natl. Acad. Sci. *115*, 201700465.

Kincaid, E.Z., Che, J.W., York, I., Escobar, H., Reyes-Vargas, E., Delgado, J.C., Welsh, R.M., Karow, M.L., Murphy, A.J., Valenzuela, D.M., et al. (2011). Mice completely lacking immunoproteasomes show major changes in antigen presentation. Nat. Immunol. *13*, 129–135.

Kirik, D., Rosenblad, C., Burger, C., Lundberg, C., Johansen, T.E., Muzyczka, N., Mandel, R.J., and Björklund, A. (2002). Parkinson-like neurodegeneration induced by targeted overexpression of α-synuclein in the nigrostriatal system. J. Neurosci. *22*, 2780–2791.

Kitada, T., Asakawa, S., Hattori, N., Matsumine, H., Yamamura, Y., Minoshima, S., Yokochi, M.,

Mizuno, Y., and Shimizu, N. (1998). Mutations in the parkin gene cause autosomal recessive juvenile parkinsonism. Nature *392*, 605–608.

Klucken, J., Shin, Y., Masliah, E., Hyman, B.T., and McLean, P.J. (2004). Hsp70 reduces α-synuclein aggregation and toxicity. J. Biol. Chem. *279*, 25497–25502.

Koller, W.C. (1984). Sensory symptoms in Parkinson's disease. Neurology *34*, 957–959.

Konijnenberg, A., Ranica, S., Narkiewicz, J., Legname, G., Grandori, R., Sobott, F., and Natalello, A. (2016). Opposite Structural Effects of Epigallocatechin-3-gallate and Dopamine Binding to α-Synuclein. Anal. Chem. *88*, 8468–8475.

Kordower, J.H., Chu, Y., Hauser, R.A., Freeman, T.B., and Olanow, C.W. (2008). Lewy body-like pathology in long-term embryonic nigral transplants in Parkinson's disease. Nat. Med. *14*, 504–506.

Kostka, M., Högen, T., Danzer, K.M., Levin, J., Habeck, M., Wirth, A., Wagner, R., Glabe, C.G., Finger, S., Heinzelmann, U., et al. (2008). Single particle characterization of iron-induced pore-forming α-synuclein oligomers. J. Biol. Chem. *283*, 10992–11003.

Kowall, N.W., Hantraye, P., Brouillet, E., Beal, M.F., McKee, A.C., and Ferrante, R.J. (2000). MPTP induces alpha-synuclein aggregation in the substantia nigra of baboons. Neuroreport *11*, 211–213.

Krueger, M.J., Singer, T.P., Casida, J.E., and Ramsay, R.R. (1990). Evidence that the blockade of mitochondrial respiration by the neurotoxin 1-methyl-4-phenylpyridinium (MPP+) involves binding at the same site as the respiratory inhibitor, rotenone. Biochem. Biophys. Res. Commun. *169*, 123–128.

Krüger, M., Moser, M., Ussar, S., Thievessen, I., Luber, C.A., Forner, F., Schmidt, S., Zanivan, S., Fässler, R., and Mann, M. (2008). SILAC Mouse for Quantitative Proteomics Uncovers Kindlin-3 as an Essential Factor for Red Blood Cell Function. Cell *134*, 353–364.

Krüger, R., Kuhn, W., Müller, T., Woitalla, D., Graeber, M., Kösel, S., Przuntek, H., Epplen, J.T., Schöls, L., and Riess, O. (1998). Ala30Pro mutation in the gene encoding alpha-synuclein in Parkinson's disease. Nat. Genet. *18*, 106–108.

Lakso, M., Vartiainen, S., Moilanen, A.-M., Sirviö, J., Thomas, J.H., Nass, R., Blakely, R.D., and Wong, G. (2003). Dopaminergic neuronal loss and motor deficits in Caenorhabditis elegans overexpressing human alpha-synuclein. J. Neurochem. *86*, 165–172.

Lambert, J.D., Kennett, M.J., Sang, S., Reuhl, K.R., Ju, J., and Yang, C.S. (2010). Hepatotoxicity of high oral dose (-)-epigallocatechin-3-gallate in mice. Food Chem. Toxicol. *48*, 409–416.

Larhammar, M., Patra, K., Blunder, M., Emilsson, L., Peuckert, C., Arvidsson, E., Rönnlund, D., Preobraschenski, J., Birgner, C., Limbach, C., et al. (2015). SLC10A4 is a vesicular amine-associated transporter modulating dopamine homeostasis. Biol. Psychiatry *77*, 526–536.

Larsen, K.E., Schmitz, Y., Troyer, M.D., Mosharov, E., Dietrich, P., Quazi, A.Z., Savalle, M., Nemani, V.M., Chaudhry, F.A., Edwards, R.H., et al. (2006). Alpha-synuclein overexpression in PC12 and chromaffin cells impairs catecholamine release by interfering with a late step in

exocytosis. J. Neurosci. *26*, 11915–11922.

Lashuel, H.A., Petre, B.M., Wall, J., Simon, M., Nowak, R.J., Walz, T., and Lansbury, P.T. (2002). A-Synuclein, Especially the Parkinson's Disease-Associated Mutants, Forms Pore-Like Annular and Tubular Protofibrils. J. Mol. Biol. *322*, 1089–1102.

Lee, H.-J. (2004). Clearance of α-Synuclein Oligomeric Intermediates via the Lysosomal Degradation Pathway. J. Neurosci. *24*, 1888–1896.

Lee, E.-N., Cho, H.-J., Lee, C.-H., Lee, D., Chung, K.C., and Paik, S.R. (2004). Phthalocyanine tetrasulfonates affect the amyloid formation and cytotoxicity of alpha-synuclein. Biochemistry *43*, 3704–3715.

Lee, H.J., Suk, J.E., Bae, E.J., Lee, J.H., Paik, S.R., and Lee, S.J. (2008). Assembly-dependent endocytosis and clearance of extracellular α-synuclein. Int. J. Biochem. Cell Biol. *40*, 1835–1849.

Lee, H.J., Suk, J.E., Patrick, C., Bae, E.J., Cho, J.H., Rho, S., Hwang, D., Masliah, E., and Lee, S.J. (2010). Direct transfer of α-synuclein from neuron to astroglia causes inflammatory responses in synucleinopathies. J. Biol. Chem. *285*, 9262–9272.

Lee, M.K., Stirling, W., Xu, Y., Xu, X., Qui, D., Mandir, A.S., Dawson, T.M., Copeland, N.G., Jenkins, N.A., and Price, D.L. (2002). Human α-synuclein-harboring familial Parkinson's disease-linked Ala-53 to Thr mutation causes neurodegenerative disease with α-synuclein aggregation in transgenic mice. Proc. Natl. Acad. Sci. *99*, 8968–8973.

Lee, V.M., Balin, B.J., Otvos, L., and Trojanowski, J.Q. (1991). A68: a major subunit of paired helical filaments and derivatized forms of normal Tau. Science *251*, 675–678.

Lees, A.J., Blackburn, N.A., and Campbell, V.L. (1988). The nighttime problems of Parkinson's disease. Clin. Pharmacol. *11*, 512–519.

Leestemaker, Y., de Jong, A., Witting, K.F., Penning, R., Schuurman, K., Rodenko, B., Zaal, E.A., van de Kooij, B., Laufer, S., Heck, A.J.R., et al. (2017). Proteasome Activation by Small Molecules. Cell Chem. Biol. *24*, 725–736.

Lennox, G., Lowe, J., Morrell, K., Landon, M., and Mayer, R.J. (1989). Anti-ubiquitin immunocytochemistry is more sensitive than conventional techniques in the detection of diffuse Lewy body disease. J. Neurol. Neurosurg. Psychiatry *52*, 67–71.

Lesage, S., Anheim, M., Letournel, F., Bousset, L., Honoré, A., Rozas, N., Pieri, L., Madiona, K., Dürr, A., Melki, R., et al. (2013). G51D α-synuclein mutation causes a novel parkinsonian-pyramidal syndrome. Ann. Neurol. *73*, 459–471.

Levin, J., Maaß, S., Schuberth, M., Respondek, G., Paul, F., Mansmann, U., Oertel, W.H., Lorenzl, S., Krismer, F., Seppi, K., et al. (2016). The PROMESA-protocol: progression rate of multiple system atrophy under EGCG supplementation as anti-aggregation-approach. J. Neural Transm. *123*, 439–445.

Levy, G., Schupf, N., Tang, M., Cote, L.J., Louis, E.D., Mejia, H., Stern, Y., and Marder, K. (2002). Combined Effect of Age and Severity on the Risk of Dementia in Parkinson ' s Disease. Ann. Neurol. *51*, 722–729.

Lewis, J., Melrose, H., Bumcrot, D., Hope, A., Zehr, C., Lincoln, S., Braithwaite, A., He, Z., Ogholikhan, S., Hinkle, K., et al. (2008). In vivo silencing of alpha-synuclein using naked siRNA. Mol. Neurodegener. *3*, 19.

Lewy, F. (1912). Paralysis agitans. I. Pathologische Anatomie. In Handbuch Der Neurologie Vol. 3, M. Lewandowsky, and G. Abelsdorff, eds. (Berlin: Springer-Verlag), pp. 920–933.

Li, J., Uversky, V.N., and Fink, A.L. (2001). Effect of familial Parkinson's disease point mutations A30P and A53T on the structural properties, aggregation, and fibrillation of human α-synuclein. Biochemistry *40*, 11604–11613.

Li, J., Zhu, M., Rajamani, S., Uversky, V.N., and Fink, A.L. (2004). Rifampicin inhibits alpha-synuclein fibrillation and disaggregates fibrils. Chem. Biol. *11*, 1513–1521.

Li, J.Y., Englund, E., Holton, J.L., Soulet, D., Hagell, P., Lees, A.J., Lashley, T., Quinn, N.P., Rehncrona, S., Björklund, A., et al. (2008). Lewy bodies in grafted neurons in subjects with Parkinson's disease suggest host-to-graft disease propagation. Nat. Med. *14*, 501–503.

Li, W., West, N., Colla, E., Pletnikova, O., Troncoso, J.C., Marsh, L., Dawson, T.M., Jakala, P., Hartmann, T., Price, D.L., et al. (2005). Aggregation promoting C-terminal truncation of α-synuclein is a normal cellular process and is enhanced by the familial Parkinson's disease-linked mutations. Proc. Natl. Acad. Sci. *102*, 2162–2167.

Lindå, H., Hammarberg, H., Piehl, F., Khademi, M., and Olsson, T. (1999). Expression of MHC class I heavy chain and beta2-microglobulin in rat brainstem motoneurons and nigral dopaminergic neurons. J. Neuroimmunol. *101*, 76–86.

Lindström, V., Fagerqvist, T., Nordström, E., Eriksson, F., Lord, A., Tucker, S., Andersson, J., Johannesson, M., Schell, H., Kahle, P.J., et al. (2014). Immunotherapy targeting α-synuclein protofibrils reduced pathology in (Thy-1)-h[A30P] α-synuclein mice. Neurobiol. Dis. *69*, 134–143.

Liu, L.L., and Franz, K.J. (2005). Phosphorylation of an α-synuclein peptide fragment enhances metal binding. J. Am. Chem. Soc. *127*, 9662–9663.

Lorenzen, N., Nielsen, S.B., Yoshimura, Y., Vad, B.S., Andersen, C.B., Betzer, C., Kaspersen, J.D., Christiansen, G., Pedersen, J.S., Jensen, P.H., et al. (2014). How epigallocatechin gallate can inhibit α-synuclein oligomer toxicity in vitro. J. Biol. Chem. *289*, 21299–21310.

Lou, X., Kim, J., Hawk, B.J., and Shin, Y.-K. (2017). α-Synuclein may cross-bridge v-SNARE and acidic phospholipids to facilitate SNARE-dependent vesicle docking. Biochem. J. *474*, 2039–2049.

Lu, Y., Prudent, M., Fauvet, B., Lashuel, H.A., and Girault, H.H. (2011). Phosphorylation of α-synuclein at Y125 and S129 alters its metal binding properties: Implications for understanding the role of α-synuclein in the pathogenesis of Parkinson's disease and related disorders. ACS Chem. Neurosci. *2*, 667–675.

Luk, K.C., Kehm, V., Carroll, J., Zhang, B., O'Brien, P., Trojanowski, J.Q., and Lee, V.M.Y. (2012a). Pathological α-synuclein transmission initiates Parkinson-like neurodegeneration in nontransgenic mice. Science *338*, 949–953.

Luk, K.C., Kehm, V.M., Zhang, B., O'Brien, P., Trojanowski, J.Q., and Lee, V.M.Y. (2012b). Intracerebral inoculation of pathological α-synuclein initiates a rapidly progressive neurodegenerative α-synucleinopathy in mice. J. Exp. Med. *209*, 975–986.

Luk, K.C., Covell, D.J., Kehm, V.M., Zhang, B., Song, I.Y., Byrne, M.D., Pitkin, R.M., Decker, S.C., Trojanowski, J.Q., and Lee, V.M.Y. (2016). Molecular and Biological Compatibility with Host Alpha-Synuclein Influences Fibril Pathogenicity. Cell Rep. *16*, 3373–3387.

Luth, E.S., Stavrovskaya, I.G., Bartels, T., Kristal, B.S., and Selkoe, D.J. (2014). Soluble, prefibrillar α-synuclein oligomers promote complex I-dependent, Ca2+-induced mitochondrial dysfunction. J. Biol. Chem. *289*, 21490–21507.

Luth, E.S., Bartels, T., Dettmer, U., Kim, N.C., and Selkoe, D.J. (2015). Purification of α-synuclein from human brain reveals an instability of endogenous multimers as the protein approaches purity. Biochemistry *54*, 279–292.

Mahul-Mellier, A.L., Vercruysse, F., Maco, B., Ait-Bouziad, N., De Roo, M., Muller, D., and Lashuel, H.A. (2015). Fibril growth and seeding capacity play key roles in α-synuclein-mediated apoptotic cell death. Cell Death Differ. *22*, 2107–2122.

Mandler, M., Valera, E., Rockenstein, E., Mante, M., Weninger, H., Patrick, C., Adame, A., Schmidhuber, S., Santic, R., Schneeberger, A., et al. (2015). Active immunization against alpha-synuclein ameliorates the degenerative pathology and prevents demyelination in a model of multiple system atrophy. Mol. Neurodegener. *10*, 1–15.

Manfredsson, F.P., Luk, K.C., Benskey, M.J., Gezer, A., Garcia, J., Kuhn, N.C., Sandoval, I.M., Patterson, J.R., O'Mara, A., Yonkers, R., et al. (2018). Induction of alpha-synuclein pathology in the enteric nervous system of the rat and non-human primate results in gastrointestinal dysmotility and transient CNS pathology. Neurobiol. Dis. *112*, 106–118.

Maraganore, D.M., Lesnick, T.G., Elbaz, A., Chartier-Harlin, M.C., Gasser, T., Krüger, R., Hattori, N., Mellick, G.D., Quattrone, A., Satoh, J.I., et al. (2004). UCHL1 Is a Parkinson's Disease Susceptibility Gene. Ann. Neurol. *55*, 512–521.

Markesbery, W., and Jicha, G. (2009). Lewy body pathology in normal elderly subjects. J. Neuropathol. Exp. Neurol. *68*, 816–822.

Maroteaux, L., and Scheller, R.H. (1991). The rat brain synucleins; family of proteins transiently associated with neuronal membrane. Brain Res. Mol. Brain Res. *11*, 335–343.

Maroteaux, L., Campanelli, J.T., and Scheller, R.H. (1988). Synuclein: a neuron-specific protein localized to the nucleus and presynaptic nerve terminal. J. Neurosci. *8*, 2804–2815.

Martinez, Z., Zhu, M., Han, S., and Fink, A.L. (2007). GM1 specifically interacts with α-synuclein and inhibits fibrillation. Biochemistry *46*, 1868–1877.

Masliah, E., Rockenstein, E., Adame, A., Alford, M., Crews, L., Hashimoto, M., Seubert, P., Lee, M., Goldstein, J., Chilcote, T., et al. (2005). Effects of alpha-synuclein immunization in a mouse model of Parkinson's disease. Neuron *46*, 857–868.

Masliah, E., Rockenstein, E., Mante, M., Crews, L., Spencer, B., Adame, A., Patrick, C., Trejo,

M., Ubhi, K., Rohn, T.T., et al. (2011). Passive immunization reduces behavioral and neuropathological deficits in an alpha-synuclein transgenic model of lewy body disease. PLoS One *6*.

Masuda, M., Suzuki, N., Taniguchi, S., Oikawa, T., Nonaka, T., Iwatsubo, T., Hisanaga, S.I., Goedert, M., and Hasegawa, M. (2006). Small molecule inhibitors of α-synuclein filament assembly. Biochemistry *45*, 6085–6094.

Masuda, M., Hasegawa, M., Nonaka, T., Oikawa, T., Yonetani, M., Yamaguchi, Y., Kato, K., Hisanaga, S. ichi, and Goedert, M. (2009). Inhibition of α-synuclein fibril assembly by small molecules: Analysis using epitope-specific antibodies. FEBS Lett. *583*, 787–791.

Mazzulli, J.R., Mishizen, A.J., Giasson, B.I., Lynch, D.R., Thomas, S.A., Nakashima, A., Nagatsu, T., Ota, A., and Ischiropoulos, H. (2006). Cytosolic Catechols Inhibit α-Synuclein Aggregation and Facilitate the Formation of Intracellular Soluble Oligomeric Intermediates. J. Neurosci. *26*, 10068–10078.

Mazzulli, J.R., Armakola, M., Dumoulin, M., Parastatidis, I., and Ischiropoulos, H. (2007). Cellular oligomerization of α-synuclein is determined by the interaction of oxidized catechols with a C-terminal sequence. J. Biol. Chem. *282*, 31621–31630.

Mazzulli, J.R., Xu, Y.H., Sun, Y., Knight, A.L., McLean, P.J., Caldwell, G.A., Sidransky, E., Grabowski, G.A., and Krainc, D. (2011). Gaucher disease glucocerebrosidase and α-synuclein form a bidirectional pathogenic loop in synucleinopathies. Cell *146*, 37–52.

Mazzulli, J.R., Burbulla, L.F., Krainc, D., and Ischiropoulos, H. (2016). Detection of Free and Protein-Bound ortho-Quinones by Near-Infrared Fluorescence. Anal. Chem. *88*, 2399–2405.

McLean, P.J., Klucken, J., Shin, Y., and Hyman, B.T. (2004). Geldanamycin induces Hsp70 and prevents α-synuclein aggregation and toxicity in vitro. Biochem. Biophys. Res. Commun. *321*, 665–669.

Meng, X., Munishkina, L.A., Fink, A.L., and Uversky, V.N. (2009). Molecular mechanisms underlying the flavonoid-induced inhibition of α-synuclein fibrillation. Biochemistry *48*, 8206–8224.

Meng, X., Munishkina, L.A., Fink, A.L., and Uversky, V.N. (2010). Effects of Various Flavonoids on the α-Synuclein Fibrillation Process. Parkinsons. Dis. *2010*, 1–16.

Mertins, P., Qiao, J.W., Patel, J., Udeshi, N.D., Clauser, K.R., Mani, D.R., Burgess, M.W., Gillette, M.A., Jaffe, J.D., and Carr, S.A. (2013). Integrated proteomic analysis of post-translational modifications by serial enrichment. Nat. Methods *10*, 634–637.

Middleton, E.R., and Rhoades, E. (2010). Effects of curvature and composition on α-synuclein binding to lipid vesicles. Biophys. J. *99*, 2279–2288.

Milber, J.M., Noorigian, J. V., Morley, J.F., Petrovitch, H., White, L., Ross, G.W., and Duda, J.E. (2012). Lewy pathology is not the first sign of degeneration in vulnerable neurons in parkinson disease. Neurology *79*, 2307–2314.

Miller, S.G., and Kennedy, M.B. (1986). Regulation of brain type II Ca2+/calmodulin-dependent protein kinase by autophosphorylation: a Ca2+-triggered molecular switch. Cell *44*, 861–870.

Minakaki, G., Menges, S., Kittel, A., Emmanouilidou, E., Schaeffner, I., Barkovits, K., Bergmann, A., Rockenstein, E., Adame, A., Marxreiter, F., et al. (2018). Autophagy inhibition promotes SNCA/alpha-synuclein release and transfer via extracellular vesicles with a hybrid autophagosome-exosome-like phenotype. Autophagy *14*, 98–119.

Mishto, M., Bellavista, E., Santoro, A., Stolzing, A., Ligorio, C., Nacmias, B., Spazzafumo, L., Chiappelli, M., Licastro, F., Sorbi, S., et al. (2006). Immunoproteasome and LMP2 polymorphism in aged and Alzheimer's disease brains. Neurobiol. Aging *27*, 54–66.

Montojo, J., Zuberi, K., Rodriguez, H., Bader, G.D., and Morris, Q. (2014). GeneMANIA: Fast gene network construction and function prediction for Cytoscape. F1000Research *3*, 153.

Moors, T.E., Hoozemans, J.J.M., Ingrassia, A., Beccari, T., Parnetti, L., Chartier-Harlin, M.C., and Van De Berg, W.D.J. (2017). Therapeutic potential of autophagy-enhancing agents in Parkinson's disease. Mol. Neurodegener. *12*, 1–18.

Mor, D.E., Tsika, E., Mazzulli, J.R., Gould, N.S., Kim, H., Daniels, M.J., Doshi, S., Gupta, P., Grossman, J.L., Tan, V.X., et al. (2017). Dopamine induces soluble α-synuclein oligomers and nigrostriatal degeneration. Nat. Neurosci. *20*, 1560–1568.

Morabito, G., Giannelli, S.G., Ordazzo, G., Bido, S., Castoldi, V., Indrigo, M., Cabassi, T., Cattaneo, S., Luoni, M., Cancellieri, C., et al. (2017). AAV-PHP.B-Mediated Global-Scale Expression in the Mouse Nervous System Enables GBA1 Gene Therapy for Wide Protection from Synucleinopathy. Mol. Ther. *25*, 2727–2742.

Moree, B., Yin, G., Lázaro, D.F., Munari, F., Strohäker, T., Giller, K., Becker, S., Outeiro, T.F., Zweckstetter, M., and Salafsky, J. (2015). Small molecules detected by second-harmonic generation modulate the conformation of monomeric α-synuclein and reduce its aggregation in cells. J. Biol. Chem. *290*, 27582–27593.

Moriguchi, S., Yabuki, Y., and Fukunaga, K. (2012). Reduced calcium/calmodulin-dependent protein kinase II activity in the hippocampus is associated with impaired cognitive function in MPTP-treated mice. J. Neurochem. *120*, 541–551.

Moscovitz, O., Ben-Nissan, G., Fainer, I., Pollack, D., Mizrachi, L., and Sharon, M. (2015). The Parkinson's-associated protein DJ-1 regulates the 20S proteasome. Nat. Commun. *6*, 1–13.

Muchamuel, T., Basler, M., Aujay, M.A., Suzuki, E., Kalim, K.W., Lauer, C., Sylvain, C., Ring, E.R., Shields, J., Jiang, J., et al. (2009). A selective inhibitor of the immunoproteasome subunit LMP7 blocks cytokine production and attenuates progression of experimental arthritis. Nat. Med. *15*, 781–787.

Murphy, D.D., Rueter, S.M., Trojanowski, J.Q., and Lee, V.M. (2000). Synucleins are developmentally expressed, and alpha-synuclein regulates the size of the presynaptic vesicular pool in primary hippocampal neurons. J. Neurosci. *20*, 3214–3220.

Nalls, M.A., Pankratz, N., Lill, C.M., Do, C.B., Hernandez, D.G., Saad, M., Destefano, A.L., Kara, E., Bras, J., Sharma, M., et al. (2014). Large-scale meta-analysis of genome-wide association data identifies six new risk loci for Parkinson's disease. Nat. Genet. *46*, 989–993.

Narhi, L., Wood, S.J., Steavenson, S., Jiang, Y., Wu, G.M., Anafi, D., Kaufman, S.A., Martin, F.,

Sitney, K., Denis, P., et al. (1999). Both familial Parkinson's disease mutations accelerate α-synuclein aggregation. J. Biol. Chem. *274*, 9843–9846.

Natalello, A., Santambrogio, C., and Grandori, R. (2017). Are Charge-State Distributions a Reliable Tool Describing Molecular Ensembles of Intrinsically Disordered Proteins by Native MS? J. Am. Soc. Mass Spectrom. *28*, 21–28.

Nathan, J.A., Spinnenhirn, V., Schmidtke, G., Basler, M., Groettrup, M., and Goldberg, A.L. (2013). Immuno- and constitutive proteasomes do not differ in their abilities to degrade ubiquitinated proteins. Cell *152*, 1184–1194.

Nelson, R., Sawaya, M.R., Balbirnie, M., Madsen, A.Ø., Riekel, C., Grothe, R., and Eisenberg, D. (2005). Structure of the cross-beta spine of amyloid-like fibrils. Nature *435*, 773–778.

Nemani, V.M., Lu, W., Berge, V., Nakamura, K., Onoa, B., Lee, M.K., Chaudhry, F.A., Nicoll, R.A., and Edwards, R.H. (2010). Increased Expression of α-Synuclein Reduces Neurotransmitter Release by Inhibiting Synaptic Vesicle Reclustering after Endocytosis. Neuron *65*, 66–79.

Neumann, M., Sampathu, D.M., Kwong, L.K., Truax, A.C., Micsenyi, M.C., Chou, T.T., Bruce, J., Schuck, T., Grossman, M., Clark, C.M., et al. (2006). Ubiquitinated TDP-43 in frontotemporal lobar degeneration and amyotrophic lateral sclerosis. Science *314*, 130–133.

Norris, E.H., Giasson, B.I., Hodara, R., Xu, S., Trojanowski, J.Q., Ischiropoulos, H., and Lee, V.M.Y. (2005). Reversible inhibition of α-synuclein fibrillization by dopaminochrome-mediated conformational alterations. J. Biol. Chem. *280*, 21212–21219.

Oaks, A.W., and Sidhu, A. (2011). Synuclein modulation of monoamine transporters. FEBS Lett. *585*, 1001–1006.

Olzscha, H., Schermann, S.M., Woerner, A.C., Pinkert, S., Hecht, M.H., Tartaglia, G.G., Vendruscolo, M., Hayer-Hartl, M., Hartl, F.U., and Vabulas, R.M. (2011). Amyloid-like aggregates sequester numerous metastable proteins with essential cellular functions. Cell *144*, 67–78.

Ono, K., and Yamada, M. (2006). Antioxidant compounds have potent anti-fibrillogenic and fibril-destabilizing effects for alpha-synuclein fibrils in vitro. J. Neurochem. *97*, 105–115.

Orre, M., Kamphuis, W., Dooves, S., Kooijman, L., Chan, E.T., Kirk, C.J., Dimayuga Smith, V., Koot, S., Mamber, C., Jansen, A.H., et al. (2013). Reactive glia show increased immunoproteasome activity in Alzheimer's disease. Brain *136*, 1415–1431.

Osterberg, V.R., Spinelli, K.J., Weston, L.J., Luk, K.C., Woltjer, R.L., and Unni, V.K. (2015). Progressive Aggregation of Alpha-Synuclein and Selective Degeneration of Lewy Inclusion-Bearing Neurons in a Mouse Model of Parkinsonism. Cell Rep. *10*, 1252–1260.

Ostrerova, N., Petrucelli, L., Farrer, M., Mehta, N., Choi, P., Hardy, J., and Wolozin, B. (1999). alpha-Synuclein shares physical and functional homology with 14-3-3 proteins. J. Neurosci. *19*, 5782–5791.

Oueslati, A., Fournier, M., and Lashuel, H.A. (2010). Role of post-translational modifications in modulating the structure, function and toxicity of α-synuclein. Implications for Parkinson's disease pathogenesis and therapies. Prog. Brain Res. *183*, 115–145.

Oueslati, A., Schneider, B.L., Aebischer, P., and Lashuel, H.A. (2013). Polo-like kinase 2 regulates selective autophagic α-synuclein clearance and suppresses its toxicity in vivo. Proc. Natl. Acad. Sci. *110*, E3945–E3954.

Ouzan, D., Chichmanian, R.M., Fuzibet, J.G., Saint-Paul, M., and Fredendrich, A. (1990). [Severe acute hepatic involvements caused by exifone]. Therapie *45*, 436–437.

Paik, S.R., Shin, H.J., Lee, J.H., Chang, C.S., and Kim, J. (1999). Copper(II)-induced self-oligomerization of alpha-synuclein. Biochem. J. *340 (Pt 3*, 821–828.

Paisán-Ruíz, C., Jain, S., Evans, E.W., Gilks, W.P., Simón, J., Van Der Brug, M., De Munain, A.L., Aparicio, S., Gil, A.M., Khan, N., et al. (2004). Cloning of the gene containing mutations that cause PARK8-linked Parkinson's disease. Neuron *44*, 595–600.

Paisán-Ruíz, C., Nath, P., Washecka, N., Gibbs, J.R., and Singleton, A.B. (2008). Comprehensive analysis of LRRK2 in publicly available Parkinson's disease cases and neurologically normal controls. Hum. Mutat. *29*, 485–490.

Paleologou, K.E., Schmid, A.W., Rospigliosi, C.C., Kim, H.Y., Lamberto, G.R., Fredenburg, R.A., Lansbury, P.T., Fernandez, C.O., Eliezer, D., Zweckstetter, M., et al. (2008). Phosphorylation at Ser-129 but not the phosphomimics S129E/D inhibits the fibrillation of α-synuclein. J. Biol. Chem. *283*, 16895–16905.

Paleologou, K.E., Oueslati, A., Shakked, G., Rospigliosi, C.C., Kim, H.-Y., Lamberto, G.R., Fernandez, C.O., Schmid, A., Chegini, F., Gai, W.P., et al. (2010). Phosphorylation at S87 Is Enhanced in Synucleinopathies, Inhibits α-Synuclein Oligomerization, and Influences Synuclein-Membrane Interactions. J. Neurosci. *30*, 3184–3198.

Parkinson, J. (1817). An Essay on the Shaking Palsy (London: Sherwood, Nealy and Jones).

Pasanen, P., Myllykangas, L., Siitonen, M., Raunio, A., Kaakkola, S., Lyytinen, J., Tienari, P.J., Pöyhönen, M., and Paetau, A. (2014). A novel α-synuclein mutation A53E associated with atypical multiple system atrophy and Parkinson's disease-type pathology. Neurobiol. Aging *35*, 2180.e1-2180.e5.

Patra, K., Lyons, D.J., Bauer, P., Hilscher, M.M., Sharma, S., Leão, R.N., and Kullander, K. (2015). A role for solute carrier family 10 member 4, or vesicular aminergic-associated transporter, in structural remodelling and transmitter release at the mouse neuromuscular junction. Eur. J. Neurosci. *41*, 316–327.

Paumier, K.L., Luk, K.C., Manfredsson, F.P., Kanaan, N.M., Lipton, J.W., Collier, T.J., Steece-Collier, K., Kemp, C.J., Celano, S., Schulz, E., et al. (2015). Intrastriatal injection of pre-formed mouse α-synuclein fibrils into rats triggers α-synuclein pathology and bilateral nigrostriatal degeneration. Neurobiol. Dis. *82*, 185–199.

Peelaerts, W., Bousset, L., Van Der Perren, A., Moskalyuk, A., Pulizzi, R., Giugliano, M., Van Den Haute, C., Melki, R., and Baekelandt, V. (2015). α-Synuclein strains cause distinct synucleinopathies after local and systemic administration. Nature *522*, 340–344.

Peng, X.M. (2005). α-Synuclein activation of protein phosphatase 2A reduces tyrosine hydroxylase phosphorylation in dopaminergic cells. J. Cell Sci. *118*, 3523–3530.

Peng, C., Gathagan, R.J., Covell, D.J., Medellin, C., Stieber, A., Robinson, J.L., Zhang, B., Pitkin, R.M., Olufemi, M.F., Luk, K.C., et al. (2018). Cellular milieu imparts distinct pathological α-synuclein strains in α-synucleinopathies. Nature 1.

Perez, R.G., Waymire, J.C., Lin, E., Liu, J.J., Guo, F., and Zigmond, M.J. (2002). A role for α-synuclein in the Regulation of Dopamine Biosynthesis. J. Neurosci. *22*, 3090–3099.

Perni, M., Galvagnion, C., Maltsev, A., Meisl, G., Müller, M.B.D., Challa, P.K., Kirkegaard, J.B., Flagmeier, P., Cohen, S.I.A., Cascella, R., et al. (2017). A natural product inhibits the initiation of α-synuclein aggregation and suppresses its toxicity. Proc. Natl. Acad. Sci. *114*, E1009–E1017.

Picconi, B., Gardoni, F., Centonze, D., Mauceri, D., Cenci, M.A., Bernardi, G., Calabresi, P., and Di Luca, M. (2004). Abnormal Ca2+-calmodulin-dependent protein kinase II function mediates synaptic and motor deficits in experimental parkinsonism. J. Neurosci. *24*, 5283–5291.

Pickering, A.M., Lehr, M., and Miller, R.A. (2015). Lifespan of mice and primates correlates with immunoproteasome expression. J. Clin. Invest. *125*, 2059–2068.

Pogačnik, L., Pirc, K., Palmela, I., Skrt, M., Kwang, K.S., Brites, D., Brito, M.A., Ulrih, N.P., and Silva, R.F.M. (2016). Potential for brain accessibility and analysis of stability of selected flavonoids in relation to neuroprotection in vitro. Brain Res. *1651*, 17–26.

Polymeropoulos, M.H., Lavedan, C., Leroy, E., Ide, S.E., Dehejia, A., Dutra, A., Pike, B., Root, H., Rubenstein, J., Boyer, R., et al. (1997). Mutation in the α-synuclein gene identified in families with Parkinson's disease. Science *276*, 2045–2047.

Powers, E.T., Morimoto, R.I., Dillin, A., Kelly, J.W., and Balch, W.E. (2009). Biological and chemical approaches to diseases of proteostasis deficiency. Annu. Rev. Biochem. *78*, 959–991.

Prabhudesai, S., Sinha, S., Attar, A., Kotagiri, A., Fitzmaurice, A.G., Lakshmanan, R., Ivanova, M.I., Loo, J.A., Klärner, F.G., Schrader, T., et al. (2012). A Novel "Molecular Tweezer" Inhibitor of α-Synuclein Neurotoxicity in Vitro and in Vivo. Neurotherapeutics *9*, 464–476.

Price, J.C., Guan, S., Burlingame, A., Prusiner, S.B., and Ghaemmaghami, S. (2010). Analysis of proteome dynamics in the mouse brain. Proc. Natl. Acad. Sci. U. S. A. *107*, 14508–14513.

Pringsheim, T., Jette, N., Frolkis, A., and Steeves, T.D.L. (2014). The prevalence of Parkinson's disease: a systematic review and meta-analysis. Mov. Disord. *29*, 1583–1590.

Prots, I., Veber, V., Brey, S., Campioni, S., Buder, K., Riek, R., Böhm, K.J., and Winner, B. (2013). α-Synuclein oligomers impair neuronal microtubule-kinesin interplay. J. Biol. Chem. *288*, 21742–21754.

Proukakis, C., Dudzik, C.G., Brier, T., MacKay, D.S., Cooper, J.M., Millhauser, G.L., Houlden, H., and Schapira, A.H. (2013). A novel α-synuclein missense mutation in Parkinson disease. Neurology *80*, 1062–1064.

Przedborski, S., Chen, Q.P., Vila, M., Giasson, B.I., Djaldatti, R., Vukosavic, S., Souza, J.M., Jackson-Lewis, V., Lee, V.M.Y., and Ischiropoulos, H. (2001). Oxidative post-translational modifications of α-synuclein in the 1-methyl-4-phenyl-1,2,3,6-tetrahydropyridine (MPTP) mouse model of Parkinson's disease. J. Neurochem. *76*, 637–640.

van der Putten, H., Wiederhold, K.H., Probst, A., Barbieri, S., Mistl, C., Danner, S., Kauffmann, S., Hofele, K., Spooren, W.P., Ruegg, M.A., et al. (2000). Neuropathology in mice expressing human alpha-synuclein. J. Neurosci. *20*, 6021–6029.

Rasia, R.M., Bertoncini, C.W., Marsh, D., Hoyer, W., Cherny, D., Zweckstetter, M., Griesinger, C., Jovin, T.M., and Fernandez, C.O. (2005). Structural characterization of copper(II) binding to α-synuclein: Insights into the bioinorganic chemistry of Parkinson's disease. Proc. Natl. Acad. Sci. *102*, 4294–4299.

Raule, M., Cerruti, F., and Cascio, P. (2014). Enhanced rate of degradation of basic proteins by 26S immunoproteasomes. Biochim. Biophys. Acta *1843*, 1942–1947.

Recasens, A., Dehay, B., Bové, J., Carballo-Carbajal, I., Dovero, S., Pérez-Villalba, A., Fernagut, P.-O., Blesa, J., Parent, A., Perier, C., et al. (2014). Lewy body extracts from Parkinson disease brains trigger α-synuclein pathology and neurodegeneration in mice and monkeys. Ann. Neurol. *75*, 351–362.

Reznichenko, L., Kalfon, L., Amit, T., Youdim, M.B.H., and Mandel, S.A. (2010). Low dosage of rasagiline and epigallocatechin gallate synergistically restored the nigrostriatal axis in MPTP-induced parkinsonism. Neurodegener. Dis. *7*, 219–231.

Rhoades, E., Ramlall, T.F., Webb, W.W., and Eliezer, D. (2006). Quantification of α-synuclein binding to lipid vesicles using fluorescence correlation spectroscopy. Biophys. J. *90*, 4692–4700.

Riederer, P., Sofic, E., Rausch, W.D., Schmidt, B., Reynolds, G.P., Jellinger, K., and Youdim, M.B. (1989). Transition metals, ferritin, glutathione, and ascorbic acid in parkinsonian brains. J. Neurochem. *52*, 515–520.

Rocha, E.M., Smith, G.A., Park, E., Cao, H., Brown, E., Hayes, M.A., Beagan, J., McLean, J.R., Izen, S.C., Perez-Torres, E., et al. (2015). Glucocerebrosidase gene therapy prevents α-synucleinopathy of midbrain dopamine neurons. Neurobiol. Dis. *82*, 495–503.

Rockenstein, E., Nuber, S., Overk, C.R., Ubhi, K., Mante, M., Patrick, C., Adame, A., Trejo-Morales, M., Gerez, J., Picotti, P., et al. (2014). Accumulation of oligomer-prone α-synuclein exacerbates synaptic and neuronal degeneration in vivo. Brain *137*, 1496–1513.

Rodriguez, J.A., Ivanova, M.I., Sawaya, M.R., Cascio, D., Reyes, F.E., Shi, D., Sangwan, S., Guenther, E.L., Johnson, L.M., Zhang, M., et al. (2015). Structure of the toxic core of α-synuclein from invisible crystals. Nature *525*, 486–490.

Rutherford, N.J., Lewis, J., Clippinger, A.K., Thomas, M.A., Adamson, J., Cruz, P.E., Cannon, A., Xu, G., Golde, T.E., Shaw, G., et al. (2013). Unbiased screen reveals ubiquilin-1 and -2 highly associated with huntingtin inclusions. Brain Res. *1524*, 62–73.

Sacino, A.N., Brooks, M., McKinney, A.B., Thomas, M.A., Shaw, G., Golde, T.E., and Giasson, B.I. (2014a). Brain Injection of α-Synuclein Induces Multiple Proteinopathies, Gliosis, and a Neuronal Injury Marker. J. Neurosci. *34*, 12368–12378.

Sacino, A.N., Brooks, M., Thomas, M.A., McKinney, A.B., Lee, S., Regenhardt, R.W., McGarvey, N.H., Ayers, J.I., Notterpek, L., Borchelt, D.R., et al. (2014b). Intramuscular injection of α-synuclein induces CNS α-synuclein pathology and a rapid-onset motor phenotype in transgenic

mice. Proc. Natl. Acad. Sci. *111*, 10732–10737.

Sampathu, D.M., Giasson, B.I., Pawlyk, A.C., Trojanowski, J.Q., and Lee, V.M.-Y. (2003). Ubiquitination of α-Synuclein Is Not Required for Formation of Pathological Inclusions in α-Synucleinopathies. Am. J. Pathol. *163*, 91–100.

Sardi, S.P., Clarke, J., Viel, C., Chan, M., Tamsett, T.J., Treleaven, C.M., Bu, J., Sweet, L., Passini, M.A., Dodge, J.C., et al. (2013). Augmenting CNS glucocerebrosidase activity as a therapeutic strategy for parkinsonism and other Gaucher-related synucleinopathies. Proc. Natl. Acad. Sci. *110*, 3537–3542.

Satake, W., Nakabayashi, Y., Mizuta, I., Hirota, Y., Ito, C., Kubo, M., Kawaguchi, T., Tsunoda, T., Watanabe, M., Takeda, A., et al. (2009). Genome-wide association study identifies common variants at four loci as genetic risk factors for Parkinson's disease. Nat. Genet. *41*, 1303–1307.

Sawaya, M.R., Sambashivan, S., Nelson, R., Ivanova, M.I., Sievers, S.A., Apostol, M.I., Thompson, M.J., Balbirnie, M., Wiltzius, J.J.W., McFarlane, H.T., et al. (2007). Atomic structures of amyloid cross-β spines reveal varied steric zippers. Nature *447*, 453–457.

Schenk, D.B., Koller, M., Ness, D.K., Griffith, S.G., Grundman, M., Zago, W., Soto, J., Atiee, G., Ostrowitzki, S., and Kinney, G.G. (2017). First-in-human assessment of PRX002, an anti–α-synuclein monoclonal antibody, in healthy volunteers. Mov. Disord. *32*, 211–218.

Scott, D.A., Tabarean, I., Tang, Y., Cartier, A., Masliah, E., and Roy, S. (2010). A pathologic cascade leading to synaptic dysfunction in alpha-synuclein-induced neurodegeneration. J. Neurosci. *30*, 8083–8095.

Seifert, U., Bialy, L.P., Ebstein, F., Bech-Otschir, D., Voigt, A., Schröter, F., Prozorovski, T., Lange, N., Steffen, J., Rieger, M., et al. (2010). Immunoproteasomes preserve protein homeostasis upon interferon-induced oxidative stress. Cell *142*, 613–624.

Serpell, L.C., Berriman, J., Jakes, R., Goedert, M., and Crowther, R.A. (2000). Fiber diffraction of synthetic alpha-synuclein filaments shows amyloid-like cross-beta conformation. Proc. Natl. Acad. Sci. U. S. A. *97*, 4897–4902.

Sharma, K., Schmitt, S., Bergner, C.G., Tyanova, S., Kannaiyan, N., Manrique-Hoyos, N., Kongi, K., Cantuti, L., Hanisch, U.-K., Philips, M.-A., et al. (2015). Cell type- and brain region-resolved mouse brain proteome. Nat. Neurosci. *18*, 1819–1831.

Sharon, R., Bar-joseph, I., Frosch, M.P., Walsh, D.M., Hamilton, J.A., and Selkoe, D.J. (2003). The Formation of Highly Soluble Oligomers of α-Synuclein Is Regulated by Fatty Acids and Enhanced in Parkinson ' s Disease Brigham and Women ' s Hospital. Neuron *37*, 583–595.

Shibayama-Imazu, T., Okahashi, I., Omata, K., Nakajo, S., Ochiai, H., Nakai, Y., Hama, T., Nakamura, Y., and Nakaya, K. (1993). Cell and tissue distribution and developmental change of neuron specific 14 kDa protein (phosphoneuroprotein 14). Brain Res. *622*, 17–25.

Shimozawa, A., Ono, M., Takahara, D., Tarutani, A., Imura, S., Masuda-Suzukake, M., Higuchi, M., Yanai, K., Hisanaga, S.I., and Hasegawa, M. (2017). Propagation of pathological α-synuclein in marmoset brain. Acta Neuropathol. Commun. *5*, 12.

Sidransky, E., Nalls, M.A., Aasly, J.O., Aharon-Peretz, J., Annesi, G., Barbosa, E.R., Bar-Shira, A., Berg, D., Bras, J., Brice, A., et al. (2009). Multicenter analysis of glucocerebrosidase mutations in Parkinson's disease. N. Engl. J. Med. *361*, 1651–1661.

Simón-Sánchez, J., Schulte, C., Bras, J.M., Sharma, M., Gibbs, J.R., Berg, D., Paisan-Ruiz, C., Lichtner, P., Scholz, S.W., Hernandez, D.G., et al. (2009). Genome-wide association study reveals genetic risk underlying Parkinson's disease. Nat. Genet. *41*, 1308–1312.

Singleton, A.B., Farrer, M., Johnson, J., Singleton, A., Hague, S., Kachergus, J., Hulihan, M., Peuralinna, T., Dutra, A., Nussbaum, R., et al. (2003). α-Synuclein Locus Triplication Causes Parkinson's Disease. Science *302*, 841.

Soper, J.H., Roy, S., Stieber, A., Lee, E., Wilson, R.B., Trojanowski, J.Q., Burd, C.G., and Lee, V.M.-Y. (2008). Alpha-synuclein-induced aggregation of cytoplasmic vesicles in Saccharomyces cerevisiae. Mol. Biol. Cell *19*, 1093–1103.

Souza, J.M., Giasson, B.I., Chen, Q., Lee, V.M.Y., and Ischiropoulos, H. (2000a). Dityrosine cross-linking promotes formation of stable α-synuclein polymers: Implication of nitrative and oxidative stress in the pathogenesis of neurodegenerative synucleinopathies. J. Biol. Chem. *275*, 18344–18349.

Souza, J.M., Giasson, B.I., Lee, V.M.Y., and Ischiropoulos, H. (2000b). Chaperone-like activity of synucleins. FEBS Lett. *474*, 116–119.

Spillantini, M.G., Schmidt, M.L., Lee, V.M.-Y., Trojanowski, J.Q., Jakes, R., and Goedert, M. (1997). alpha-Synuclein in Lewy bodies. Nature *388*, 839–840.

Spillantini, M.G., Crowther, R.A., Jakes, R., Hasegawa, M., and Goedert, M. (1998). alpha-Synuclein in filamentous inclusions of Lewy bodies from Parkinson's disease and dementia with lewy bodies. Proc. Natl. Acad. Sci. U. S. A. *95*, 6469–6473.

Sulzer, D., Alcalay, R.N., Garretti, F., Cote, L., Kanter, E., Agin-Liebes, J., Liong, C., McMurtrey, C., Hildebrand, W.H., Mao, X., et al. (2017). T cells from patients with Parkinson's disease recognize α-synuclein peptides. Nature *546*, 656–661.

Tabner, B.J., Turnbull, S., El-Agnaf, O.M.A., and Allsop, D. (2002). Formation of hydrogen peroxide and hydroxyl radicals from A(beta) and alpha-synuclein as a possible mechanism of cell death in Alzheimer's disease and Parkinson's disease. Free Radic. Biol. Med. *32*, 1076–1083.

Takeda, A., Mallory, M., Sundsmo, M., Honer, W., Hansen, L., and Masliah, E. (1998). Abnormal accumulation of NACP/α-synuclein in neurodegenerative disorders. Am. J. Pathol. *152*, 367–372.

Tavassoly, O., Nokhrin, S., Dmitriev, O.Y., and Lee, J.S. (2014). Cu(II) and dopamine bind to α-synuclein and cause large conformational changes. FEBS J. *281*, 2738–2753.

Tehranian, R., Montoya, S.E., Van Laar, A.D., Hastings, T.G., and Perez, R.G. (2006). Alpha-synuclein inhibits aromatic amino acid decarboxylase activity in dopaminergic cells. J. Neurochem. *99*, 1188–1196.

Teoh, C.Y., and Davies, K.J.A. (2004). Potential roles of protein oxidation and the immunoproteasome in MHC class I antigen presentation: the "PrOxI" hypothesis. Arch. Biochem.

Biophys. *423*, 88–96.

Thomas, B., Mandir, A.S., West, N., Liu, Y., Andrabi, S.A., Stirling, W., Dawson, V.L., Dawson, T.M., and Lee, M.K. (2011). Resistance to MPTP-Neurotoxicity in α-synuclein knockout mice is complemented by human α-synuclein and associated with increased β-synuclein and Akt activation. PLoS One *6*.

Tran, H.T., Chung, C.H.Y., Iba, M., Zhang, B., Trojanowski, J.Q., Luk, K.C., and Lee, V.M.Y. (2014). α-Synuclein Immunotherapy Blocks Uptake and Templated Propagation of Misfolded α-Synuclein and Neurodegeneration. Cell Rep. *7*, 2054–2065.

Trétiakoff, C. (1919). Contribution a l'étude de l'anatomie pathologique du locus niger de Soemmering avec quelques dedutions relatives a la pathogenie des troubles du tonus musculaire et de la maladie de Parkinson. (Paris: Université de Paris).

Trexler, A.J., and Rhoades, E. (2009). α-Synuclein binds large unilamellar vesicles as an extended helix. Biochemistry *48*, 2304–2306.

Trexler, A.J., and Rhoades, E. (2012). N-terminal acetylation is critical for forming α-helical oligomer of α-synuclein. Protein Sci. *21*, 601–605.

Tsika, E., Moysidou, M., Guo, J., Cushman, M., Gannon, P., Sandaltzopoulos, R., Giasson, B.I., Krainc, D., Ischiropoulos, H., and Mazzulli, J.R. (2010). Distinct region-specific alpha-synuclein oligomers in A53T transgenic mice: implications for neurodegeneration. J. Neurosci. *30*, 3409–3418.

Tuttle, M.D., Comellas, G., Nieuwkoop, A.J., Covell, D.J., Berthold, D.A., Kloepper, K.D., Courtney, J.M., Kim, J.K., Barclay, A.M., Kendall, A., et al. (2016). Solid-state NMR structure of a pathogenic fibril of full-length human α-synuclein. Nat. Struct. Mol. Biol. *23*, 409–415.

Tyanova, S., Temu, T., Sinitcyn, P., Carlson, A., Hein, M.Y., Geiger, T., Mann, M., and Cox, J. (2016). The Perseus computational platform for comprehensive analysis of (prote)omics data. Nat. Methods *13*, 731–740.

Tyson, T., Steiner, J.A., and Brundin, P. (2016). Sorting out release, uptake and processing of alpha-synuclein during prion-like spread of pathology. J. Neurochem. *139*, 275–289.

Uéda, K., Fukushima, H., Masliah, E., Xia, Y., Iwai, A., Yoshimoto, M., Otero, D.A., Kondo, J., Ihara, Y., and Saitoh, T. (1993). Molecular cloning of cDNA encoding an unrecognized component of amyloid in Alzheimer disease. Proc. Natl. Acad. Sci. *90*, 11282–11286.

Ulmer, T.S., and Bax, A. (2005). Comparison of structure and dynamics of micelle-bound human α-synuclein and Parkinson disease variants. J. Biol. Chem. *280*, 43179–43187.

Uversky, V.N., Li, J., and Fink, A.L. (2001a). Metal-triggered structural transformations, aggregation, and fibrillation of human α-synuclein: A possible molecular link between parkinson's disease and heavy metal exposure. J. Biol. Chem. *276*, 44284–44296.

Uversky, V.N., Li, J., and Fink, A.L. (2001b). Evidence for a Partially Folded Intermediate in α-Synuclein Fibril Formation. J. Biol. Chem. *276*, 10737–10744.

Valente, E.M., Bentivoglio, A.R., Dixon, P.H., Ferraris, A., Ialongo, T., Frontali, M., Albanese, A., and Wood, N.W. (2001). PARK7, a Novel Locus for Autosomal Recessive Early-Onset Parkinsonism, on Chromosome 1p36. Am. J. Hum. Genet. *68*, 895–900.

Valente, E.M., Abou-sleiman, P.M., Caputo, V., Muqit, M.M.K., Harvey, K., Gispert, S., Ali, Z., Turco, D. Del, Bentivoglio, A.R., Healy, D.G., et al. (2004). Hereditary Early-Onset Parkinson ' s Disease Caused by Mutations in PINK1. Science *304*, 1158–1161.

Vargas, K.J., Makani, S., Davis, T., Westphal, C.H., Castillo, P.E., and Chandra, S.S. (2014). Synucleins Regulate the Kinetics of Synaptic Vesicle Endocytosis. J. Neurosci. *34*, 9364–9376.

Vilar, M., Chou, H.-T., Luhrs, T., Maji, S.K., Riek-Loher, D., Verel, R., Manning, G., Stahlberg, H., and Riek, R. (2008). The fold of α-synuclein fibrils. Proc. Natl. Acad. Sci. *105*, 8637–8642.

Vilariño-Güell, C., Wider, C., Ross, O.A., Dachsel, J.C., Kachergus, J.M., Lincoln, S.J., Soto-Ortolaza, A.I., Cobb, S.A., Wilhoite, G.J., Bacon, J.A., et al. (2011). VPS35 mutations in parkinson disease. Am. J. Hum. Genet. *89*, 162–167.

Wagner, J., Ryazanov, S., Leonov, A., Levin, J., Shi, S., Schmidt, F., Prix, C., Pan-Montojo, F., Bertsch, U., Mitteregger-Kretzschmar, G., et al. (2013). Anle138b: A novel oligomer modulator for disease-modifying therapy of neurodegenerative diseases such as prion and Parkinson's disease. Acta Neuropathol. *125*, 795–813.

Wakabayashi, K., Yoshimoto, M., Tsuji, S., and Takahashi, H. (1998). Alpha-synuclein immunoreactivity in glial cytoplasmic inclusions in multiple system atrophy. Neurosci. Lett. *249*, 180–182.

Walter, W., Sánchez-Cabo, F., and Ricote, M. (2015). GOplot: an R package for visually combining expression data with functional analysis. Bioinformatics *31*, 2912–2914.

Walther, D.M., and Mann, M. (2011). Accurate Quantification of More Than 4000 Mouse Tissue Proteins Reveals Minimal Proteome Changes During Aging. Mol. Cell. Proteomics *10*, M110.004523.

Wang, H., Qian, W.-J., Chin, M.H., Petyuk, V.A., Barry, R.C., Liu, T., Gritsenko, M.A., Mottaz, H.M., Moore, R.J., Camp Ii, D.G., et al. (2006). Characterization of the mouse brain proteome using global proteomic analysis complemented with cysteinyl-peptide enrichment. J. Proteome Res. *5*, 361–369.

Wang, L., Das, U., Scott, D.A., Tang, Y., McLean, P.J., and Roy, S. (2014). α-Synuclein multimers cluster synaptic vesicles and attenuate recycling. Curr. Biol. *24*, 2319–2326.

Wang, W., Perovic, I., Chittuluru, J., Kaganovich, A., Nguyen, L.T.T., Liao, J., Auclair, J.R., Johnson, D., Landeru, A., Simorellis, A.K., et al. (2011). A soluble α-synuclein construct forms a dynamic tetramer. Proc. Natl. Acad. Sci. *108*, 17797–17802.

Waxman, E.A., and Giasson, B.I. (2010). NIH Public Access. J. Neuropathol. Exp. Neurol. *67*, 402–416.

Waxman, E.A., Duda, J.E., and Giasson, B.I. (2008). Characterization of antibodies that selectively detect α-synuclein in pathological inclusions. Acta Neuropathol. *116*, 37–46.

Webb, J.L., Ravikumar, B., Atkins, J., Skepper, J.N., and Rubinsztein, D.C. (2003). α-synuclein Is Degraded by Both Autophagy and the Proteasome. J. Biol. Chem. *278*, 25009–25013.

Weinreb, P.H., Zhen, W., Poon, A.W., Conway, K.A., and Lansbury, P.T. (1996). NACP, a protein implicated in Alzheimer's disease and learning, is natively unfolded. Biochemistry *35*, 13709–13715.

White, L., and al, et (1996). Prevalence of dementia in older Japanese-American Men in Hawaii. J. Am. Med. Assoc. *276*, 955–960.

Wilms, H., Rosenstiel, P., Romero-Ramos, M., Arlt, a, Schäfer, H., Seegert, D., Kahle, P.J., Odoy, S., Claasen, J.H., Holzknecht, C., et al. (2009). Suppression of MAP kinases inhibits microglial activation and attenuates neuronal cell death induced by alpha-synuclein protofibrils. Int. J. Immunopathol. Pharmacol. *22*, 897–909.

Winner, B., Jappelli, R., Maji, S.K., Desplats, P.A., Boyer, L., Aigner, S., Hetzer, C., Loher, T., Vilar, M., Campioni, S., et al. (2011). In vivo demonstration that α-synuclein oligomers are toxic. Proc. Natl. Acad. Sci. *108*, 4194–4199.

Wirdefeldt, K., Adami, H.-O., Cole, P., Trichopoulos, D., and Mandel, J. (2011). Epidemiology and etiology of Parkinson's disease: a review of the evidence. Eur. J. Epidemiol. *26*, 1–58.

Withers, G.S., George, J.M., Banker, G.A., and Clayton, D.F. (1997). Delayed localization of synelfin (synuclein, NACP) to presynaptic terminals in cultured rat hippocampal neurons. Dev. Brain Res. *99*, 87–94.

Woerner, A.C., Frottin, F., Hornburg, D., Feng, L.R., Meissner, F., Patra, M., Tatzelt, J., Mann, M., Winklhofer, K.F., Hartl, F.U., et al. (2016). Cytoplasmic protein aggregates interfere with nucleocytoplasmic transport of protein and RNA. Science *351*, 173–176.

Wood, S.J., Wypych, J., Steavenson, S., Louis, J., Citron, M., and Biere, A.L. (1999). α-Synuclein Fibrillogenesis is Nucleation-dependent. Biochemistry 19509–19512.

Woods, W.S., Boettcher, J.M., Zhou, D.H., Kloepper, K.D., Hartman, K.L., Ladror, D.T., Qi, Z., Rienstra, C.M., and George, J.M. (2007). Conformation-specific binding of α-synuclein to novel protein partners detected by phage display and NMR spectroscopy. J. Biol. Chem. *282*, 34555–34567.

Wrasidlo, W., Tsigelny, I.F., Price, D.L., Dutta, G., Rockenstein, E., Schwarz, T.C., Ledolter, K., Bonhaus, D., Paulino, A., Eleuteri, S., et al. (2016). A de novo compound targeting α-synuclein improves deficits in models of Parkinson's disease. Brain *139*, 3217–3236.

Wu, C.C., MacCoss, M.J., Howell, K.E., Matthews, D.E., and Yates, J.R. (2004). Metabolic labeling of mammalian organisms with stable isotopes for quantitative proteomic analysis. Anal. Chem. *76*, 4951–4959.

Yang, J.E., Rhoo, K.Y., Lee, S., Lee, J.T., Park, J.H., Bhak, G., and Paik, S.R. (2017). EGCG-mediated Protection of the Membrane Disruption and Cytotoxicity Caused by the "Active Oligomer" of α-Synuclein. Sci. Rep. *7*, 1–10.

Yang, W., Wang, G., Wang, C.-E., Guo, X., Yin, P., Gao, J., Tu, Z., Wang, Z., Wu, J., Hu, X., et

al. (2015). Mutant Alpha-Synuclein Causes Age-Dependent Neuropathology in Monkey Brain. J. Neurosci. *35*, 8345–8358.

Yavich, L. (2004). Role of α-Synuclein in Presynaptic Dopamine Recruitment. J. Neurosci. *24*, 11165–11170.

Ysselstein, D., Joshi, M., Mishra, V., Griggs, A.M., Asiago, J.M., McCabe, G.P., Stanciu, L.A., Post, C.B., and Rochet, J.C. (2015). Effects of impaired membrane interactions on α-synuclein aggregation and neurotoxicity. Neurobiol. Dis. *79*, 150–163.

Yun, Y.S., Kim, K.H., Tschida, B., Sachs, Z., Noble-Orcutt, K.E., Moriarity, B.S., Ai, T., Ding, R., Williams, J., Chen, L., et al. (2016). mTORC1 Coordinates Protein Synthesis and Immunoproteasome Formation via PRAS40 to Prevent Accumulation of Protein Stress. Mol. Cell *61*, 625–639.

Zarranz, J.J., Alegre, J., Gómez-Esteban, J.C., Lezcano, E., Ros, R., Ampuero, I., Vidal, L., Hoenicka, J., Rodriguez, O., Atarés, B., et al. (2004). The New Mutation, E46K, of α-Synuclein Causes Parkinson and Lewy Body Dementia. Ann. Neurol. *55*, 164–173.

Zharikov, A.D., Cannon, J.R., Tapias, V., Bai, Q., Horowitz, M.P., Shah, V., El Ayadi, A., Hastings, T.G., Greenamyre, J.T., and Burton, E.A. (2015a). shRNA targeting α-synuclein prevents neurodegeneration in a Parkinson's disease model. J. Clin. Invest. *125*, 2721–2735.

Zharikov, A.D., Cannon, J.R., Tapias, V., Bai, Q., Horowitz, M.P., Shah, V., El Ayadi, A., Hastings, T.G., Greenamyre, J.T., and Burton, E. (2015b). shRNA targeting α-synuclein prevents neurodegeneration in a Parkinson's disease model. J. Clin. Invest. *125*, 2721–2735.

Zhu, M., and Fink, A.L. (2003). Lipid binding inhibits α-synuclein fibril formation. J. Biol. Chem. *278*, 16873–16877.

Zhu, J.-H., Guo, F., Shelburne, J., Watkins, S., and Chu, C.T. (2003a). Localization of phosphorylated ERK/MAP kinases to mitochondria and autophagosomes in Lewy body diseases. Brain Pathol. *13*, 473–481.

Zhu, M., Li, J., and Fink, A.L. (2003b). The association of α-synuclein with membranes affects bilayer structure, stability, and fibril formation. J. Biol. Chem. *278*, 40186–40197.

Zimprich, A., Biskup, S., Leitner, P., Lichtner, P., Farrer, M., Lincoln, S., Kachergus, J., Hulihan, M., Uitti, R.J., Calne, D.B., et al. (2004). Mutations in LRRK2 cause autosomal-dominant parkinsonism with pleomorphic pathology. Neuron *44*, 601–607.

Zimprich, A., Benet-Pagès, A., Struhal, W., Graf, E., Eck, S.H., Offman, M.N., Haubenberger, D., Spielberger, S., Schulte, E.C., Lichtner, P., et al. (2011). A mutation in VPS35, encoding a subunit of the retromer complex, causes late-onset parkinson disease. Am. J. Hum. Genet. *89*, 168–175.